

N, S-Doped Carbon Quantum Dots/TiO₂ Nanocomposites for Visible-Light-Driven Photocatalytic Degradation of Water Pollutants

by

Lantian Chang

submitted to the School of Graduate Studies in partial fulfillment
of the requirements for the degree of

Master of Engineering

Faculty of Engineering and Applied Science

Memorial University of Newfoundland

July 2022

St. John's Newfoundland and Labrador

Abstract

This thesis presents the synthesis and application of a novel carbon quantum dots (CQDs) sensitized TiO₂ composite in the treatment of water pollutants. Firstly, nitrogen and sulfur co-doped carbon quantum dots (N, S-CQDs) were synthesized from citric acid and thiourea through hydrothermal method. The as-prepared N, S-CQDs demonstrated strong visible-light absorption and green-light emission. By incorporating N, S-CQDs into TiO₂, a composite (N, S-CQDs/TiO₂) with great improvement in visible-light-harvesting and reduced band gap were obtained, which was subsequently used as a visible-light-responsive catalyst for the photocatalytic reduction of Cr (VI) from water. Experimental results from batch reaction processes indicated that the composite was able to completely reduce Cr (VI) to Cr (III) at pH2.0 after 3 hours' exposure to visible light with the initial Cr (VI) concentration being 20.0 mg/L and a catalyst dosage of 1.0g/L. It was also found that lower pH and lower initial concentration of Cr (VI) led to high reduction efficiency. Compare with pure TiO₂, a four-fold increase in reduction efficiency of Cr (VI) was achieved by the N, S-CQDs/TiO₂ composite under the same reaction conditions.

The N, S-CQDs/TiO₂ nanocomposite was also applied for synergistic photocatalytic reduction of Cr (VI) and degradation of erythromycin (ERY) from water under visible light irradiation. Because of the instant consumptions of photo-generated electrons and holes at conduction and valence bands, the composite exhibited improved Cr (VI) reduction efficiency in the binary Cr (VI)-ERY system compared to single Cr (VI) system, leading to complete reduction of Cr (VI) and 96.0% degradation of ERY with the increased initial concentration ($c_0 = 30.0$ mg/L for each and catalyst dosage being 1.0 g/L). Moreover, the composite also exhibited very high chemical stability, and less than 10% decrease in Cr (VI) reduction rate and ERY degradation efficiency were achieved

after four sequential runs. The results from radical trapping experiments proved that hole (h^+) and hydroxyl radical ($\bullet OH$) were the major active species for ERY degradation, whereas photo-generated electrons (e^-) reduced Cr (VI) to Cr (III). Results from this study reveals that sensitization of TiO_2 with CQDs is efficient in broadening the light absorption range of TiO_2 , expanding its application in visible-light-driven photocatalysis.

Acknowledgments

First and foremost, I would like to convey my heartfelt appreciation to my supervisors, Dr. Yan Zhang, for her constant encouragement and support throughout my Master's study. Dr. Yan Zhang unreservedly passing on to me her knowledge and skills required to carry out the research work and present the research outcomes.

I am grateful to Memorial University and the Natural Sciences and Engineering Research Council of Canada (NSERC) for providing the financial assistance of my research study.

I am incredibly grateful to my parents and my husband for their love, care, support, and sacrifice for my educating and daily life.

Finally, my thanks to all the people who have supported me to complete the research work directly or indirectly.

Table of Contents

ABSTRACT.....	I
ACKNOWLEDGMENTS	III
TABLE OF CONTENTS	IIIV
LIST OF TABLES	VIII
LIST OF FIGURES	IX
LIST OF ABBREVIATIONS AND SYMBOLS	X
CHAPTER 1. INTRODUCTION	1
1.1 BACKGROUND	1
1.2 RESEARCH OBJECTIVES	4
1.3 STRUCTURE OF THE THESIS	5
REFERENCES:	6
CHAPTER 2. LITERATURE REVIEW	9
2.1 CARBON QUANTUM DOTS AND THEIR APPLICATIONS IN PHOTOCATALYSIS	9
2.1.1 <i>Fabrication of carbon quantum dots</i>	9
2.1.2 <i>Functionalization of carbon quantum dots</i>	11
2.1.3 <i>CQDs as photocatalysts</i>	17
2.2 CQDs FOR ENHANCEMENT OF THE PHOTOCATALYTIC ACTIVITY OF TiO ₂	18
2.2.1 <i>CQDs as a photosensitizer to enhance the photocatalytic activity of TiO₂</i>	18

2.2.2 Preparation methods of CQDs/TiO ₂ composites.....	21
2.2.3 Characterisation methods of CQDs/TiO ₂ composites.....	24
2.3 APPLICATION OF CQDs/TiO ₂ COMPOSITES IN WASTEWATER TREATMENT	24
2.3.1 Photocatalytic reduction of heavy metal ions	24
2.3.2 Photocatalytic degradation of organic pollutants in water	28
2.4 INFLUENCES OF ENVIRONMENTAL CONDITIONS ON THE PHOTOCATALYTIC DEGRADATION/REDUCTION	34
2.4.1 Effect of pH	34
2.4.2 Effect of Catalyst Loading	35
2.4.3 initial concentration of contaminants	36
REFERENCES.....	37
CHAPTER 3. VISIBLE-LIGHT-DRIVEN PHOTOCATALYTIC REDUCTION OF CR (VI) BY CARBON QUANTUM DOTS-SENSITIZED TiO₂.....	49
3.1 INTRODUCTION	49
3.2 MATERIALS AND METHODS	51
3.2.1 Materials.....	51
3.2.2 Synthesis of N, S-CQDs	51
3.2.3 Preparation of the N, S-CQDs/TiO ₂ nanocomposites	52
3.2.4 Characterization.....	52
3.2.5 Reduction of Cr (VI) under visible light irradiation.....	53
3.3 RESULTS AND DISCUSSION	54
3.3.1 Characterization of N, S-CQDs and N, S-CQDs/TiO ₂	54
3.3.2 Photocatalytic study of N, S-CQDs/TiO ₂ composite	59

3.3.3	<i>Effect of pH on photocatalytic performance</i>	600
3.3.4	<i>Effect of initial concentration of Cr (VI)</i>	62
3.3.5	<i>Recyclability</i>	64
3.3.6	<i>Photocatalytic reduction mechanisms</i>	65
3.4	REDUCTION OF CR (VI) FROM REAL WATER SAMPLES	67
3.5	CONCLUSION	68
	REFERENCES	70
	CHAPTER 4. SYNERGISTIC PHOTOCATALYTIC REDUCTION OF CR (VI) AND ERYTHROMYCIN DEGRADATION BY CARBON QUANTUM DOTS-SENSITIZED TiO₂ UNDER VISIBLE-LIGHT IRRADIATION	75
4.1	INTRODUCTION	75
4.2	MATERIALS AND METHODS	78
4.2.1	<i>Materials, synthesis and characterization of N, S-CQDs/TiO₂</i>	78
4.2.2	<i>Synergistic photocatalytic reduction of Cr (VI) and ERY degradation</i>	79
4.3	RESULTS AND DISCUSSION	80
4.3.1	<i>Characterization</i>	800
4.3.2	<i>Photocatalytic study of N, S-CQDs/TiO₂ nanocomposite</i>	81
4.3.3	<i>Effect of initial concentrations of Cr (VI) and ERY</i>	82
4.3.4	<i>Radicals trapping experiments</i>	85
4.3.5	<i>Photocatalytic mechanisms</i>	87
4.3.6	<i>Recyclability</i>	88
4.4	CONCLUSION	89
	REFERENCES	90

CHAPTER 5. CONCLUSIONS AND RECOMMENDATION	94
5.1 CONCLUSIONS	94
5.2 RECOMMENDATIONS FOR FUTURE WORK.....	95
APPENDIX A: THE CALIBRATION CURVE FOR CR (VI) UV-VIS DETERMINATION.....	98

List of Tables

Table 2.1	Methods of synthesis and performance parameters for heteroatoms-doped CQDs....	16
Table 2.2	Various methods for the preparation of CQDs/TiO ₂ nanocomposites.....	23
Table 3.1	Reduction rate constants of Cr (VI) at different pH by N, S-CQDs/TiO ₂ under visible light irradiation.....	62
Table 3.2	Reduction rate constants of Cr (VI) at different initial concentration of Cr (VI) by N, S-CQDs/TiO ₂ under visible light irradiation.	62
Table 4. 1	The 1 st order rate constants of Cr (VI) reduction and ERY degradation at different initial concentrations by N, S-CQDs/TiO ₂ under visible light irradiation	85
Table 4. 2	The 2 nd order rate constants of Cr (VI) reduction and ERY degradation at different initial concentrations by N, S-CQDs/TiO ₂ under visible light irradiation.....	85

List of Figures

Figure 2.1	The electronic energy band diagram for a semiconductor [61].	20
Figure 2.2	First-order kinetic profiles (a) and reduction rate constants (b) of Cr (VI) via indicated catalysts under visible light.	26
Figure 2.3	A putative mechanism of photocatalytic Cr (VI) reduction over N, S-CQDs/TiO ₂ nanocomposites.	28
Figure 2.4	A basic photo-catalytic mechanism in photocatalytic degradation of organic pollutants by CQDs/TiO ₂ composites.	30
Figure 2.5	UV-Vis DRS (a), Tauc's plots for the band gap values (b), photocatalytic activity (c), and reusability (d) of CQDs/TiO ₂ composites. (Reproduced with permission from [108])	31
Figure 2.6	(a) Effect of initial concentration of cefradine on the photocatalytic activities of CQDs/TiO ₂ composite (inset: degradation rates versus concentration of cefradine); (b) effect of amount of CQDs/TiO ₂ composite on its photocatalytic activities (inset: plots of degradation rates versus concentration of CQDs/TiO ₂ composite); (c) effect of pH of reaction solution on the photocatalytic activities of CQDs/TiO ₂ composite (inset: plots of degradation rates versus pH); (d) the changes of pH value before and after reaction during the reaction solution with different initial pH value; (e) effect of foreign inorganic ions on the photocatalytic activities of CQDs/TiO ₂ composite under the visible irradiation, respectively; [115]	34
Figure 3. 1	HRTEM (a), high resolution XPS spectra of C 1s (b), N1s (c), O 1s(d) and S 2p (e), FT-IR spectrum (f), UV-vis absorption (g), and PL emission spectra (h) of N, S-CQDs.	56
Figure 3. 2.	Powder XRD (a), diffuse reflectance UV/Vis spectra (b), Tauc plot (c), and valence band XPS spectra of N, S-CQDs/TiO ₂ .	58
Figure 3. 3.	Photocatalytic reduction of Cr (VI) over N, S-CQDs/TiO ₂ prepared from 4% N, S-CQDs solution) (a); efficiency of photoreduction of Cr (VI) by N, S-CQDs/TiO ₂ composites prepared from different weight percentages of N, S-CQDS solutions .	59
Figure 3. 4.	Photocatalytic degradation of Cr (VI) at different pH values by N, S-CQDs/TiO ₂ under visible light irradiation (a), first-order (b) and second order (c) reduction	

kinetics of Cr (VI) at different pH values. Reaction condition: Cr (VI) concentration = 20.0 mg/L, catalyst dosage = 1.0 g/L.	611
Figure 3. 5. Photocatalytic degradation of Cr (VI) at different initial concentration by N, S-CQDs/TiO ₂ under visible irradiation (a), first order (b) and second order (c) reduction kinetics of Cr(VI) at different initial concentration	63
Figure 3. 6. Reusability of N, S-CQDs/TiO ₂ nanocomposites toward degradation of Cr (VI) for four reaction cycles.....	644
Figure 3. 7. Schematic diagram of photocatalytic reduction of Cr (VI) by N, S-CQDs/TiO ₂ composite	66
Figure 3. 8. High resolution XPS spectra and deconvoluted BE peaks of Ti 2p, and O 1s before and after photocatalytic reduction of Cr (VI)	666
Figure 3. 9. Photocatalytic degradation of Cr (VI) from surface wastewater by N, S-CQDs/TiO ₂ with different initial concentration of Cr (VI).....	688
Figure 4. 1. The chemical structure of erythromycin.....	788
Figure 4. 2. XPS survey spectrum of N, S-CQDs/TiO ₂	800
Figure 4. 3. Photocatalytic reduction of Cr (VI) (a) and ERY degradation (b) over TiO ₂ and N, S-CQDs/TiO ₂	822
Figure 4. 4. Photocatalytic reduction of Cr (VI) (a, b & c) and ERY degradation (d, e & f) by N, S-CQDs/TiO ₂ at different initial concentrations.....	84
Figure 4. 5. ERY degradation in the presence of different radicals' scavengers.	86
Figure 4. 6. Photocatalytic mechanism of synergic Cr (VI) reduction and ERY degradation by N, S-CQDs/TiO ₂	888
Figure 4. 7. Reusability of N, S-CQDs/TiO ₂ nanocomposite for (a) ERY degradation, and (b) reduction of Cr (VI) with four reaction cycles.....	899

List of Abbreviations and Symbols

A	The absorbance measured at excited wavelength
A _C	The absorbance of carbon dots
Abs	The absorption spectra
CQDs	Carbon quantum dots
E _x	The excitation spectra
E _m	The emission spectra
FTIR	Fourier-transform infrared spectroscopy
N, S-CQDs	Nitrogen, sulphur-doped carbon quantum dots
PL	Photoluminescence
XPS	X-ray Photoelectron spectroscopy
DPC	Diphenylcarbazine
ERY	Erythromycin
TEM	Transmission electron microscopy
CB	Conduction band
VB	Valence band
XRD	X-ray diffraction
UV-Vis	Ultraviolet-visible spectroscopy
λ _{ex}	The excitation wavelength

Chapter 1. Introduction

1.1 Background

Water is one of the most important natural resources on the planet. Water can dissolve more substances than any other liquid on earth, it is thus vulnerable to pollution. Numerous organic or inorganic pollutants have been identified as severe toxicants capable of negatively impacting ecosystem and human health [1, 2]. Among these, heavy metal ions and persistent organic pollutants (POPs) are of particular concern due to their high toxicity, long persistence, bioaccumulation, and biomagnification [3, 4]. Removal of toxic heavy metals and POPs from water and/or wastewater is an imperative and a serious challenge to industries and human life. Although adsorption, electro dialysis, and membrane filtration have long been used to remove heavy metals and POPs from wastewater, re-release of these toxic pollutants is typically involved during the regeneration of the used adsorbents and membranes [5, 6]. Heterogeneous photocatalysis plays an important role in converting toxic heavy metals and POPs into less toxic compounds or completely mineralizing them into carbon dioxide and water, and thus is considered as one of the most effective water treatment techniques [7, 8].

TiO₂ is the most widely used photocatalyst because of its photostability, nontoxicity, low cost, and stability in water under most environmental conditions [9]. However, TiO₂ is an intrinsic wide band gap (3.07–3.2 eV) semiconductor and therefore limited by its absorption of UV light which covers only ~5% of the solar spectrum [10, 11]. To overcome this limitation, doping nanoclusters that absorb visible light onto TiO₂ has recently been employed to broaden the light absorption to visible-light and infrared regions, and to extend the application of TiO₂-based catalysts in wastewater treatment [12].

Carbon quantum dots (CQDs), a new family of carbonaceous nanomaterials (CNMs), have attracted great attention since their discovery in 2004 by virtue of their outstanding optical properties, photo-stability, low toxicity, and low cost [13]. The incorporation of CQDs into TiO₂ has been proved to extend the adsorption spectrum to the visible light region, and the CQDs sensitized TiO₂ composites have been applied to the photodegradation of dyes and phenols, water splitting, and CO₂ conversion [14-16]. Nonetheless, research explorations on utilizing CQDs-sensitized TiO₂ for heavy metal reduction were scarcely reported.

CQDs are amorphous quasi-spherical (0D) carbon nanoparticles made up of carbon, oxygen, hydrogen and nitrogen with particle size less than 10 nm [17]. CQDs typically exhibit two absorption bands that correspond to the π - π^* and n - π^* transitions in C=C and C=O/C=N bonds, respectively [18]. Their fluorescence stems from the band gap transitions from the conjugated π -domain or the surface defects [19]. Most CQDs contain carboxylic acid moieties at their surfaces, leading to excellent aqueous solubility and suitability for subsequent functionalization with various organic, polymeric, inorganic, or biological species [20]. CQDs are chemically stable, water soluble, and non-toxic, making them extremely suitable in photocatalytic wastewater treatment [21].

However, neither CQDs powder nor CQD solutions are suitable to be used as photocatalyst because CQDs cannot be reused when they dissolve in water solutions. To improve the reusability and practical application performance, CQDs have to be deposited on solid matrices, such as TiO₂, Al₂O₃, Fe₂O₃, etc. Generally, CQDs incorporated TiO₂ (CQDs/TiO₂) composites can be fabricated by either one-pot (*in situ*) synthesis or multi-step hybridization route [22, 23]. In one-pot synthesis, all the starting materials are mixed for hydro-/solvothermal treatment [24, 25]. CQDs/TiO₂ composites prepared by one-pot synthesis are very stable and able to promote charge separation at their interfaces. More often, CQDs/TiO₂ composites are prepared by multi-step hybridization

process, in which the pre-made CQDs are combined with TiO₂ matrix by either physical mixing or chemical bonding [22]. Although facile and rapid, the interaction between CQDs and TiO₂ by physical mixing is generally weak and unstable, limiting the charge separation and transfer at their interfaces [26]. The construction of CQDs/TiO₂ composites by chemical bonding via hydrothermal deposition or calcination method is mainly through the formation of a covalent (Ti–O–C) bond between TiO₂ and –OH group on the CQDs surface [27, 28]. Obviously, multi-step hybridization provides more flexibility in tuning the surface properties of CQDs, leading to the enhanced photocatalytic performance of the composites.

The CQDs/TiO₂ composites demonstrate the common features of narrow band gap, enhanced absorption of visible light, and prolonged lifetime of excited electrons and holes, which significantly improve the photocatalytic performance in degrading various water pollutants [29, 30]. Different mechanisms have been proposed to explain the enhanced photocatalytic properties of CQDs/TiO₂ composites. Firstly, CQDs can absorb visible or near infrared (NIR) light due to the presence of various functional groups (–COOH, –OH, –NH₂, etc.) on the outer layer of CQDs and the molecular fluorophores generated in most CQDs synthetic protocols [31]. Incorporation of CQDs into TiO₂ makes the resultant composites capable of absorbing visible or NIR light due to the electronic coupling between the π states of graphite essential CQDs and the CB states of TiO₂ [21]. Such electronic coupling induces a narrower bandgap energy compared to pure TiO₂ and bring about a red shift of the composites. Moreover, CQDs can also act as electron scavengers and improve the carrier separation by retarding the recombination of photo-excited electrons and holes at the junction interface [21].

So far, CQDs/TiO₂ composites have not been widely applied as visible-light-active photocatalysts to photodegradation of POPs and reduction of heavy metal ions. The synthetic conditions and the

proper CQDs loading that result in the best optical properties and the optimum photocatalytic activities of CQDs/TiO₂ needs to be further studied. The effects of the environmental conditions, such as temperature, solution pH, initial concentration of the pollutants on the photocatalytic degradation efficiency should be investigated. The efficiency and photocatalytic degradation mechanisms of this new class of photocatalysts deserve additional attention and comprehensive study.

1.2 Research Objectives

To address the research gaps, the current study is focused on the development of a novel nitrogen and sulfur co-doped CQDs/TiO₂ composite (N, S-CQDs/TiO₂) as a visible-light-active photocatalyst for the degradation of toxic heavy metal ions and antibiotics from polluted water. By incorporating N, S-CQDs into TiO₂, the resultant composite is anticipated to have a narrower bandgap and extended light absorption range. This study is a new attempt in simultaneous reduction of heavy metal ions and degradation of antibiotics by photocatalysis and helps generate new knowledge and cost-effective technologies in wastewater treatment.

This study entails the following tasks: 1) preparation of nitrogen and sulfur co-doped CQDs (N, S-CQDs) from citric acid and thiourea using hydrothermal method; 2) preparation of N, S-CQDs sensitized TiO₂ (N, S-CQDs/TiO₂) composite; 3) photocatalytic application of N, S-CQDs/TiO₂ for Cr (VI) reduction under visible light irradiation; 4) synergistic photocatalytic reduction of Cr (VI) and degradation of erythromycin by N, S-CQDs/TiO₂ under visible light irradiation; and 5) clarification of the mechanisms for photocatalytic reduction of Cr (VI) and degradation of erythromycin by the N, S-CQDs/TiO₂ composite.

1.3 Structure of the Thesis

This thesis includes five chapters. A brief introduction on the research scope and objectives is presented in Chapter 1, which is followed by a thorough literature review on the relevant research topics. Chapter 3 focuses on the preparation and the characterization of N, S-CQDs and N, S-CQDs/TiO₂ composite as well as the application of N, S-CQDs/TiO₂ as a visible-light-active photocatalyst for the photocatalytic reduction of Cr (VI). Chapter 4 presents the application of N, S-CQDs/TiO₂ to synergistic photocatalytic reduction of Cr (VI) and degradation of erythromycin under visible light irradiation. The major conclusions drawn from this study and recommendations for future works are summarized in Chapter 5.

References

- [1] M. Engel, B. Chefetz, Removal of triazine-based pollutants from water by carbon nanotubes: Impact of dissolved organic matter (DOM) and solution chemistry, *Water Res.*, 106 (2016), 146-154.
- [2] A. Yadav, A. Raj, D. Purchase, L. F. R. Ferreira, G. D. Saratale, and R. N. Bharagava, Phytotoxicity, cytotoxicity and genotoxicity evaluation of organic and inorganic pollutants rich tannery wastewater from a Common Effluent Treatment Plant (CETP) in Unnao district, India using *Vigna radiata* and *Allium cepa*, *Chemosphere*, 224 (2019), 324–332.
- [3] M. Balali-Mood, K. Naseri, Z. Tahergorabi, M.R. Khazdair, M. Sadeghi, Toxic mechanisms of five heavy metals: mercury, lead, chromium, cadmium, and arsenic, *Front. Pharmacol.* 12 (2021), 643972.
- [4] J. O. Tijani, O. O. Fatoba, G. Madzivire, L. F. Petrik, A review of combined advanced oxidation technologies for the removal of organic pollutants from water, *Water Air Soil Poll.*, 225 (2014), 2102.
- [5] X. Gao, M. Li, Y. Zhao, Y. Zhang, Mechanistic study of selective adsorption of Hg^{2+} ion by porous alginate beads, *Chem. Eng. J.* 378 (2019), 122096.
- [6] R. Li, D. Hu, K. Hu, H. Deng, M. Zhang, A. Wang, R. Qiu, K. Yan, Coupling adsorption-photocatalytic reduction of Cr (VI) by metal-free N-doped carbon, *Sci. Total Environ.* 704 (2020), 135284.
- [7] S.G. Kumar, L.G. Devi, Review on modified TiO_2 photocatalysis under UV/visible light: Selected results and related mechanisms on interfacial charge carrier transfer dynamics, *J. Phys. Chem. A* 115 (2011), 13211–13241.
- [8] S.N. Ahmed, W. Haider, Heterogeneous photocatalysis and its potential applications in water and wastewater treatment: a review, *Nanotechnology* 29 (2018), 342001.
- [9] X. Chen, S. S. Mao, Titanium Dioxide Nanomaterials: Synthesis, Properties, Modifications, and Applications, *Chem. Rev.*, 107 (2007), 2891–2959.
- [10] D. Kanakaraju, B.D. Glass, M. Oelgemöller, Titanium dioxide photocatalysis for pharmaceutical wastewater treatment, *Environ. Chem. Lett.* 12 (2014), 27–47.
- [11] M. Pelaez, N.T. Nolan, S.C. Pillai, M.K. Seery, P. Falaras, A.G. Kontos, P.S.M. Dunlop, J.W.J. Hamilton, J.A. Byrne, K. O’Shea, M.H. Entezari, D.D. Dionysiou, A review on the visible light active titanium dioxide photocatalysts for environmental applications, *Appl. Catal. B: Environ.* 125 (2012), 331–349.

- [12] J. Tian, Z. Zhao, A. Kumar, R.I. Boughton, H. Liu, Recent progress in design, synthesis, and applications of one-dimensional TiO₂ nanostructured surface heterostructures: a review, *Chem. Soc. Rev.* 43(2014), 6920–6937.
- [13] J. Zhou, C. Booker, X. Zhou, T. Sham, X. Sun, Z. Ding, An electrochemical avenue to blue luminescent nanocrystals from multiwalled carbon nanotubes (MWCNTs), *J. Am. Chem. Soc.*, 129 (2007), 744–745.
- [14] H. Yu, R. Shi, Y. Zhao, G.I.N. Waterhouse, L.-Z. Wu, C.-H. Tung, T. Zhang, Smart utilization of carbon dots in semiconductor photocatalysis, *Adv. Mater.* 28 (2016), 9454–9477.
- [15] A. Ansón-Casaos, J. Hernández-Ferrer, L. Vallan, H. Xie, M. Lira-Cantú, A.M. Benito, W.K. Maser, Functionalized carbon dots on TiO₂ for perovskite photovoltaics and stable photoanodes for water splitting, *Int. J. Hydrog. Energy* 46 (2021), 12180–12191.
- [16] J. Yu, J. Jin, B. Cheng, M.J. Jaroniec, A noble metal-free reduced graphene oxide-CdS nanorod composite for the enhanced visible-light photocatalytic reduction of CO₂ to solar fuel, *Mater. Chem. A* 2 (2014), 3407–3416.
- [17] Y. Sun, B. Zhou, Y. Lin, W. Wang, K. Fernando, P. Pathak et al., Quantum-Sized Carbon Dots for Bright and Colorful Photoluminescence, *J. Am. Chem. Soc.*, 128 (2006), 7756–7757.
- [18] K. Jiang, S. Sun, L. Zhang, Y. Lu, A. Wu, C. Cai et al., Red, Green, and Blue Luminescence by Carbon Dots: Full-Color Emission Tuning and Multicolor Cellular Imaging, *Angew. Chem. Int. Ed.*, 54 (2015), 5360–5363.
- [19] K. A. S. Fernando, S. Sahu, Y. Liu, W. Lewis, E. Gulians, A. Jafariyan et al., Carbon Quantum Dots and Applications in Photocatalytic Energy Conversion, *ACS Appl. Mater. Interfaces*, 7 (2015), 8363–8376.
- [20] H. Li, X. He, Z. Kang, H. Huang, Y. Liu, J. Liu et al., Water-Soluble Fluorescent Carbon Quantum Dots and Photocatalyst Design, *Angew. Chem. Int. Ed.*, 49 (2010), 4430–4434.
- [21] R. Wang, K. Lu, Z. Tang, Y. Xu, Recent progress in carbon quantum dots: synthesis, properties and applications in photocatalysis, *J. Mater. Chem. A*, 5 (2017), 3717–3734.
- [22] B.B. Chen, M.L. Liu, C.Z. Huang, Carbon dot-based composites for catalytic applications, *Green Chem.* 22(2020), 4034–4054.
- [23] K.-W. Chu, S.L. Lee, C.-J. Chang, L. Liu, Recent progress of carbon dot precursors and photocatalysis applications, *Polymers* 11(2019), 689.
- [24] W. Wang, Y. Ni, Z. Xu, One-step uniformly hybrid carbon quantum dots with high-reactive TiO₂ for photocatalytic application, *J. Alloy. Compd.* 622(2015), 303–308.

- [25] M. Rahbar, M. Mehrzad, M. Behpour, S. Mohammadi-Aghdam, M. Ashrafi, S, N co-doped carbon quantum dots/TiO₂ nanocomposite as highly efficient visible light photocatalyst, *Nanotechnology* 30 (2019), 505702.
- [26] Z. P. Zeng, F. X. Xiao, H. Phan, S. F. Chen, Z. Z. Yu, R. Wang, T. Q. Nguyen, T. T. Y. Tan, Unraveling the cooperative synergy of zero-dimensional graphene quantum dots and metal nanocrystals enabled by layer-by-layer assembly, *J. Mater. Chem. A* 6(2018), 1700–1713.
- [27] N.C.T. Martins, J. Ângelo, A.V. Girão, T. Trindade, L. Andrade, A. Mendes, N-doped carbon quantum dots/TiO₂ composite with improved photocatalytic activity, *Appl. Catal. B: Environ.* 193 (2016), 67–74.
- [28] G. Rajendera, J. Kumarb, P.K. Giri, Interfacial charge transfer in oxygen deficient TiO₂-graphene quantum dot hybrid and its influence on the enhanced visible light photocatalysis, *Appl. Catal. B: Environ.* 224 (2018), 960–972.
- [29] Y. Zhang, K. Hawboldt, L. Zhang, J. Lu, L. Chang, A. Dwyer, Carbonaceous nanomaterials-TiO₂ heterojunctions for visible-light-driven photocatalytic degradation of aqueous organic pollutants, *Appl. Catal. A-Gen.* 630 (2022), 118460.
- [30] H. Xu, S. Ouyang, L. Liu, P. Reunchan, N. Umezawa, J. Ye, Recent advances in TiO₂-based photocatalysis, *J. Mater. Chem. A*, 2 (2014), 12642–12661.
- [31] K. Akbar, E. Moretti, A. Vomiero, Carbon dots for photocatalytic degradation of aqueous pollutants: recent advancements, *Adv. Optical Mater.* 9(2021), 2100532

Chapter 2. Literature Review

Advanced oxidation processes mediated by semiconductor photocatalyst TiO_2 is recognized as one of the most efficient solutions for reducing contaminants in water [1]. However, low activity under visible light and recombination of photogenerated electron and hole pairs make semiconductor photocatalysts unsuitable for large-scale water filtration. Carbon quantum dots (CQDs) are used to modify semiconductor photocatalysts to improve the photocatalytic performance. CQDs are an intriguing type of carbon nanoparticles with a diameter less than 10 nanometers [1, 2]. Low toxicity, chemical inertness, great biocompatibility, photo-induced electron transfer, and highly tunable photoluminescence behavior are all characteristics of CQDs. The excellent optical property and narrow band gap make CQDs good candidate as photosensitizers of TiO_2 . The photogenerated electrons and holes generated by the composite catalyst of CQDs/ TiO_2 can be separated between the two semiconductors (TiO_2 and CQDs) effectively through effective internal charge transfer, thus improving the photocatalytic performance of the catalyst. The physical and chemical features of CQDs, the raw materials and methods utilized in CQDs/ TiO_2 manufacture, and their prospective applications in wastewater treatment will all be reviewed in this chapter.

2.1 Carbon quantum dots and their applications in photocatalysis

2.1.1 Fabrication of carbon quantum dots

Carbon quantum dots (CQDs) are fluorescent nanomaterials with highly controllable photoluminescent and optoelectronic capabilities due to their strong quantum confinement effect [3]. CQDs are an intriguing type of carbon nanoparticles made up primarily of carbon nanoparticles. CQDs' surface structures and particle sizes have been altered by oxygenated-functional groups on

their surfaces, resulting in quantum confinement effects [4]. Aside from that, photo-generated electrons can be separated using electron transfers and CQD reservoir features [5].

According to previous studies, CQDs have been fabricated from various sources, such as natural carbon sources [6, 7], food wastes [8], grass [9], and waste biomass [10]. However, just a few studies have looked into how to produce CQDs from waste biomass. In future investigations, the fundamental material can be replaced with sustainable materials with a comparable chemical structure to achieve near-zero waste discharge [3]. CQDs are typically generated by surface-functionalizing organic or inorganic compounds by carbonising and oxidising source materials [11]. Using green carbon sources or waste organic materials to make CQDs has a number of advantages, including cost-effectiveness, environmental friendliness, and widespread availability in nature [12]. Furthermore, due to their high quantum effects and self-passivation of precursors, the production of CQDs using natural carbon sources without acidic or chemical exposure could be actively promoted [13].

The synthetic methods of CQDs can be divided into two categories: top-down and bottom-up [14]. The former creates CQDs by chemically, electrochemically, or physically cracking or shattering carbonaceous material. The heteroatoms in the carbonaceous material have previously been doped or are being doped throughout the process. In contrast, the bottom-up methods mainly involve pyrolysis, electrochemical carbonization, hydrothermal/solvothermal treatment, microwave radiation, and so on [14, 15]. The top-down method has the benefits of low-cost raw materials, mass production, and ease of use [16]. However, this method requires costly experimental equipment and a nonselective chemical cutting process that makes it impossible to precisely control the shape or size of the output. Bottom-up approaches, such as hydrothermal carbonization, microwave radiation, and electrochemical carbonization, provide substantial advantages in

controlling the molecular weight and form of carbon dots [17, 18]. However, bottom-up methods also have some drawbacks like complex synthesis processes and a strong tendency for aggregation. Luckily, surfactants or co-surfactants can be added to the solution to avoid aggregation [14].

2.1.2 Functionalization of carbon quantum dots

Heteroatom doping and surface passivation are two efficient approaches to the functionalization of CQDs. Heteroatom (B, N, P, and S) doping is a simple and effective method of improving the luminous characteristics of CQDs [9, 17]. Doped CQDs with highly electronegative atoms (e.g., N and S) produce blue-shifted PL emissions, while those doped with low electronegativity atoms (e.g., P, B) produce red-shifted PL emissions [19]. The size and structure of N and C atoms are comparable, and they both have five valence electrons that can interact with other C atoms. By giving a high number of reactive groups ($-\text{OH}$, $-\text{COOH}$, $-\text{N}=\text{C}-$, $-\text{CN}$, and $-\text{NH}_2$), N-doping raises the surface-state defects of CQDs and improves their electrical characteristics and surface chemical reactivity [19, 20, 21]. The fluorescence quantum yield (QY) of CQDs is increased as a result of these reactive groups. For example, Aghamali et al. [23] synthesized N-doped CQDs in which a one-step hydrothermal process was used to produce CQDs and surface passivation simultaneously. Surprisingly, up to 95% of the as-prepared N-CQDs showed an extremely high QY, which is the highest QY that CQDs have achieved so far. The prominent light-harvesting ability and high capacitance of N-CQDs demonstrate the excellent degradation efficiency of methylene blue [24].

Compared to N-CQDs, S-CQDs have been less studied because C-S bonds are harder to form, making them more challenging to synthesize than N-CQDs. In addition, S has a larger atomic radius than C, and the C-S bond is 25 % longer than the C-C bond. However, the mismatch between the outermost S and C orbitals results in an uneven distribution of the spin density,

conferring surface reactivity and catalytic capabilities to S-CQDs. The chemical characteristics of CQDs are altered by S-doping [24, 25]. For instance, Dai et al. firstly used thioacetic as the carbon and sulfur source to synthesis S-CQDs. The S-CQDs showed good optical characteristics and a uniform shape by TEM and PL [27]. S-CQDs are attractive candidates for catalytic applications because of their exceptional electrical characteristics and surface chemical activity.

In P-CQDs, the separated sp^2 carbon clusters and defect sites coexist [20]. P increases the photoelectric characteristics of the CQDs by acting as an n-type donor, and P-doping can alter the electrical characteristics of CQDs while also producing a large number of active sites [20]. An electrochemical method is used to make phosphorus-doped graphene quantum dots with a high phosphorus doping percentage ($>7\%$). The results showed that in both hydroxyl radicals ($\cdot\text{OH}$) and 2,2-diphenyl-1-picrylhydrazyl (DPPH) radical scavenging, the P in the P-GQDs played a key role [28].

Based on the previous studies, N, P, and S are n-type dopants that can boost CQD electron concentration. B-doping, on the other hand, can change the optical characteristics of CQDs by creating a high number of active sites [19, 28]. Different boron precursor compounds were investigated by Jana et al. Boron absorption in CQDs has been clearly demonstrated to vary with different boron precursors producing changed emissive CQDs [30]. Shen et al. [31] hydrothermally treated Ethylenediamine and boric acid under $260\text{ }^\circ\text{C}$ for 12h to produce B-CQDs with green color and small size of 1-6 nm. The results showed that the only way to make solid-state luminous CQDs is to combine BA and EDA in a hydrothermal reaction, which could be due to the B element being introduced. This is mainly because (1) the electron-deficient B atom could prevent intermolecular charge transfer among CQDs, which is caused by electron donors and acceptors interacting, thus reducing aggregation-induced quenching. (2) The H-bond interactions

created by the surface B–OH groups could give agminated nanodots a dispersive state comparable to that found in liquid environments. (3) The CQDs' zeta potential is around 25 mV due to the abundance of negative electricity functional groups, and the high electrostatic repulsions among the carbon dots may prevent them from aggregating excessively [31].

In addition to the elements mentioned above, some other elements like Florine (F), Si, and I. Florine is usually used in medicine because it could improve selectivity between drugs and receptors. F-doping can affect the chemical, structural, and electronic characteristics of CQDs, thus increasing their fluorescence and magnetic and biological capabilities [32]. As a result, F-CQDs have considerable potential in medical applications [33]. Si has sp^3 -like bonding which could change the electronic and structural properties of CQDs [34]. I, on the other hand, could be applied to disease diagnosis. Su et al. prepared iodine-doped carbon quantum dots (I-CQDs) using the hydrothermal method. The results demonstrate that HCC827 cells fluoressed brightly, implying that cetuximab-conjugated I-CQDs might specifically target cancer cells with EGFR overexpression via EGFR-mediated endocytosis [35].

CQD doping allows for the creation of new energy states resulting from distinct electronic configurations of doped atoms, hence improving physic-chemical and catalytic characteristics [36]. Sulfur, phosphorus, or boron co-doped CQDs Sulfur, phosphorus, and boron-doped CQDs have great biocompatibility and minimal toxicity, making them ideal for detecting ions in human blood and multicolor cell imaging. N, S co-coped CQDs, for example, S and N, are both made up of lone pair electrons, and they can work together to give electrons, accelerate radiation recombination, and boost the fluorescence QY of CQDs, giving them new features [37]. Dong et al. synthesized carbon-based dots co-doped with nitrogen and sulfur through a facile bottom-up method using citric acid and L- cysteine as a precursor. The inserted Sulphur atoms appear to be able to erase

the O-states and augment the N-state in the N, S-CQDs, resulting in the original surface states being almost ignored. As a result, the N, S-CQDs have a high fluorescence QY and emit excitation independently [37]. CQDs emit blue light under UV radiation and absorb low visible light in normal conditions. To make CQDs with green fluorescence, N, a popular doping element, is employed as a co-dopant with P. The flaws caused by P and N co-doping around the Fermi level cause this green emission [38]. Compared to N, S/P-CQDs, N and B not only efficiently dope the skeleton of CQDs, but also produce functional groups such as $-\text{COOH}$, $-\text{CONH}$, $-\text{OH}$, and boric acid on their surface, according to some researchers [39, 40]. Because of the intricate procedures and reaction conditions needed, multi-doping has not been frequently reported in comparison to dual-atom co-doping CQDs. In addition, the three atom-doped CQDs' rich functional groups on the surface involve many excited states, among which the excited electrons in CQDs undergo inter-state conversion and radiative recombination, resulting in a variety of fluorescence emissions at different wavelengths [14]. For example, N, P, S co-doped graphene quantum dots (NPS-GQDs) were made using anthracite coal as the raw material in a one-step wet chemical plus dialysis approach by Xu et al [41]. During XPS detection, local doping of N, P, and S on GQDs can reach high levels of 5.6 %, 3.7 %, and 3.7 % (by atomic), respectively. Excitation-dependent fluorescence and quench by trace metals were both good features of the produced N,P,S-GQDs. Huang et al. [42] prepared an N,S,B-CQD via one-step hydrothermal synthesis by using 2,5-diaminobenzenesulfonic acid and 3-aminobenzenboronic acid. The optical characteristics of such N,B,S-CDs were outstanding, with a comparatively high absolute fluorescence QY (11.6 %). In particular, red emission exhibits great absorption under visible light that could be used in many fields. Increasing evidence suggests that modifying the surface functional groups or defects of

CQDs has a significant impact on the fluorescence emissions measured. The different methods of synthesis and performance parameters for heteroatom-doped CQDs are shown in Table 2.1.

Surface passivation is a technique for increasing the endurance and photostability of CQDs by forming a thin insulating layer on an acid-treated CQD surface. That is because CQD surfaces are extremely sensitive to contaminants in their environment, and even small amounts of pollutants can have a significant impact on their properties. Non-emissive polymers such as ethylenediamine, polyethyleneimine (PEI), poly (ethylenimine)-co-poly (ethylene glycol)-co-poly (ethyl-enimide) (PPEI), and 4,7,10-trioxa-1,13-tridecanediamine are common passivation agents. Niu et al. [43] used ethylenediamine as a surface passivation agent to synthesize the passivated CQDs. Because of the esterification process between the cis-diols group in dihydro-nicotinamide adenine dinucleotide (NADH) and the carboxyl group on the surface of N-CQDs, a simple, green, extremely sensitive, and selective fluorescence sensor for NADH was developed. Hasanzadeh et al. [44] synthesized CQDs with poly-l-lysine (PLL) as a passivation agent. The results show that under physiological settings, the CQD/PLL core-shell NPs demonstrated robust photoluminescence in both solid and aqueous forms, as well as high cellular uptake in HEK-293T cells.

Table 2.1 Methods of synthesis and performance parameters for heteroatom doped CQDs.

Heteroatoms	Precursors	Synthetic methods	Particle size, nm	PL color	QY	Ref.
N	Citric acid & ethylenediamine	Hydrothermal treatment	2-6 nm	blue	80%	[45]
N	Acetylacetone and $\text{NH}_3 \cdot \text{H}_2\text{O}$	Microwave synthesis	< 4 nm	blue	51.61%	[46]
S	Thioacetic acid	Hydrothermal treatment	3.8-7.4 nm	blue		[27]
P	Sodium pyruvate	Electrochemical synthesis	~4 nm	green		[28]
B	Phosphorous tribromide and hydroquinone silicon	Solvent thermal method	< 6 nm	green	7 %	[30]
F	fluorinated graphite & Fluorine	Microwave-assisted method	6 nm	blue	57.7%	[33]
Si	SiCl_4 & hydroquinone	Solvothermal treatment	5-9 nm	blue	19.2%	[34]
I	Citric acid & iohexol	Hydrothermal method	3.7 nm	blue	18 %	[35]
N, S	Citric acid and L-cysteine	Hydrothermal method	< 10 nm	blue	70 %	[37]
N, P	Glucose & ethylenediamine & phosphoric	Microwave assisted method	2-5 nm	green		[47]
N, B	Boric acid & urea & citric acid	Microwave assisted method	20 nm	blue		[48]
N, S, P	Anthracite coal concentrated sulphury acid and nitric acid	Wet chemical plus dialysis	1-7 nm	blue		[41]
N, S, B	2,5-diaminobenzenesulfonic acid & 3-aminobenzeneboronic acid	Hydrothermal method	2.84 nm	red	11.6%	[42]

2.1.3 CQDs as photocatalysts

CQDs have a high sensitivity to visible light, which can improve photocatalytic efficiency because they can convert the spectrum of sunlight to the required wavelength for photocatalysis [49]. The nanoscale properties of CQDs, which can boost the oxidation reaction during photo-catalysis, can explain the improvement in photocatalytic activity [50]. CQDs also has excellent performance in trapping and transferring electrons [24]. The size-dependent optical features of CQDs, in which the distance between charge carriers is short and generally less than the carrier diffusion length, contribute to improved charge transport. CQDs' edge-abundant properties are particularly advantageous for photo-catalysis, as this oxidation reaction happens more frequently at the edges than at the basal planes [51]. According to Hu et al. [52], the presence of O and Cl radicals resulted in low photocatalytic activity. However, the presence of O and N radicals in CQDs resulted in high photocatalytic activity. This is due to the O, N, and Cl causing varying degrees and directions of energy-band bending from the inner region to the surface of the CQDs. The presence of upward and downward band bending in the CQDs, generated by the O and Cl radicals, respectively, created an internal electronic field that aided carrier migration and electron–hole pair separation. The photocatalytic activity of the CQDs was improved as a result of this [52]. Accordingly, CQDs are promising photocatalytic candidates for the breakdown of contaminants.

Although significant progress has been achieved in this field over the last decade, there are still a number of concerns that need to be investigated further. First of all, photogenerated electrons and holes are easy to recombine on the surface of carbon quantum dots, which show considerable absorption in the ultraviolet light region and weak absorption in the visible light region. Therefore, in order to improve these shortcomings, combined carbon quantum dots

were combined with several other lightweight heteroatoms, which not only improved the absorption in the visible light region but also promoted the transfer speed of electrons and holes. The redox conversion efficiency is significantly improved. Another consideration is if carbon quantum dots alone are used as photocatalysts, the catalytic efficiency is relatively low. Carbon quantum dot composite catalysts have become popular as a result of this. Because of its low cost, great chemical stability, and ability to use sunlight, the semiconductor catalyst TiO_2 is appealing.

2.2 CQDs for enhancement of the photocatalytic activity of TiO_2

2.2.1 CQDs as a photosensitizer to enhance the photocatalytic activity of TiO_2

Semiconducting materials are crucial in the electronics industry and in environmental remediation because they can generate charge carriers when activated with a particular amount of energy [58]. Some semiconductors have been used as photocatalysts due to a good combination of electronic structure, light absorption qualities, charge transport characteristics, and stimulated lifetimes. Many binary compounds that consist of precisely two elements are classed as semiconductors; however, not all are suitable for photocatalytic applications. Silicon and gallium arsenides, for example, have been discovered to have considerable practical promise; however, due to a lack of chemical stability, they are not ideal for photocatalytic applications. As a result, a semiconductor suitable for heterogeneous photocatalysis must have the following properties: a suitable band gap (in the range of 1.7–3.2 eV), efficient light absorption, high carrier mobility, and precise band edge positions that straddle the water redox potentials, nontoxic and chemically stable. Titanium dioxide (TiO_2) in anatase form and zinc oxide (ZnO) in the wurtzite phase is the most used metal oxides as photocatalysts because of

their electronic band structure. Specifically, TiO_2 was utilized as a photo electrocatalyst to split water into hydrogen by Fujishima et al. in 1972 [59]. Since then, TiO_2 has been the subject of increased research.

A semiconductor has a band structure, which is roughly defined as a series of energetically closed-spaced energy levels associated with covalent bonding between atoms in the crystallite (the valence band) and the second series of spatially diffuse, energetically similar levels of higher energy associated with conduction in the macromolecular crystallite (the conduction band). The band gap is defined as the difference in energy between the conduction and valence bands [58]. The oxygen vacancies in TiO_2 , which should be spelled TiO_{2-x} , are compensated by adopting the 3+ oxidation state with an equivalent amount of titanium atoms. The Ti^{3+} ions operate as electron donors, making the material an n-type semiconductor. Additionally, the energy level at the top of the valence band E_{VB} corresponds to the energy that determines the oxidizing ability of holes in an electronic energy level diagram of a semiconductor as shown in Figure 2.1, and the energy level at the bottom of the conduction band corresponds to the energy that determines the oxidizing ability of electrons. The energy of electrons in reduction processes is E_{CB} . The energies of electrons in a solid are compared to the vacuum level, which is used as a point of reference for zero energy values [60]. Because of their propensity to form electron and hole pairs when exposed to light, semiconductors have been employed in the construction of electronic components and to solve environmental concerns.

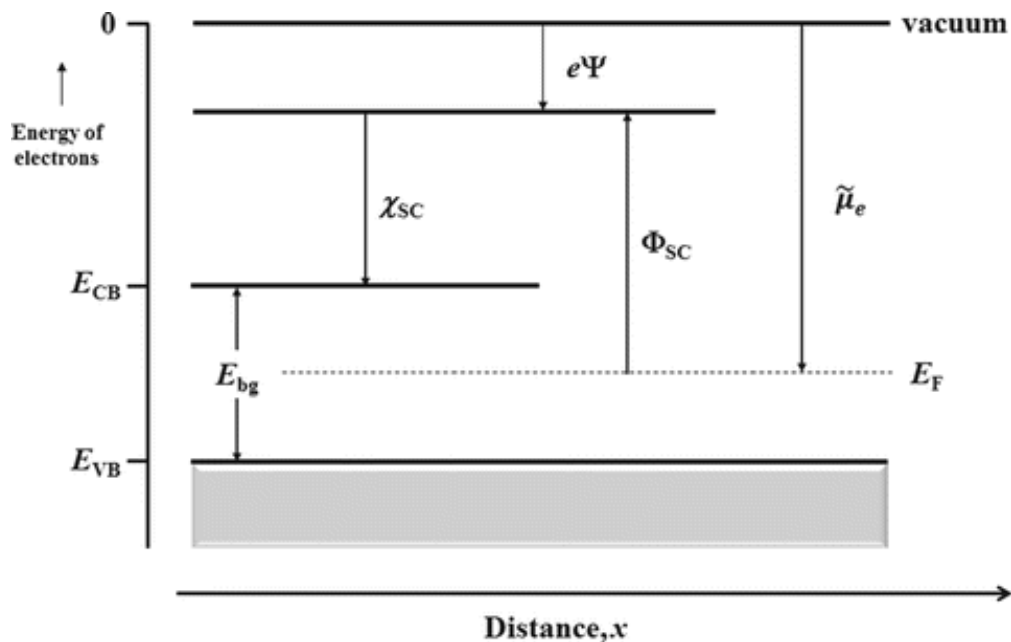


Figure 2.1 The electronic energy band diagram for a semiconductor [61].

However, the inefficient use of visible light as a source of irradiation is a major obstacle to its successful use, since less than 5% of sunlight is available or absorbed by undoped TiO₂ due to its large intrinsic band distance. This can be costly if it only relies on UV light [62]. At the same time, during TiO₂ migration via the majority to the surface, the recombination of charge carriers occurs rampantly in semiconductor particles, where photocatalytic reactions are initiated. The TiO₂'s low photocatalytic activity is the rapid recombination time of photo-generated charge carriers in the order of 10⁻⁹s, whereas TiO₂ and adsorbed pollutants have a chemical reaction time of 10⁻⁸-10⁻³s [63]. Thus, the two approaches to boost photocatalytic efficiency are to reduce the TiO₂ band gap and lower recombination rates for the photo-generated carriers [64, 65]. Combined with carbonaceous materials like CQDs, this is an effective method because of their conjugated π -domains, which makes them similar to polycyclic aromatic hydrocarbons [66] and confers unique photo-conversion and excellent electron transfer properties [67, 68]. Moreover, CQDs contain carboxylic acid moieties at their surfaces, resulting in excellent aqueous solubility and suitability for subsequent

functionalization with various organic, polymeric, inorganic, or biological species [69]. The power and tunable luminescence of carbonaceous materials also enhance their flexible properties fundamentally and technologically. Importantly, CQDs also satisfy the specifications for a fast migration of electric charge and effective surface redox reactions throughout photocatalytic reactions. Thus, in the design of a photocatalyst for wider light response and encouraged electron-hole separation, they can serve not only as an effective photocatalyst alone but also as a multifunctional constituent.

2.2.2 Preparation methods of CQDs/TiO₂ composites

Metallic semiconductors have been widely used in photocatalysis, which is critical for the creation of sustainable energy and the reduction of pollutants. Metallic semiconductors (such as TiO₂ and ZnO) have a tiny band gap; therefore, they are only active in UV light, which accounts for a small portion of total solar radiation reaching the Earth's surface. It has been demonstrated that doping nanoclusters on semiconductors extends the light absorption of these semiconductors to visible and infrared irradiations. However, despite the fact that CQDs can act as both electron donors and acceptors, making them a possible catalyst, there have been few investigations on employing CQDs as photocatalysts directly.

Photocatalysts can be made in a single pot or in a multi-step synthetic process [70, 71]. In the one-pot method, all the composite's raw components are combined before being processed further. Wang et al., for example, used a one-pot synthetic technique to make a hybrid CQDs/TiO₂ photocatalyst by hydrothermally treating a mixed solution of sodium citrate and hydrogen fluoride-containing Ti foil [72]. Under visible light, the CQDs/TiO₂ hybrid dramatically improves photocatalytic degradation of rhodamine B. Photocatalysts are most often manufactured in a multi-step procedure, either by incubating CQDs or separately

prepared photocatalyst particles or by treating a photocatalyst precursor solution including pre-made CQDs. Multi-step synthesis, as opposed to one-pot synthesis, allows for more freedom in tuning CQD characteristics, resulting in improved photocatalytic performance. Table 2.2 summarizes the various preparation methods of CQDs/TiO₂ nanocomposites.

Table 2.2 Various methods for the preparation of CQDs/TiO₂ nanocomposites.

Synthetic route	Starting carbon	Ti pre-cursor	Details	Ref.
Solvo-thermal method	Orange peels	Titanium isopropoxide	CQDs prepared by microwave solvothermal method, TiO ₂ by sol-gel method. The mole ratios of TiO ₂ :CQDs are 1:1, 1:2, and 1:3, stirred for 12 hours at $T=35$ °C.	[73]
	Coal tar pitch (CTP)	Commercial P25	TiO ₂ nanoparticles were added to CQDs solution at $T=180$ °C for 12 h in autoclave.	[74]
In situ synthesis	Glucose	Tetrabutyl-titanate (TBOT)	TiO ₂ prepared by sol-gel method. TiO ₂ microspheres were dispersed in DI water and mixed with glucose in a Teflon-lined autoclave at $T=90$ °C for 4 h.	[75]
Sol-gel	L-ascorbic acid	Titanium (IV)-n-butoxide (Ti(OBu) ₄)	CQDs prepared by hydrothermal method; hydrolysis of Ti(OBu) ₄ and iminodiacetic acid in ethanol for TiO ₂ nanoparticles; mixing TiO ₂ and CQDs followed by drying in a vacuum oven.	[76]
	L-ascorbic acid	Titanium (IV) isopropoxide	CQDs prepared by an ultrasonic-hydrothermal method; TiO ₂ by sol-gel method; mixing TiO ₂ and CQDs followed by drying in a vacuum oven at 80 °C.	[77]
Hydro-thermal	Citric acid	Tetra-butyl titanate (TBT)	CQDs prepared by hydrothermal method; TBT was hydrolyzed in acetic acid solution; CQDs, FeCl ₃ and TBT were mixed and autoclaved at $T=180$ °C for 24 h.	[79]
	Citric acid	Titanium tetraisopropoxide	CQDs prepared by hydrothermal method, TiO ₂ nanofiber by electrospinning process. TiO ₂ nanofiber and CQDs were mixed and autoclaved at $T=140$ °C for 4h.	[57]
	Citric acid	Commercial P25	CQDs prepared via bottom-up method. P25 and CQDs were mixed and autoclaved at $T=140$ °C for 4h.	[80]

2.2.3 Characterisation methods of CQDs/TiO₂ composites

The XRD findings have confirmed the high crystalline structure of the synthesized hybrid nanocomposites, which can be inferred from the effective incorporation of relatively small atomic CQDs by forming Ti-O-C bonds into TiO₂ nanoparticles. Morphological analysis by SEM and field-emission transmission electron microscopy (TEM) tested the active decoration of nano-sized semiconductors over CQD platforms, while the EDS and XPS analysis verified the presence of all components in the hybrid nanocomposites. In particular, XPS spectra analyze the basic binding conditions of nanocomposite compositional components (the surface chemical composition and the chemical bonding state). Lastly, TEM observation and XPS characterization indicate that the CQDs are well anchored on the surface of nanoparticles [78]. To validate the respective distributions of the compositional elements, EDX elemental maps have been explored. In order to research the separation of charge carriers in the as-prepared samples, steady-state PL and time-resolved PL spectra were used. A higher PL strength indicates a higher likelihood of recombination of electron-hole pairs under light irradiation. Fourier transform infrared (FT-IR) spectra were conducted by a spectrometer with the ATR accessories (Nicolet X700). And UV-Vis diffuse reflectance spectra were measured.

2.3 Application of CQDs/TiO₂ composites in wastewater treatment

2.3.1 Photocatalytic reduction of heavy metal ions

Heavy metal pollution in water is a global environmental problem that has put human health and ecosystems in jeopardy. Cations (e.g., Hg²⁺, Pb²⁺, Cd²⁺, and Cu²⁺) and oxygen anions (e.g., CrO₄²⁻/Cr₂O₇²⁻, SeO₃²⁻/SeO₄²⁻, and HAsO₄²⁻/AsO₄³⁻) are the most prevalent heavy metal pollutants in water [82]. When compared to organic pollutants, these heavy metal ions in water are harder to

biodegrade into environmentally benign molecules. As a result, it is critical to dispose of them in a real-world water environment. S,N-CQD/TiO₂ composites have sparked considerable interest in the capture of dangerous heavy metal ions in water in recent years [83]. Zhao et al., for example, proposed using a sol-gel technique to combine TiO₂ with rGO in an ethanol-water solvent. TiO₂ nanoparticles are densely packed on the surface of rGO, indicating that rGO and TiO₂ are a good combination. The photocatalytic activity and stability of nanocomposites generated with this material are exceptional. In comparison to prior investigations [59, 60], a high level of Cr (VI) removal is accomplished along the surface, with up to 86.5 % removal of Cr (VI) [128]. Chen et al. announced new rGO-Mn-doped-TiO₂ composites with strong photocatalytic activity in one-point hydrothermal light, resulting in Cr (VI) elimination of 98.72 % in 30 minutes under visible light. The visibility of photocatalytic flexibility can be increased.

In 2018, a unique CQDs-N-TiO₂-x nanocomposite was successfully produced for the first time by adopting a simple hydrothermal-calcination process to decorate carbon quantum dots (CQDs) on nitrogen (N) and Ti³⁺ co-doped TiO₂ nanoparticles. The generated CQDs-N-TiO₂-x nanocomposite demonstrated efficient photocatalytic performance in real laboratory wastewater to reduce Cr (VI) (94%) [84]. Some CQDs/TiO₂ nanoparticles prepared by the hydrothermal method with different CQDs loadings were used for photocatalytic degradation of Cr (VI) under visible irradiation. The band gap energies of the prepared CQDs/TiO₂ nanoparticles were narrower than those of pure TiO₂ and decreased with the increased amount of CQDs, leading to enhanced visible light absorption. The composite with the optimum CQDs content (3.0 wt%) was capable of degrading almost 100% of Cr (VI) in 40 minutes as shown in Figure 2.2, with a degradation rate constant 8.6 times faster than that of pure TiO₂ [85].

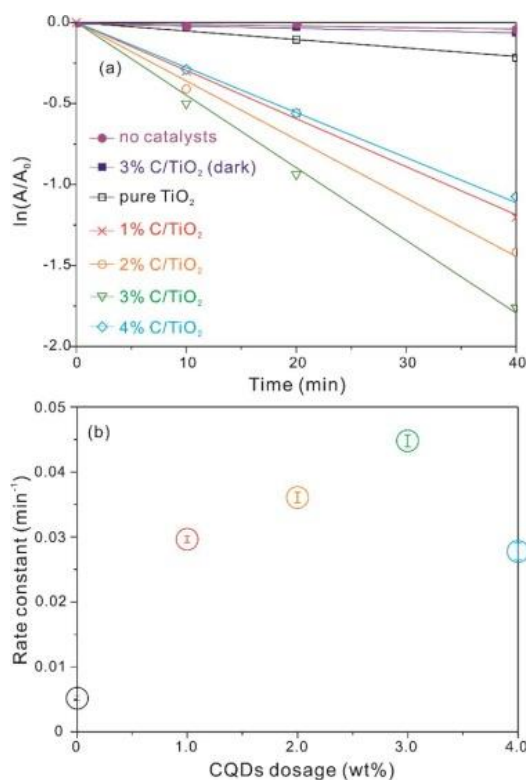


Figure 2.2 First-order kinetic profiles (a) and reduction rate constants (b) of Cr (VI) via indicated catalysts under visible light.

Similar to Cr (VI), Arsenic (As) compound pollution in natural water can also pose a serious hazard to the environment and public health, even at extremely low concentrations, due to its carcinogenic and mutagenic properties [86]. Previous research has mostly focused on the oxidation of acutely poisonous arsenite (As(III)) to arsenate (As(V)); nevertheless, As (V)'s absorbability on soil may have negative consequences for bacteria and microscopic fungi [87]. For instance, Li et al. used a TiO₂ photocatalyst in deoxygenated aqueous suspension to investigate its photoreduction performance over As(V). They discovered that converting As(V) to As(IV) directly by accepting photogenerated electrons in the conduction band was not thermodynamically feasible. However, adding sacrificial electron donors (such as alcohols or carboxylic acids) to the photocatalytic media

could result in the generation of strongly reductive radicals, hence enhancing As' indirect reductive process (V) [88].

A putative mechanism of photocatalytic Cr (VI) reduction over N, S-CQDs/TiO₂ nanocomposites is postulated (As shown in Figure 2.3):



Photo-excited electrons (e⁻) and holes (h⁺) with energies equivalent to or greater than the energy gap of semiconductors are produced in the conduction band (CB) and valence band (VB), respectively, under the light. To dissipate energy, such charge carriers (e⁻/h⁺) may be captured at defective sites in the semiconductor lattice or recombined as heat or light emissions [89]. Furthermore, when photo-excited electrons and holes are transported to the semiconductor surface and create strong radicals, they will initiate a redox process (OH⁻, O₂⁻, etc.) [58, 59]. Lin et al. [90] discovered that by employing TiO₂ as a photocatalyst, the initial reduction rate of Cr (VI) follows the Langmuir reaction model. They also studied the pH-related thermodynamic characteristics of the photocatalytic reduction of Cr (VI) and discovered that photo corrosion of TiO₂ in basic solutions is particularly unfavorable. They also discovered that in an acidic medium, photocatalytic reduction of Cr (VI) is faster than in a basic medium [91]. The highly positively charged TiO₂ surfaces, as well as the existence of fewer competing molecules for the redox reaction at the lower pH, are responsible for the greater photocatalytic reduction rate of Cr (VI) in acidic media.

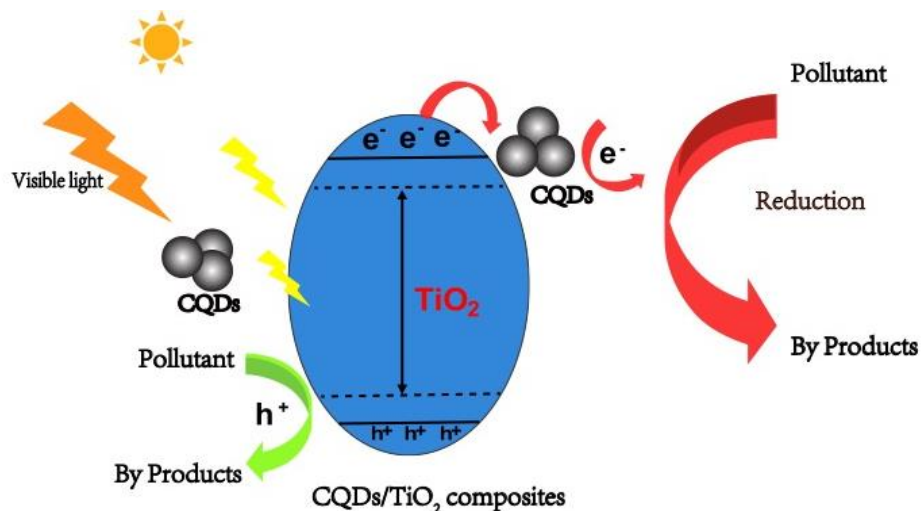


Figure 2.3 A putative mechanism of photocatalytic Cr (VI) reduction over N, S-CQDs/TiO₂ nanocomposites [89]

2.3.2 Photocatalytic degradation of organic pollutants in water

Water pollution by diverse organic contaminants has increased as a result of industrialization and anthropogenic activity (e.g. dyes, phenolic compounds, pesticides, and pharmaceutically active compounds, etc.) [92]. These pollutants are highly poisonous, carcinogenic, and resistant to degradation. Photocatalysis, which involves speeding up a light-induced reaction in the presence of heterogeneous catalysts, can reduce or eliminate water contamination by converting it to harmless or less hazardous components by chemical conversion [93]. Photocatalysis research is primarily focused on the creation of visible-light responsive photocatalysts [94]. It has been demonstrated that combining TiO₂ with non-toxic carbonaceous nanomaterials like CQDs can increase TiO₂ light absorption from ultraviolet (UV) to visible and even near-infrared light. Herein, a summary of and future directions for exploring high-performance CQDs/TiO₂ photocatalysts will be discussed [95, 96].

A sequence of oxidative and reductive processes on the surface of CQD/TiO₂ composites is involved in the photocatalytic destruction of organic contaminants (Fig. 2.4) [97]. The photo-

generated electron/hole pairs participate in oxidation-reduction processes on the photocatalyst surface with adsorbed H₂O and O₂, generating reactive oxygen species such as hydroxyl (\bullet OH) and superoxide ($O_2^{\bullet -}$) radicals [98]. In aqueous situations, the photogenerated holes (h^+) react with surface OH⁻ groups to produce \bullet OH radicals [99]. It is thought that the reaction of \bullet OH radicals with organic contaminants causes these molecules to decompose [100, 101]. In general, only photons with energies greater than the bandgap energy (ΔE) can excite valence band (VB) electrons, which can then enhance organic pollutant processes. Energy is frequently dissipated in the form of heat when photons with energies less than ΔE or longer wavelengths are absorbed. The creation of a positive hole (h^+) in the valence band and an electron (e^-) in the conduction band is caused by sufficient energy lighting of the photocatalytic surface (CB). To form the hydroxyl radical OH \bullet , the positive hole oxidises either the pollutant or water directly. However, the electron in the conduction band reduces the amount of oxygen adsorbed on the photocatalyst. When the reduction of oxygen and the oxidation of pollutants do not proceed at the same time in photocatalytic degradation, an electron accumulates in the conduction band, causing an increase in the rate of e^- and h^+ recombination. The following processes and equations can be used to describe the radical formation and the interaction of generated radicals with organic pollutants [102-106]:



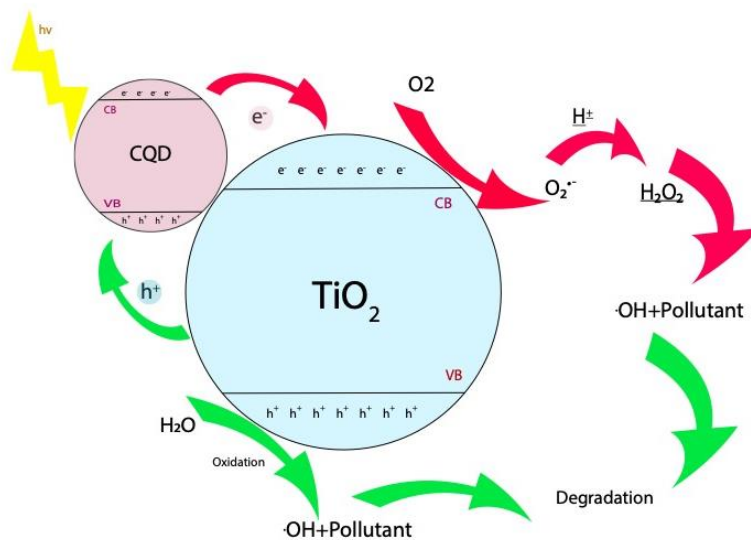


Figure 2.4 A basic photo-catalytic mechanism in photocatalytic degradation of organic pollutants by CQDs/TiO₂ composites.

The photocatalytic destruction of organic contaminants (dyes, pesticides, medicinal components, and phenols, etc.) from water using CQDs/TiO₂ has been studied extensively. The following is a summary of this study, organized by target pollutant (s). Textile, cosmetic, paper, food, agriculture, and pharmaceutical industries all employ organic colors. Organic dyes thrown into bodies of water produce an unpleasant color and block sunlight, resulting in a variety of severe environmental effects such as the decreased photosynthetic activity of algae, aquatic life death, and surface/groundwater toxicity [107]. Photocatalytic degradation of organic dyes using CQDs/TiO₂ has been proven to be an efficient method of dyes from wastewater. For example, for photocatalytic degradation of RhB (10.0 mg/L) under visible irradiation, CQDs/TiO₂ composites produced by an energy-efficient impregnation process with varied CQD loadings were utilised. The band gap energies of the synthesised CQDs/TiO₂ composites were significantly lower than those of pure TiO₂ and declined as the amount of CQDs grew, resulting in greater visible light

absorption. The composite with the highest CQDs content (6.0 wt%) degraded 93.4 % of RhB in 4 hours, at a pace 42.7 times faster than pure TiO₂. The synthesised composites showed good chemical stability, with no appreciable loss in photocatalytic degradation [108] (As shown in Figure 2.5).

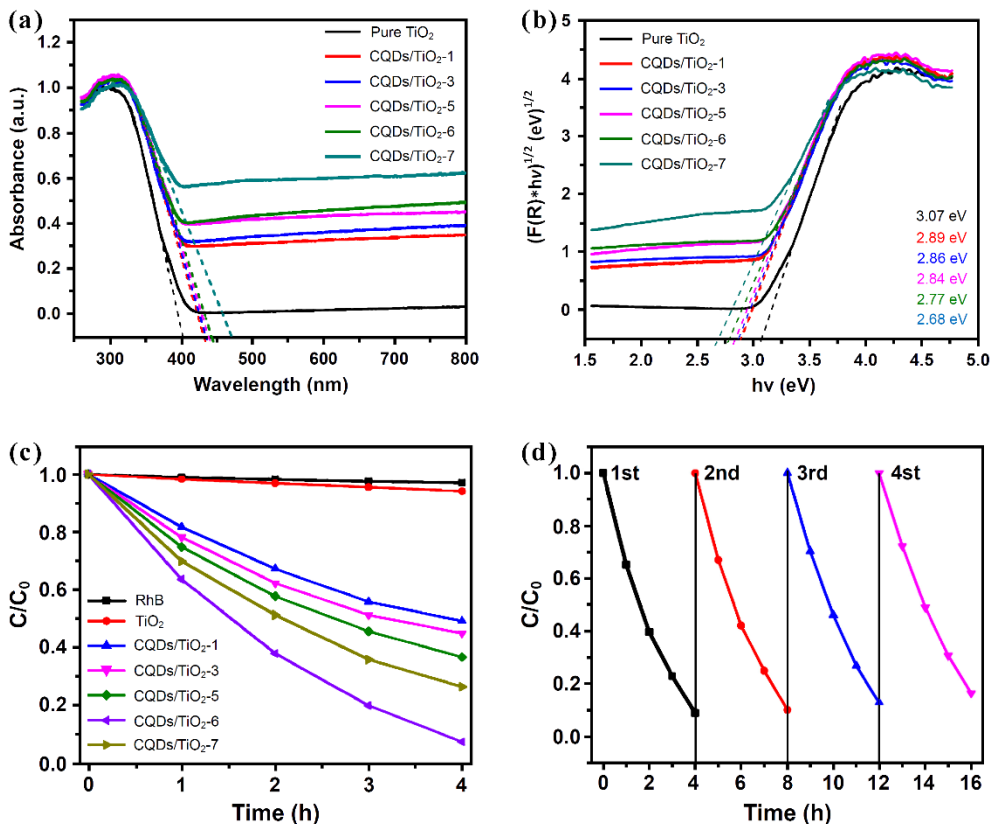


Figure 2.5 UV-Vis DRS (a), Tauc's plots for the band gap values (b), photocatalytic activity (c), and reusability (d) of CQDs/TiO₂ composites. (Reproduced with permission from [108])

The superior stability and recyclability of the hybrid composites, which are important factors considering their economic effectiveness, also need to be tested. In order to determine the recyclability of the catalysts, after each experiment, the catalyst was removed from the reaction mixture by filtration and washed with deionized water and acetone, then dried in the air. It is evident from Yan et al. that up to seven cycles without apparent loss of catalytic activity, the 82%

CQDs-TiO₂ catalyst could be reused, demonstrating the stability of the catalyst [109]. An on-off recycling system was used in most of the recycling experiments [110]. The experimental results from Chu et al. showed that the degradation rate of dye pollutant after 1h of UV light irradiation reached 95%, and even after 10 cycles of the catalyst, the degradation rate of the dye still reached 88% compared with the pure TiO₂ particles [111]. Considerable research illustrated the high catalyst stability and demonstrated the catalyst is highly usable.

Another important category of organic contaminants in water bodies is phenols. Phenols are mostly introduced into the aquatic system from the agriculture sector, effluents of phenol manufacturing industries, and plant growth regulators [112]. Phenols used in excess of the permitted limit have adverse impacts on human health, including dermatological, gastrointestinal, neurological, carcinogenic, respiratory, reproductive, and endocrine consequences [113]. To protect humans and aquatic organisms from probable contamination of these harmful substances, complete removal of phenolic compounds from the aquatic environment is required. Chemical removal procedures that can break down harmful chemicals are recommended over physical removal methods. Photocatalysis of phenols using visible light is a potentially more sustainable and cost-effective approach for removing phenolic chemicals from water. By using a simple hydrothermal-calcining procedure, a highly solar-active nanocomposite with a sheet-like WO₃ skeleton and equally loaded TiO₂ and carbon quantum dots (CQDs) was created by Sun et al. [114], and it demonstrated 3.1 and 46.6 times more activity on antibiotic (cephalexin) degradation, respectively than TiO₂ and WO₃. The TiO₂/CQDs composite's structure decreased the band gap and made electron-hole separation easier. By photosensitization, conjugated CQDs were shown to increase charge separation and expand the visible light sensitivity. The photocatalytic mineralization efficiency can reach 92.4% in 4 hours, showing that cephalexin and its intermediates have low ecotoxicity.

Pharmaceuticals and personal care are mainly made up of polar compounds that have a wide range of physicochemical properties. Industrial wastewater, runoff, and landfill leachate all convey pharmaceuticals to bodies of water. Chen et al. first removed cefradine from water by CQDs/TiO₂ nanocomposite in 2016 [115]. The CQDs/TiO₂ nanocomposite was proposed via a sol-gel approach. In comparison with pure TiO₂, the photocatalyst absorption was extended into the visible light range and photocatalytic activity was increased with the simple decorating of CQDs. The result showed that the photocatalytic degradation of cefradine by CQDs/TiO₂ composite was in accordance with pseudo-first-order kinetics, and the degradation rate constant was 0.02585 min⁻¹. The circumstances of photocatalytic degradation, such as the initial concentration of cefradine, the amount of catalyst, and the pH value of the reaction liquid, were tuned in order to improve the degradation efficiency of cefradine by CQDs/TiO₂ composite. Experimental results showed that the degradation degree peaked at pH 2.85 in the acid range, but peaked at pH 9.46 when the pH was higher than pH 7. Cefradine deterioration in the acid range could be due to cefradine's instability in acidic conditions, which can speed up photodegradation. And when the initial concentration of cefradine was increased, the degradation rate constants were reduced. However, the degradation rate constants were found to be favorably correlated with photocatalyst concentrations in the range of 0–2.0 g/L, with the best efficiency at the correct concentration (2.0 g/L). This could be due to increasing turbidity of the reaction solution with increased photocatalyst concentration, resulting in a drop in degradation efficiency as UV transmission decreased, as shown in Figure 2.6.

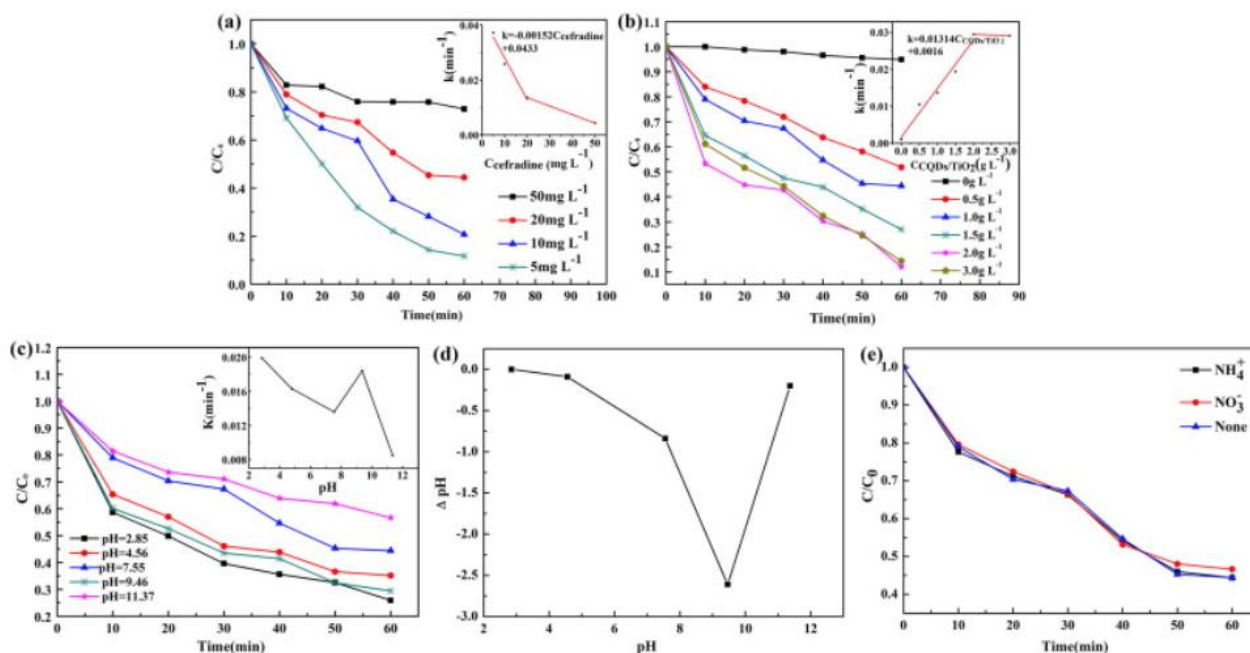


Figure 2.6 (a) Effect of initial concentration of cefradine on the photocatalytic activities of CQDs/TiO₂ composite (inset: plots of degradation rates versus concentration of cefradine); (b) effect of amount of CQDs/TiO₂ composite on its photocatalytic activities (inset: plots of degradation rates versus concentration of CQDs/TiO₂ composite); (c) effect of pH of reaction solution on the photocatalytic activities of CQDs/TiO₂ composite (inset: plots of degradation rates versus pH); (d) the changes of pH value before and after reaction during the reaction solution with different initial pH value; (e) effect of foreign inorganic ions on the photocatalytic activities of CQDs/TiO₂ composite under the visible irradiation, respectively; [115]

2.4 Influences of environmental conditions on the photocatalytic degradation/reduction

The effectiveness and performance of a photocatalytic system can be affected by many influences such as pH, catalyst loading, and initial concentration of contaminants for suspended systems, and the starting concentration of pollutants are all factors to consider. These aspects will be discussed in further detail in the sections below.

2.4.1 Effect of pH

pH is one of the most critical operational parameters in a heterogeneous photocatalytic reactor because it influences catalyst particle charges, target chemical adsorption capacity, dissociation, catalyst aggregate size, conductance, and valence band locations [114-116]. Previous studies have

proven that the surface charge of semiconductors depends on pH [119-121]. Because there is no electrostatic force between the contaminants and the photocatalyst at a pH equal to the point of zero charges of TiO_2 (PZC), there is no attraction between the contaminants and the photocatalyst [122]. Under this water pH level, the suspended catalyst has a proclivity to agglomerate. The net surface charge of the catalyst is positive at pH levels lower than PZC, which could result in an electrostatic interaction between the positively charged catalyst and anionic organic molecules in the water. Conversely, the photocatalyst's surface will be negatively charged at pH levels higher than PZC, creating a repulsive force between the catalyst and the anionic compounds in the water [123]. Kazeminezhad et al. [124] have studied the effect of pH on ZnO nanoparticle photocatalytic activity for photodegradation of Rose Bengal (RB), Methylene blue (MB), and Bromocresol green (BG) dyes. The dye adsorption on the outer surface of ZnO nanoparticles is greatly influenced by the pH of the solution, which plays a crucial role in photocatalytic degradation. Abbasi et al. [125] also investigated the influence of pH on the photocatalytic activity of MO in ZnO-SnO₂ suspension. The results of their analysis of variance revealed that pH has a significant effect on the photocatalytic activity of all nanoparticles and hybrids.

2.4.2 Effect of Catalyst Loading

The efficiency of photocatalytic degradation is greatly reliant on catalyst loading. According to previous studies [126], the photocatalytic degradation rate increases linearly with catalyst loading but begins to decline at extremely high concentrations when light scattering and screening effects decrease. Because of agglomeration (particle-particle interaction) at high catalyst loading, the surface area of the photocatalyst tends to decrease, affecting light absorption. Take organic pollutants as an example [127]. The rate of photocatalytic degradation of organic pollutants increases with photocatalyst dosage in general due to an increase in active sites [128]. This effect

is mostly due to an increase in the amount of hydroxyl radical produced by photocatalysts that have been irradiated [129]. Because more light passes through the reactor with lower catalyst loadings, the organic molecule breakdown is reduced, and less radiation is transmitted to be used exclusively in photocatalytic activity [130]. However, when the light is above the optimum quantity of catalyst loading, the degradation rate may be lower due to a rise in the opacity of the suspension, which increases light scattering and also reduces photon infiltration depth, resulting in fewer photocatalysts being activated [131]. Akyol et al. [132] studied the catalyst loading for its effects on the photocatalytic degradation performance in terms of TOC removal and decolorization. Due to the limited catalyst surface area, photonic adsorption regulates the reaction extent at lower loading levels, and whole light scattering by catalyst particles predominates over photonic adsorption at higher loading levels. Decolorization and TOC removal reach their highest levels at about 2g/l catalyst loading due to these negative effects.

2.4.3 Initial concentration of contaminants

The number of contaminants in the wastewater is a critical factor that influences photocatalytic efficiency. With all other reaction parameters held constant, the reaction rate constant drops as the contaminant concentration rise. At greater pollutant concentrations, a longer irradiation period is required to achieve complete degradation and mineralization of the contaminants because of this reduction in reaction rate constant [133]. This behavior can be explained by the fact that when the initial concentration rises, more organic compounds are adsorbed on the surface of the semiconductor. Because there are fewer active sites for the adsorption of hydroxyl ions and the formation of hydroxyl radicals, the generation of hydroxyl radicals is reduced. Furthermore, as the solution concentration rises, photons are intercepted before reaching the catalyst surface. As a result, the catalyst's photon absorption lowers, and the degradation rate decreases [134].

References

- [1] S. Sharma V. Dutta, P. Singh, P. Raizada, A. Sani, A. Bandegharaei, V. Thakur, Carbon quantum dot supported semiconductor photocatalysts for efficient degradation of organic pollutants in water: A review, *J. Clean. Prod.*, 228 (2019), 755–769.
- [2] B. Xue, Y. Yang, Y. Sun, J. Fan, X. Li, Z. Zhang, Photoluminescent lignin hybridized carbon quantum dots composites for bioimaging applications, *Int. J. Biol. Macromol.*, 122 (2019), 954–961.
- [3] U. A. Rani, L. Y. Ng, C. Y. Ng, E. Mahmoudi, A review of carbon quantum dots and their applications in wastewater treatment, *Adv. Colloid Interface Sci.*, 278 (2020), 102124.
- [4] P. N. Joshi, A. Mathias, A. Mishra, Synthesis of ecofriendly fluorescent carbon dots and their biomedical and environmental applications, *Adv. Perform. Mater.*, 33 (2018), 672–680.
- [5] Z. Liang, J. Yang, C. Zhou, Q. Mo, Y. Zhang, Carbon quantum dots modified BiOBr microspheres with enhanced visible light photocatalytic performance, *Inorg. Chem. Commun.*, 90 (2018), 97–100.
- [6] P. Cui, Y. Kuai, Q. Wu, Y. Zheng, X. Liu, Synthesis of a fluorescent cation surfactant derived from carbon quantum dots, *Mater. Lett.*, 235 (2019), 161–163.
- [7] L. Zhou, M. Qiao, L. Zhang, L. Sun, Y. Zhang, W. Liu, Green and efficient synthesis of carbon quantum dots and their luminescent properties, *J. Lumin.*, 206 (2019), 158–163.
- [8] H. Fan, M. Zhang, B. Bhandari, C. Yang, Food waste as a carbon source in carbon quantum dots technology and their applications in food safety detection, *Trends Food Sci. Tech.*, 95 (2020), 86–96.
- [9] M. Sabet, K. Mahdavi, Green synthesis of high photoluminescence nitrogen-doped carbon quantum dots from grass via a simple hydrothermal method for removing organic and inorganic water pollutions, *Appl. Surf. Sci.*, 463 (2019), 283–291.
- [10] Y. Shi, X. Liu, M. Wang, J. Huang, X. Jiang, J. Pang, et al., Synthesis of N-doped carbon quantum dots from bio-waste lignin for selective irons detection and cellular imaging, *Int. J. Biol.*, 128 (2019), 537–545.
- [11] G. Kalaiyarasan, J. Joseph, Cholesterol derived carbon quantum dots as fluorescence probe for the specific detection of hemoglobin in diluted human blood samples, *Mater.Sci. Eng. C*, 94 (2019), 580–586.
- [12] R. Das, R. Bandyopadhyay, P. Pramanik, Carbon quantum dots from natural resource: A review, *Mater. Today Chem.*, 8 (2018), 96–109.

- [13] P. Devi, P. Rajput, A. Thakur, K.-H. Kim, P. Kumar, Recent advances in carbon quantum dot-based sensing of heavy metals in water, *TrAC- Trends Anal. Chem.*, 114 (2019), 171–195.
- [14] X. Kou, S. Jiang, S.-J. Park, L.-Y. Meng, A review: recent advances in preparations and applications of heteroatom-doped carbon quantum dots, *Dalton Trans.*, 49 (2020), 6915–6938.
- [15] M. M. Mohideen, Y. Liu, S. Ramakrishna, Recent progress of carbon dots and carbon nanotubes applied in oxygen reduction reaction of fuel cell for transportation, *Appl. Energy*, 257 (2020), 114027.
- [16] S. Y. Lim, W. Shen, Z. Gao, Carbon quantum dots and their applications, *Chem. Soc. Rev.*, 44 (2015), 362–381.
- [17] J. Hagen, N. Young, A. Every, C. Pagel, C. Schnoeller, J. Scheerlinck et al. Omega-1 knockdown in schistosoma mansoni eggs by lentivirus transduction reduces granuloma size in vivo, *Nat. Commun.*, 5 (2014), 5375.
- [18] T. Madrakian, S. Maleki, S. Gilak, A. Afkhami, Turn-off fluorescence of amino-functionalized carbon quantum dots as effective fluorescent probes for determination of isotretinoin, *Sens. Actuators B: Chem.*, 247 (2017), 428–435.
- [19] A. Nasrin, M. Hassan, G. Mann, V. G. Gomes, Conjugated ternary doped carbon dots from vitamin B derivative: Multispectral nanoprobe for targeted melanoma bioimaging and photosensitization, *J. Lumin.*, 217 (2020), 116811.
- [20] J. Zhou, H. Zhou, J. Tang, S. Deng, F. Yan, W. Li et al., Carbon dots doped with heteroatoms for fluorescent bioimaging: a review, *Microchim. Acta*, 184 (2017), 343–368.
- [21] A. Rehman, S.-J. Park, Comparative study of activation methods to design nitrogen-doped ultra-microporous carbons as efficient contenders for CO₂ capture, *Chem. Eng. J.*, 352 (2018), 539–548.
- [22] C. Lee, B. Pant, B. Kim, R. Jang, S. Park, S. Park et al., Carbon quantum dots incorporated keratin/polyvinyl alcohol hydrogels: Preparation and photoluminescent assessment, *Mater. Lett.*, 201 (2017), 57–61.
- [23] Z. W. Heng, W. C. Chong, Y. L. Pang, C. H. Koo, An overview of the recent advances of carbon quantum dots/metal oxides in the application of heterogeneous photocatalysis in photodegradation of pollutants towards visible-light and solar energy exploitation, *J. Environ. Chem. Eng.*, 9 (2021), 105199.

- [24] A. Aghamali, M. Khosravi, H. Hamishehkar, N. Modirshahla, M. A. Behnajady, Synthesis and characterization of high efficient photoluminescent sunlight driven photocatalyst of N-carbon quantum dots, *J. Lumin.*, 201 (2018), 265–274.
- [25] S. Bian, C. Shen, Y. Qian, J. Liu, F. Xi, X. Dong, Facile synthesis of sulfur-doped graphene quantum dots as fluorescent sensing probes for Ag⁺ ions detection, *Sens. Actuators B: Chem.*, 242 (2017), 231–237.
- [26] H. Gao, Z. Liu, L. Song, W. Guo, W. Gao, L. Ci et al., Synthesis of S-doped graphene by liquid precursor, *Nanotechnology*, 23 (2012), 275605.
- [27] B. Dai, C. Wu, Y. Lu, D. Deng, S. Xu, Synthesis and formation mechanism of s-doped carbon dots from low-molecule-weight organics, *J. Lumin.*, 190 (2017), 108–114.
- [28] Y. Li, S. Li, Y. Wang, J. Wang, H. Liu, X. Liu et al., Electrochemical synthesis of phosphorus-doped graphene quantum dots for free radical scavenging, *Phys. Chem. Chem. Phys.*, 19 (2017), 11631–11638.
- [29] F. Wang, Q. Hao, Y. Zhang, Y. Xu, W. Lei, Fluorescence quenchometric method for determination of ferric ion using boron-doped carbon dots, *Microchim. Acta*, 183 (2016), 273–279.
- [30] J. Jana, M. Ganguly, K. R. S. Chandrakumar, G. Mohan Rao, T. Pal, Boron Precursor-Dependent Evolution of Differently Emitting Carbon Dots, *Langmuir*, 3 (2017), 573–584.
- [31] C. Shen, J. Wang, Y. Cao, Y. Lu, Facile access to B-doped solid-state fluorescent carbon dots toward light emitting devices and cell imaging agents, *J. Mater. Chem. C*, 3 (2015), 6668–6675.
- [32] P. Godard, P.-O. Renault, D. Faurie, D. Thiaudière, Relaxation mechanisms in a gold thin film on a compliant substrate as revealed by X-ray diffraction, *Appl. Phys. Lett.*, 110 (2017), 211901.
- [33] H. Sun, H. Ji, E. Ju, Y. Guan, J. Ren, X. Qu, Synthesis of fluorinated and nonfluorinated graphene quantum dots through a new top-down strategy for long-time cellular Imaging, *Eur. J. Chem.*, 21 (2015), 3791–3797.
- [34] Z. Qian, X. Shan, L. Chai, J. Ma, J. Chen, H. Feng, Si-doped carbon quantum dots: A facile and general preparation strategy, bioimaging application, and multifunctional sensor,” *ACS Appl. Mater. Interfaces*, 6 (2014), 6797–6805.
- [35] H. Su, Y. Liao, F. Wu, X. Sun, H. Liu, K. Wang et al., Cetuximab-conjugated iodine doped carbon dots as a dual fluorescent/CT probe for targeted imaging of lung cancer cells, *Colloids Surf. B.*, 170 (2018), 194–200.

- [36] M. Wang, Y. Wang, M. Zhao, F. Wang, C. Zhao, Metabolic profiling analysis of fatty acids from hyperlipidemic rats treated with gynostemma pentaphyllum and atorvastatin based on GC/MS, *Anal. Methods*, 6 (2014), 8660–8667.
- [37] Y. Dong, H. Pang, H. Yang, C. Guo, J. Shao, Y. Chi et al., Carbon-based dots co-doped with nitrogen and sulfur for high quantum yield and excitation-independent emission, *Angew. Chem. Int. Ed.*, 52 (2013), 7800–7804.
- [38] N. Parvin, T. K. Mandal, Dually emissive P,N-co-doped carbon dots for fluorescent and photoacoustic tissue imaging in living mice, *Microchim. Acta*, 184 (2017), 1117–1125.
- [39] M.-C. Rong, K.-X. Zhang, Y.-R. Wang, X. Chen, The synthesis of B, N-carbon dots by a combustion method and the application of fluorescence detection for Cu^{2+} , *Chin. Chem. Lett.*, 28 (2017), 1119–1124.
- [40] T. Tian, Y. He, Y. Ge, G. Song, One-pot synthesis of boron and nitrogen co-doped carbon dots as the fluorescence probe for dopamine based on the redox reaction between Cr (VI) and dopamine, *Sens. Actuators B: Chem.*, 240 (2017), 1265–1271.
- [41] Y. Xu, S. Wang, X. Hou, Z. Sun, Y. Jiang, Z. Dong et al., Coal-derived nitrogen, phosphorus and sulfur co-doped graphene quantum dots: A promising ion fluorescent probe, *Appl. Surf. Sci.*, 445 (2018), 519–526.
- [42] S. Huang, E. Yang, J. Yao, Y. Liu, Q. Xiao, Red emission nitrogen, boron, sulfur co-doped carbon dots for ‘on-off-on’ fluorescent mode detection of Ag^+ ions and l-cysteine in complex biological fluids and living cells, *Anal. Chim. Acta*, 1035 (2018), 192–202.
- [43] W. Niu, Y. Li, R. Zhu, D. Shan, Y. Fan, X. Zhang, Ethylenediamine-assisted hydrothermal synthesis of nitrogen-doped carbon quantum dots as fluorescent probes for sensitive biosensing and bioimaging, *Sens. Actuators B: Chem.*, 218 (2015), 229–236.
- [44] A. Hasanzadeh, M. Jahromi, A. Abdoli, H. Beigi, Y. Fatahi, H. Nourizadeh et al., Photoluminescent carbon quantum dot/poly-l-Lysine core-shell nanoparticles: A novel candidate for gene delivery, *J. Drug Deliv. Sci. Tec.*, 61 (2021), 102118.
- [45] S. Zhu, Q. Meng, L. Wang, J. Zhang, Y. Song, H. Jin et al., Highly photoluminescent carbon dots for multicolor patterning, sensors, and bioimaging, *Angew. Chem. Int. Ed.*, 52 (2013), 3953–3957.
- [46] G. He, M. Shu, Z. Yang, Y. Ma, D. Huang, S. Xu et al., Microwave formation and photoluminescence mechanisms of multi-states nitrogen doped carbon dots, *Appl. Surf. Sci.*, 422 (2017), 257–265.

- [47] H. J. Yashwanth, S. R. Rondiya, N. Y. Dzade, S. D. Dhole, D. M. Phase, K. Hareesh, Enhanced photocatalytic activity of N, P, co-doped carbon quantum dots: An insight from experimental and computational approach, *Vacuum*, 180 (2020), 109589.
- [48] N. Xiao, S. Liu, S. Mo, N. Li, Y. Ju, Y. Ling et al., Highly selective detection of p-nitrophenol using fluorescence assay based on boron, nitrogen co-doped carbon dots, *Talanta*, 184 (2018), 184–192.
- [49] Z. Wang, X. Zhao, Z. Guo, P. Miao, X. Gong, Carbon dots based nanocomposite thin film for highly efficient luminescent solar concentrators, *Org. Electron.*, 62 (2018), 284–289.
- [50] Q. Chen, L. Chen, J. Qi, Y. Tong, Y. Lv, C. Xu et al., Photocatalytic degradation of amoxicillin by carbon quantum dots modified $K_2Ti_6O_{13}$ nanotubes: Effect of light wavelength, *Chin. Chem. Lett.*, 30 (2019), 1214–1218.
- [51] B. Hemmateenejad, P. Shadabipour, T. Khosousi, M. Shamsipur, Chemometrics investigation of the light-free degradation of methyl green and malachite green by starch-coated CdSe quantum dots, *J. Ind. Eng. Chem.*, 27 (2015), 384–390.
- [52] S. Hu, R. Tian, Y. Dong, J. Yang, J. Liu, Q. Chang, Modulation and effects of surface groups on photoluminescence and photocatalytic activity of carbon dots, *Nanoscale*, 5 (2013), 11665–11671.
- [53] Y. Park, J. Yoo, B. Lim, W. Kwon, S. Rhee, Improving the functionality of carbon nanodots: doping and surface functionalization, *J. Mater. Chem. A*, 4 (2016), 11582–11603.
- [54] Q. Wang, G. Wang, X. Liang, X. Dong, X. Zhang, Supporting carbon quantum dots on NH₂-MIL-125 for enhanced photocatalytic degradation of organic pollutants under a broad spectrum irradiation, *Appl. Surf. Sci.*, 467–468 (2019), 320–327.
- [55] Z. Zhang, L. Wu, P. Wang, Y. Zhang, S. Wan, X. Guo et al., Carbon quantum dots modified La₂Ti₂O₇ nanosheets for visible light photocatalysis, *Mater. Lett.*, 230 (2018), 72–75.
- [56] Y. Zhang, L. Wang, M. Yang, J. Wang, J. Shi, Carbon quantum dots sensitized ZnSn(OH)₆ for visible light-driven photocatalytic water purification, *Appl. Surf. Sci.*, 466 (2019), 515–524.
- [57] P. S. Saud, B. Pant, A.-M. Alam, Z. K. Ghouri, M. Park, H.-Y. Kim, Carbon quantum dots anchored TiO₂ nanofibers: Effective photocatalyst for waste water treatment, *Ceram. Int.*, 41 (2015), 11953–11959.
- [58] A. Hernandez-Ramírez, I. Medina-Ramírez, Semiconducting Materials in *Photocatalytic Semiconductors: Synthesis, Characterization, and Environmental Applications*, A.

- Hernández-Ramírez and I. Medina-Ramírez, Eds. Cham: Springer International Publishing, 2015, pp. 1–40.
- [59] A. Fujishima, K. Honda, Electrochemical photolysis of water at a semiconductor electrode, *Nature*, 238 (1972), 37–38.
- [60] M. I. Litter, Heterogeneous photocatalysis: Transition metal ions in photocatalytic systems, *Appl. Catal., B*, 23 (1999), 89–114.
- [61] D. Ravelli, D. Dondi, M. Fagnoni, A. Albini, Photocatalysis. A multi-faceted concept for green chemistry, *Chem. Soc. Rev.*, 38 (2009), 1999..
- [62] X. Chen, S. S. Mao, Titanium dioxide nanomaterials: synthesis, properties, modifications, and applications, *Chem. Rev.*, 107 (2007), 2891–2959.
- [63] N. R. Khalid, A. Majid, M. B. Tahir, N. A. Niaz, S. Khalid, Carbonaceous-TiO₂ nanomaterials for photocatalytic degradation of pollutants: A review, *Ceram. Int.*, 43 (2017), 14552–14571.
- [64] T. M. Breault, B. M. Bartlett, Lowering the band gap of anatase-structured TiO₂ by coalloying with Nb and N: Electronic structure and photocatalytic degradation of methylene blue dye, *J. Phys. Chem.*, 116 (2012), 5986–5994.
- [65] C. Chen, T. Wei, J. Li, Broadband photocatalytic activity of mesoporous Cd(II)-doped TiO₂,” *ChemistrySelect*, 2 (2017), 3648–3656.
- [66] Y. Sun, B. Zhou, Y. Lin, W. Wang, K. Fernando, P. Pathak et al., Quantum-sized carbon dots for bright and colorful photoluminescence, *J. Am. Chem. Soc.*, vol. 128, no. 24, pp., 128 (2006), 7756–7757.
- [67] K. Jiang, S. Sun, L. Zhang, Y. Lu, A. Wu, C. Cai et al., Red, green, and blue luminescence by carbon dots: full-color emission tuning and multicolor cellular imaging, *Angew. Chem. Int. Ed.*, 54 (2015), 5360–5363.
- [68] K. A. S. Fernando, S. Sahu, Y. Liu, W. Lewis, E. Gulians, A. Jafariyan et al., Carbon quantum dots and applications in photocatalytic energy conversion, *ACS Appl. Mater. Interfaces*, 7 (2015), 8363–8376.
- [69] H. Li, X. He, Z. Kang, H. Huang, Y. Liu, J. Liu et al., Water-soluble fluorescent carbon quantum dots and photocatalyst design, *Angew. Chem. Int. Ed.*, 49 (2010), 4430–4434.
- [70] C. Wang, K. Yang, X. Wei, S. Ding, F. Tian, F. Li, One-pot solvothermal synthesis of carbon dots/Ag nanoparticles/TiO₂ nanocomposites with enhanced photocatalytic performance, *Ceram. Int.*, 44 (2018), 22481–22488.

- [71] M. Feng, Y. Liu, N. Wei, S. Ma, Z. Li, H. Li et al., Alumina anchored CQDs/TiO₂ nanorods by atomic layer deposition for efficient photoelectrochemical water splitting under solar light, *J. Mater. Chem. A*, 6 (2018), 18293–18303.
- [72] W. Wang, Y. Ni, Z. Xu, One-step uniformly hybrid carbon quantum dots with high-reactive TiO₂ for photocatalytic application, *J. Alloys Compd.*, 622 (2015), 303–308.
- [73] P. M. Olmos-Moya, S. Velazquez-Martinez, C. Pineda-Arellano, J. R. Rangel-Mendez, L. F. Chazaro-Ruiz, High added value functionalized carbon quantum dots synthesized from orange peels by assisted microwave solvothermal method and their performance as photosensitizer of mesoporous TiO₂ photoelectrodes, *Carbon*, 187 (2022), 216–229.
- [74] J. Zhang, Q. Liu, H. He, F. Shi, G. Huang, B. Xing et al., Coal tar pitch as natural carbon quantum dots decorated on TiO₂ for visible light photodegradation of rhodamine B, *Carbon*, 152 (2019), 284–294.
- [75] R. Liu, H. Li, L. Duan, H. Shen, Y. Zhang, X. Zhao, In situ synthesis and enhanced visible light photocatalytic activity of C-TiO₂ microspheres/carbon quantum dots, *Ceram. Int.*, 43 (2017), 8648–8654.
- [76] J. Ke, X. Li, Q. Zhao, B. Liu, S. Liu, S. Wang, Upconversion carbon quantum dots as visible light responsive component for efficient enhancement of photocatalytic performance, *J. Colloid Interface Sci.*, 496 (2017), 425–433.
- [77] R. Miao, Z. Luo, W. Zhong, S. Chen, T. Jiang, B. Dutta et al., Mesoporous TiO₂ modified with carbon quantum dots as a high-performance visible light photocatalyst, *Appl. Catal., B*, 189 (2016), 26–38.
- [78] F. Zhao, Y. Rong, J. Wan, Z. Hu, Z. Peng, B. Wang, High photocatalytic performance of carbon quantum dots/TNTs composites for enhanced photogenerated charges separation under visible light, *Catal. Today*, 315 (2018), 162–170.
- [79] J. Zhang, M. Kuang, J. Wang, R. Liu, S. Xie, Z. Ji, Fabrication of carbon quantum dots/TiO₂/Fe₂O₃ composites and enhancement of photocatalytic activity under visible light,” *Chem. Phys. Lett.*, 730 (2019), 391–398.
- [80] H. Zhao, X. Yu, C. Li, A. Wang, Z. Hu, S. Larter et al., Carbon quantum dots modified TiO₂ composites for hydrogen production and selective glucose photoreforming, *J. Energy Chem.*, 64 (2022), 201–208.
- [81] M. A. Ahsan, V. Jabbari, M. Islam, R. Turley, N. Dominguez, H. Kim et al., Sustainable synthesis and remarkable adsorption capacity of MOF/graphene oxide and MOF/CNT based hybrid nanocomposites for the removal of Bisphenol A from water, *Sci. Total Environ.*, 673 (2019), 306–317.

- [82] D. Häder, A. Banaszak, V. Villafañe, M. Narvarte, R. González, E. Helbling, Anthropogenic pollution of aquatic ecosystems: Emerging problems with global implications,” *Sci. Total Environ.*, 713 (2020), 136586.
- [83] Z. Li, L. Wang, L. Qin, C. Lai, Z. Wang, M. Zhou et al., Recent advances in the application of water-stable metal-organic frameworks: Adsorption and photocatalytic reduction of heavy metal in water,” *Chemosphere*, 285 (2021), 131432.
- [84] L. Xu, X. Bai, L. Guo, S. Yang, P. Jin, L. Yang, Facial fabrication of carbon quantum dots (CDs)-modified N-TiO_{2-x} nanocomposite for the efficient photoreduction of Cr (VI) under visible light,” *Chem. Eng. J.*, 357 (2019), 473–486.
- [85] D. Choi, S. Ham, D. Jang, Visible-light photocatalytic reduction of Cr (VI) via carbon quantum dots-decorated TiO₂ nanocomposites, *J. Environ. Chem. Eng.*, 6 (2018), 1–8.
- [86] T. M. Clancy, K. F. Hayes, L. Raskin, Arsenic waste management: A critical review of testing and disposal of arsenic-bearing solid wastes generated during arsenic removal from drinking water, *Environ. Sci. Technol.*, 47 (2013), 10799–10812.
- [87] B. Neppolian, A. Doronila, F. Grieser, M. Ashokkumar, Simple and efficient sonochemical method for the oxidation of arsenic(III) to arsenic(V), *Environ. Sci. Technol.*, 43 (2009), 6793–6798.
- [88] I. K. Levy, M. Mizrahi, G. Ruano, G. Zampieri, F. G. Requejo, M. I. Litter, TiO₂-photocatalytic reduction of pentavalent and trivalent arsenic: Production of elemental arsenic and arsine,” *Environ. Sci. Technol.*, 46 (2012), 2299–2308.
- [89] S. C. Ray, A. Saha, N. R. Jana, R. Sarkar, Fluorescent carbon nanoparticles: Synthesis, characterization, and bioimaging application,” *J. Phys. Chem. C*, 113 (2009), 18546–18551.
- [90] W. Lin, C. Wei, K. Rajeshwar, Photocatalytic reduction and immobilization of hexavalent chromium at titanium dioxide in aqueous basic media, *J. Electrochem. Soc.*, 140 (1993), 2477–2482.
- [91] A. Shoneye, J. Sen Chang, M. N. Chong, J. Tang, Recent progress in photocatalytic degradation of chlorinated phenols and reduction of heavy metal ions in water by TiO₂-based catalysts, *Int. Mater. Rev.*, 67 (2021), 47-64.
- [92] M. Lorenzo, J. Campo, Y. Picó, Analytical challenges to determine emerging persistent organic pollutants in aquatic ecosystems, *Trends Analyt. Chem.*, 103 (2018), 137–155.
- [93] A. Zhitkovich, Chromium in drinking water: Sources, metabolism, and cancer risks, *Chem. Res. Toxicol.*, 24 (2011), 1617–1629.

- [94] D. Chen, Y. Cheng, N. Zhou, P. Chen, Y. Wang, K. Li et al., Photocatalytic degradation of organic pollutants using TiO₂-based photocatalysts: A review, *J. Clean. Prod.*, 268 (2020), 121725.
- [95] A. Di Mauro, M. E. Fragalà, V. Privitera, G. Impellizzeri, ZnO for application in photocatalysis: From thin films to nanostructures, *Mater. Sci. Semicond Process*, 69 (2017), 44–51.
- [96] L. G. Devi, R. Kavitha, A review on non metal ion doped titania for the photocatalytic degradation of organic pollutants under UV/solar light: Role of photogenerated charge carrier dynamics in enhancing the activity, *Appl. Catal., B*, 140–141 (2013), 559–587.
- [97] F. Khan, M. S. Khan, S. Kamal, M. Arshad, S. I. Ahmad, S. A. A. Nami, Recent advances in graphene oxide and reduced graphene oxide based nanocomposites for the photodegradation of dyes, *J. Mater. Chem. C*, 8 (2020), 15940–15955.
- [98] C. N. C. Hitam, A. A. Jalil, A review on exploration of Fe₂O₃ photocatalyst towards degradation of dyes and organic contaminants, *J. Environ. Manage.*, 258 (2020), 110050.
- [99] W. Ong, L. Tan, S. Chai, S. Yong, and A. Mohamed, Facet-dependent photocatalytic properties of TiO₂-based composites for energy conversion and environmental remediation, *ChemSusChem*, 7 (2014), 690–719.
- [100] S. N. Ahmed, W. Haider, Heterogeneous photocatalysis and its potential applications in water and wastewater treatment: a review, *Nanotechnology*, 29 (2018), 342001.
- [101] R. Gusain, K. Gupta, P. Joshi, O. Khatri, Adsorptive removal and photocatalytic degradation of organic pollutants using metal oxides and their composites: A comprehensive review, *Adv. Colloid Interface Sci.*, 272 (2019), 102009.
- [102] C. Chiou, C. Wu, R. Juang, Influence of operating parameters on photocatalytic degradation of phenol in UV/TiO₂ process, *Chem. Eng. J.*, 139 (2008), 322–329.
- [103] W. Bahnemann, M. Muneer, M. M. Haque, Titanium dioxide-mediated photocatalysed degradation of few selected organic pollutants in aqueous suspensions, *Catal. Today*, 124 (2007), 133–148.
- [104] D. Saha, M. Desipio, T. Hoinkis, E. Smeltz, R. Thorpe, D. Hensley et al., Influence of hydrogen peroxide in enhancing photocatalytic activity of carbon nitride under visible light: An insight into reaction intermediates, *J. Environ. Chem. Eng.*, 6 (2018), 4927–4936.
- [105] P. Phonsy, S. Anju, K. Jyothi, S. Yesodharan, E. Yesodharan, Semiconductor mediated photocatalytic degradation of plastics and recalcitrant organic pollutants in water: Effect of additives and fate of insitu formed H₂O₂, *J. Adv. Oxid. Technol.*, 18 (2015), 0111.

- [106] H. Zhu, J. Wang, Z. Gong, Y. D. Kim, J. Hone, X. Zhu, Interfacial charge transfer circumventing momentum mismatch at two-dimensional van der waals composites, *Nano Lett.*, 17 (2017), 3591–3598.
- [107] A. Bhatnagar, A. K. Jain, A comparative adsorption study with different industrial wastes as adsorbents for the removal of cationic dyes from water, *J. Colloid Interface Sci.*, 281 (2005), 49–55.
- [108] J. Zhang, Q. Liu, J. Wang, H. He, F. Shi, B. Xing et al., Facile preparation of carbon quantum dots/TiO₂ composites at room temperature with improved visible-light photocatalytic activity, *J. Alloys Compd.*, 869 (2021), 159389.
- [109] Y. Yan, W. Kuang, L. Shi, X. Ye, Y. Yang, X. Xie et al., Carbon quantum dot-decorated TiO₂ for fast and sustainable antibacterial properties under visible-light, *J. Alloys Compd.*, 777 (2019), 234–243.
- [110] R. Shi, Z. Li, H. Yu, L. Shang, C. Zhou, G. Waterhouse et al., Effect of nitrogen doping level on the performance of N-doped carbon quantum dot/TiO₂ composites for photocatalytic hydrogen evolution, *ChemSusChem.*, 10 (2017), 4650–4656.
- [111] Z. Chu, L. Qiu, Y. Chen, Z. Zhuang, P. Du, J. Xiong, TiO₂-loaded carbon fiber: Microwave hydrothermal synthesis and photocatalytic activity under UV light irradiation, *J. Phys. Chem. Solids*, 136 (2020), 109138.
- [112] D. J. Hamilton, A. Ambrus, R. M. Dieterle, A. Felsot, C. A. Harris, P. Holland et al., Regulatory limits for pesticide residues in water (IUPAC technical report), *Pure Appl. Chem.*, 75 (2003), 1123–1155.
- [113] S. Mostafalou, M. Abdollahi, Pesticides and human chronic diseases: Evidences, mechanisms, and perspectives, *Toxicol. Appl. Pharmacol.*, 268 (2013), 157–177.
- [114] X. Sun, W. He, T. Yang, H. Ji, W. Liu, J. Lei et al., Ternary TiO₂/WO₃/CQDs nanocomposites for enhanced photocatalytic mineralization of aqueous cephalixin: Degradation mechanism and toxicity evaluation, *Chem. Eng. J.*, 412 (2021), 128679.
- [115] J. Chen, J. Shu, Z. Anqi, H. Juyuan, Z. Yan, J. Chen, Synthesis of carbon quantum dots/TiO₂ nanocomposite for photo-degradation of Rhodamine B and cefradine, *Diam. Relat. Mater.*, 70 (2016), 137–144.
- [116] A. Carabin, P. Drogui, D. Robert, Photo-degradation of carbamazepine using TiO₂ suspended photocatalysts, *J. Taiwan Inst. Chem. Eng.*, 54 (2015), 109–117.

- [117] A. F. Alkaim, A. M. Aljeboree, N. A. Alrazaq, S. J. Baqir, F. H. Hussein, A. J. Lilo, Effect of pH on adsorption and photocatalytic degradation efficiency of different catalysts on removal of methylene blue, *Asian J. Chem.*, 26 (2014), 8445–8448.
- [118] L. Haroune, M. Salaun, A. Ménard, C. Legault, J. Bellenger, Photocatalytic degradation of carbamazepine and three derivatives using TiO₂ and ZnO: Effect of pH, ionic strength, and natural organic matter, *Sci. Total Environ.*, 475 (2014), 16–22.
- [119] S. S. Chin, K. Chiang, A. Fane, The stability of polymeric membranes in a TiO₂ photocatalysis process, *J. Membr. Sci.*, 275 (2006), 202–211.
- [120] A. P. Toor, A. Verma, C. K. Jotshi, P. K. Bajpai, V. Singh, Photocatalytic degradation of direct yellow 12 dye using UV/TiO₂ in a shallow pond slurry reactor, *Dyes and Pigm.*, 68 (2006), 53–60.
- [121] I. Ochuma, R. Fishwick, J. Wood, J. Winterbottom, Optimisation of degradation conditions of 1,8-diazabicyclo[5.4.0]undec-7-ene in water and reaction kinetics analysis using a cocurrent downflow contactor photocatalytic reactor, *Appl. Catal., B*, 73 (2007), 259–268.
- [122] E. K. Putra, R. Pranowo, J. Sunarso, N. Indraswati, S. Ismadji, Performance of activated carbon and bentonite for adsorption of amoxicillin from wastewater: Mechanisms, isotherms and kinetics, *Water Res.*, 43 (2009), 2419–2430.
- [123] Y. Xu, C. H. Langford, Variation of Langmuir adsorption constant determined for TiO₂-photocatalyzed degradation of acetophenone under different light intensity, *J. Photochem. Photobiol. A: Chem.*, 133 (2000), 67–71.
- [124] K. Iraj, A. Sadollahkhani, Influence of pH on the photocatalytic activity of ZnO nanoparticles, *J. Mater. Sci.: Mater. Electron.*, 27 (2016), 4206–4215.
- [125] S. Abbasi, M. Hasanpour, The effect of pH on the photocatalytic degradation of methyl orange using decorated ZnO nanoparticles with SnO₂ nanoparticles, *J. Mater. Sci.: Mater. Electron.*, 28 (2017), 1307–1314.
- [126] N. N. Yunus, F. Hamzah, M. S. So'aib, J. Krishnan, Effect of catalyst loading on photocatalytic degradation of phenol by using N, S co-doped TiO₂, *IOP Conf. Ser.: Mater. Sci. Eng.*, 206 (2017), 012092.
- [127] A. Gnanaprakasam, V. M. Sivakumar, M. Thirumarimurugan, Influencing parameters in the photocatalytic degradation of organic effluent via nanometal oxide catalyst: A review, *Indian J. Mater. Sci.*, 15 (2015), 1–16.

- [128] L. Karimi, S. Zohoori, M. E. Yazdanshenas, Photocatalytic degradation of azo dyes in aqueous solutions under UV irradiation using nano-strontium titanate as the nanophotocatalyst, *J. Saudi Chem. Soc.*, 18 (2014), 581–588.
- [129] X. Zhang, F. Wu, X. Wu, P. Chen, N. Deng, Photodegradation of acetaminophen in TiO₂ suspended solution, *J. Hazard. Mater.*, 157 (2008), 300–307.
- [130] F. Mai, C. Lu, C. Wu, C. Huang, J. Chen, C. Chen, Mechanisms of photocatalytic degradation of victoria blue R using nano-TiO₂, *Sep. Purif. Technol.*, 62 (2008), 423–436.
- [131] H. Seshadri, S. Chitra, K. Paramasivan, P. K. Sinha, Photocatalytic degradation of liquid waste containing EDTA, *Desalination*, 232 (2008), 139–144.
- [132] A. Akyol, M. Bayramoğlu, Photocatalytic degradation of remazol red F3B using ZnO catalyst, *J. Hazard. Mater.*, 124 (2005), 241–246.
- [133] A. Nageswara Rao, B. Sivasankar, V. Sadasivam, Kinetic study on the photocatalytic degradation of salicylic acid using ZnO catalyst, *J. Hazard. Mater.*, 166 (2009), 1357–1361.
- [134] M. A. Behnajady, N. Modirshahla, R. Hamzavi, Kinetic study on photocatalytic degradation of C.I. acid yellow 23 by ZnO photocatalyst, *J. Hazard. Mater.*, 133 (2006), 226–232.

Chapter 3. Visible-Light-Driven Photocatalytic Reduction of Cr (VI) by Carbon Quantum Dots-Sensitized TiO₂

3.1 Introduction

The pollution of heavy metals in water resources is a worldwide challenge due to the adverse health effects of heavy metals. Chromium is one of the toxic heavy metals, generally existing in hexavalent (Cr (VI)) and trivalent (Cr (III)) forms, of which Cr (VI) is highly toxic, carcinogenic, mutagenic and results in several health issues such as liver damage, pulmonary problems, vomiting, and diarrhea [1-3]. Nonetheless, Cr (III) is relatively inert and non-toxic. As a result, reduction of Cr (VI) to Cr (III) is one of the most effective ways to eliminate hazardous Cr (VI) from wastewater. Compared with conventional catalytic reduction of Cr (VI) using noble metal catalysts [4, 5], photocatalytic reduction of Cr (VI) has attracted widespread attention and strong interest because of its high degradation rate and relatively low cost [6–8]. Various semiconductors both with a wide band gap (TiO₂, ZnO, ZnS, CeO₂ etc.) and narrow band gap (CdS, MnO₂, α -Fe₂O₃, SnS₂ etc.) have been developed [9-15]. Nonetheless, these photocatalysts suffer from limitation of fast recombination of the electron–hole pairs, low solar energy utilization efficiency, and/or potential secondary pollution due to the leaching of heavy metal ions under acidic environment. Therefore, development non-toxic and efficient visible-light responsive photocatalysts is desirable.

Recently, carbonaceous nanomaterial (CNM) sensitized TiO₂ has been developed as visible-light active photocatalysts in wastewater treatment. Combining non-toxic CNM with TiO₂ can effectively reduce the band gap energy [16], broaden the light absorption range [17, 18] and improve the separation efficiency of photogenerated charges of TiO₂ [19, 20], leading to enhanced photocatalytic performance. Carbon quantum dots (CQDs) are zero-dimensional (0D) CNMs with

excellent optical and chemical properties [21]. CQDs are currently the most promising CNMs for applications in photocatalysis, electrocatalysis, bioimaging and sensing applications due to their quantum confinement, edge effect, biocompatibility, low toxicity, and photostability [22–24]. Moreover, most CQDs contain hydroxyl and carboxylic acid moieties at their surfaces, resulting in excellent aqueous solubility and suitability for subsequent functionalization with various organic, polymeric, inorganic, or biological species [25]. Finally, by doping lightweight heteroatoms (B, N, P, and S), electric conductivity and light absorption and emission range of CQDs can be fine-tuned [26–28]. As such, CQDs can serve as photosensitizers to extend the visible-light photocatalytic activity of TiO₂.

To date, variety of CQDs/TiO₂ composites have been fabricated as visible-light responsive photocatalysts for Cr (VI) reduction [29–34]. Carbon dots-TiO₂ nanosheets (CDs-TNs) were synthesized by facile hydrothermal method and applied for photoreduction of Cr (VI) under simulated sunlight illumination. The CDs-TNs can be excited by a broad range of sunlight and exhibit higher photoreduction efficiency under simulated sunlight [30]. A carbon dot-sensitized Ti³⁺ self-doped TiO₂ composite was constructed using low-temperature (135°C) hydrothermal method and was applied to simultaneously reduce Cr (VI) and degrade Rhodamine B (RhB) under visible light irradiation. The experimental results indicated that RhB (10 mg/L) and Cr (VI) (40 mg/L) solutions were degraded completely in 30 and 120 min respectively, with the catalyst loading of 1.0 g/L [31]. In a related work, a CQDs and Ti³⁺ co-modified TiO₂-graphene (CQDs-TiO_{2-x}/rGO) nanocomposite was fabricated to degrade bisphenol A and reduce Cr (VI) synergistically. Due to the introduction of CQDs and rGO, the prepared composite exhibited extended visible light absorption and large BET surface area, leading to enhanced photocatalytic activities towards organic degradation and Cr (VI) reduction [33]. Although these studies have

confirmed that CQDs/TiO₂ composites demonstrate great potential as efficient photocatalysts driven by visible light to reduce Cr (VI), it is still worth investigating their reusability and photocatalytic reduction performance in real water samples.

In this study, a facile hydrothermal method was used to fabricate a novel nitrogen and sulfur co-doped CQDs, which were then incorporated into TiO₂ to form the N, S-CQDs/TiO₂ composite. Different analyses were used to assess the morphology, chemical content, and optical properties of the prepared N, S-CQDs and N, S-CQDs/TiO₂. The photocatalytic activity of the as-prepared composite was tested by the reduction of Cr (VI) from water under visible light irradiation. The effects of initial substrate concentration, catalyst dosage, and solution pH were thoroughly examined. Based on the obtained experimental results, a plausible mechanism for the Cr (VI) reduction by N, S-CQDs/TiO₂ was proposed. The reusability and the photocatalytic performance of N, S-CQDs/TiO₂ in real water samples were also investigated.

3.2 Materials and methods

3.2.1 Materials

Citric acid (99.9%), thiourea (>99%), sodium sulfite, commercial TiO₂ (P25), sodium dichromate dihydrate, diphenylacarbazine (DPC), hydrochloride acid, phosphoric acid, sulfuric acid, sodium hydroxide, and ethanol were purchased from Fisher Scientific Canada. All the chemicals were used as received without further purification. The ultrapure deionized (DI) water used in all experiments.

3.2.2 Synthesis of N, S-CQDs

N, S-CQDs were synthesized via a modified one-pot hydrothermal method according to previous studies [35, 36]. Specifically, 1.09 mmol (0.21g) of citric acid and 3.0 mmol (0.23g) of thiourea were dissolved in 40.0 mL of DI water by ultrasonication. The mixture was then transferred to a

100 mL Teflon-lined stainless-steel autoclave and heated at 180 °C for 6 h. After cooling to room temperature, the products were centrifuged at 4000 rpm for 35 min to remove the large particles. The supernatant was withdrawn and filtered through 0.22 µm membrane filters, followed by a further purification using dialysis membrane (molecular cut of 500 Da) against DI water for 8 h. Finally, the solid N, S-CQDs product was collected after freeze drying.

3.2.3 Preparation of the N, S-CQDs/TiO₂ nanocomposites

The N, S-CQDs/TiO₂ nanocomposites were prepared by mixing 0.2 g of P25 and 40.0 mL of N, S-CQDs solutions with different weight percentages (1.0–5.0 w%) of solid N, S-CQDs. The pH of the solutions was adjusted to 3.5 using HCl and NaOH solutions, and then mixed with 20.0 mL of ethanol separately under vigorous stirring for 6 h. The solution mixtures were then transferred to 100 mL Teflon-sealed autoclaves and heated at 150 °C for 6h. After the hydrothermal reaction, the N, S-CQDs/TiO₂ nanocomposites were collected after centrifugation of the product solutions, sample washing (twice) with DI water and ethanol and air-drying at 70 °C for 24 h.

3.2.4 Characterization

The morphology and composition of N, S-CQDs and N, S-CQDs/TiO₂ were characterized using high-resolution transmission electron microscopy (HRTEM, Titan 80-300, FEI, USA) and X-ray photoelectron spectroscopy (XPS, PHI 5000 VPIII, ULVAC-PHI, Japan) as well as The Fourier transform infrared (FTIR, Tensor II, Bruker, Germany) spectroscopy over a range from 400 to 4000 cm⁻¹. XRD was used to determine the crystallinity of the prepared photocatalyst. The UV-Vis absorption spectra of N, S-CQDs and N, S-CQDs/TiO₂ were measured using a UV-3600 UV-Vis-Nir spectrophotometer (Shimadzu, Japan). The valence-band positions of N, S-CQDs and N, S-CQDs/TiO₂ were evaluated by performing valence-band XPS.

3.2.5 Reduction of Cr (VI) under visible light irradiation

The photocatalytic performance of the as-prepared N, S-CQDs/TiO₂ composites was investigated toward the reduction of Cr (VI) irradiated by visible light (300W Xenon lamp with a 420-nm cutoff filter) at 30°C. The temperature of photocatalytic reaction was controlled by a circulating water system (FP50-HL, Julabo, USA). For each run, 50.0 mg of the N, S-CQDs/TiO₂ composite was mixed with 50.0 mL of Cr (VI) aqueous solution under constant stirring. After 1 h of dark adsorption/reaction, photocatalytic reduction of Cr (VI) was triggered by turning on the xenon lamp. At each sampling time, 1.0 mL aliquot of suspension was withdrawn from the reactor and filtered using 0.22µm membrane filter. The Cr (VI) concentration was determined using Cari-100 UV-vis spectrophotometer. To verify the repeatability of the reduction experiments, three repeated experimental runs were carried out with 20.0 mg/L of initial concentration of Cr (VI), pH 3.0 and 1.0 g/L of catalyst dosage. The average experimental error was within ±3.0%, demonstrating a very good experimental repeatability.

The concentration of Cr (VI) was determined via a diphenylcarbazide (DPC) colorimetric method, and the detailed steps are as follows: 1.0 mL of the filtered sample was mixed with 4.0 mL of DI water. Then, 100.0 µL of 1+1 H₂SO₄ and 100 µL of 1+1 H₃PO₄ were added to the mixture and mixed completely. Next, 400.0 µL of freshly prepared DPC solution was added to the mixture and allowed to sit for 5-10 min for full color development. Finally, the concentration of Cr (VI) was determined by monitoring the absorbance of the solution at 540 nm wavelength using DI water as the reference.

3.3 Results and discussion

3.3.1 Characterization of N, S-CQDs and N, S-CQDs/TiO₂

High resolution TEM was used to characterize the morphology and size of the N, S-CQDs particles. The HRTEM image of the as-prepared N, S-CQDs is presented in Fig. 3.1a. As can be seen the average particle size of spherical N, S-CQDs are less than 10 nm which meets the size criteria of carbon quantum dots.

XPS and FTIR spectroscopy were performed to analyze the elemental composition and functional groups existing on the surface of N, S-CQDs. Both XPS survey spectrum and high resolution spectra (Figs. 3.1b-e) indicate that N, S-CQDs are mainly composed of elements of C, O, N and S. Three deconvoluted peaks at 284.8, 286.35 and 288.81 eV for C 1s can be seen from Fig. 3.1b, which are attributed to the sp² C (C–C/C=C) in graphite, the sp³ C (C–O/C–N), and the oxidized C (C=O), respectively [37, 38]. Similarly, the N 1s spectrum (Fig. 3.1c) was deconvoluted into three BE peaks centering at 400.64, 401.48 and 402.17 eV, which can be attributed to pyridinic-N, pyrrolic-N, and N–H, respectively. XPS spectrum of N 1s for N, S-CQDs from this study are consistent with those reported from open literature [37, 39, 40]. The two peaks of the O 1s spectrum (Fig. 3.1d) at 531.61 and 533.02 eV are assigned to the C=O, and C–O bonds respectively [38, 39]. The S 2p spectrum of N, S-CQDs was fitted into four peaks: BE peaks at 163.32 and 163.34 eV are the S 2p_{3/2} and S 2p_{1/2} doublet for C–S–C covalent bond, whereas peak at 164.33 and 168.67 eV are assigned to oxidized sulfur (SO_x) groups [41]. XPS results illustrated in Fig. 3.1 clearly indicate that heteroatom doping of CQDs by N and S were successful.

FT-IR spectrum of N, S-CQDs can be found in Fig. 3.1f, from which broad peaks in 3500-3100 cm⁻¹ are observed for O–H and N–H groups in the as-prepared N, S-CQDs. A peak at 2815.9 cm⁻¹ is for C–H stretching vibrations. Characteristic peaks at 2058, 1712, 1627 and 1525 cm⁻¹ are

attributed to the stretching vibrations of N=C=S, C=O, C=N and C=C of N, S-CQDs, respectively. Band peaks at 1402 and 1208 cm^{-1} can be ascribed to the stretching vibrations of C–N and C–O. Whereas, peaks at 1080 and 677 cm^{-1} are for for C–S vibrations. The results show good agreement with the results found in the literature using similar source of carbon and nitrogen [42, 43].

The UV-Vis absorption spectrum of N, S-CQDs (Fig. 3.1g) indicate three absorption bands at 333 nm, 420 nm, and 600 nm which are originated from the n to π^* transition of C=O, C=N, and C=S/S=O bonds [44]. The UV-vis results prove the visible light absorption ability of N, S-CQDs. To study the optical properties of the synthesized N, S-CQDs, photoluminescence (PL) analysis was carried out under different excitation wavelengths, as shown in Fig. 3.1h. The N, S-CQDs exhibit excitation-dependent photoluminescence. Furthermore, many studies have revealed that the PL behaviour of carbon dots is highly associated with the amount of oxygen-containing moieties [45]. The degree of surface oxidation that varies with the synthesis approach would determine the number of oxygenated groups produced Journal Pre-proof [36, 46] during partial decomposition of the C=C conjugated structure.

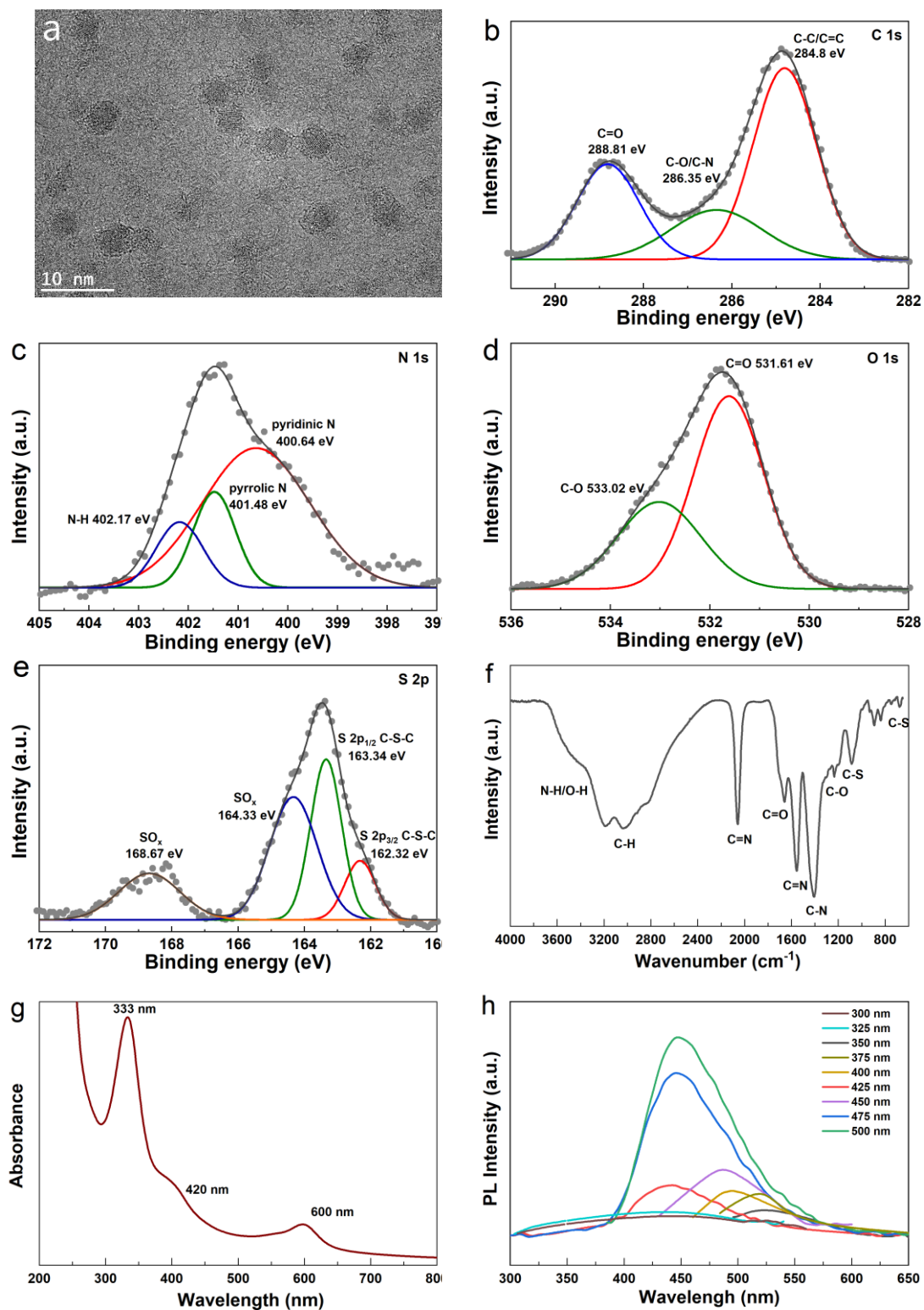


Figure 3. 1. HRTEM (a), high resolution XPS spectra of C 1s (b), N1s (c), O 1s(d) and S 2p (e), FT-IR spectrum (f), UV-vis absorption (g), and PL emission spectra (h) of N, S-CQDs.

To characterize the prepared N, S-CQDs/TiO₂ composite, powder x-ray diffraction (XRD) analysis was carried out. As shown in Fig. 3.2a, N, S-CQDs/TiO₂ showed similar XRD pattern to that of TiO₂, indicating that the phase structure of TiO₂ did not vary after the deposition of N, S-CQDs. Because of the low crystallinity or doping amount of N, S-CQDs in the composite, no characteristic peaks attributed to N, S-CQDs could be observed. Characteristic diffraction peaks of the N, S-CQDs/TiO₂ composite are in good agreement with the those of pure TiO₂ by the exposure of 25.32°, 37.84°, 48.04°, 54.08°, 62.72°, 68.96°, 70.3° and 75.2° peaks, corresponding to the reflections from (101), (004), (200), (105), (204), (116), (220) and (215) crystal facets [47].

Ultraviolet-visible diffuse reflectance spectroscopy (UV-Vis DRS) was used to study the optical properties of TiO₂ (P25) and N, S-CQDs/TiO₂ composite. Fig. 3.2b illustrates UV absorbance spectra of P25 and the N, S-CQDs/TiO₂ composite. As seen from Fig. 2b that TiO₂ can only absorb the light with a wavelength below 393 nm, however, after incorporation of N, S-CQDs into TiO₂, the absorption edge of the N, S-CQDs/TiO₂ was significantly increased from 393 nm to 426 nm. This indicates that photosensitizing TiO₂ with N, S-CQDs helps to improve the visible-light harvesting efficiency. The bandgap energy (E_g) of TiO₂ and N, S-CQDs/TiO₂ composite were estimated based on the Tauc plot (Fig. 3.2c), from which E_g can be determined using the following equations [48],

$$(\alpha h\nu)^2 = A(h\nu - E_g) \quad (3-1)$$

$$h\nu = hc / \lambda \quad (3-2)$$

where α is the optical absorption coefficient; A is a transition probability-dependent constant; c ($3.0 \times 10^8 \text{ m} \cdot \text{s}^{-1}$) is the speed of light; h ($6.626 \times 10^{-34} \text{ J} \cdot \text{Hz}^{-1}$) is the Plank's constant, and ν is the radiation frequency. As shown in Fig. 3.2c, the E_g value of N, S-CQDs/TiO₂ is 3.04 eV, which is lower than that (3.20 eV) of the pure TiO₂.

XPS valence band (VB) spectrum of N, S-CQDs/TiO₂ was measured to determine the VB energy (E_{VB}) of the composite photocatalyst, as seen from Fig. 3.2d, the E_{VB} value of N, S-CQDs/TiO₂ is estimated to be 2.7 eV, almost identical to the E_{VB} value of TiO₂ [49]. The conduction band energy ($E_{CB}=-0.34$ eV) of the N, S-CQDs/TiO₂ composite can be calculated by Mulliken electronegativity theory by Eq. (3–3),

$$E_{CB} = E_{VB} - E_g \quad (3-3)$$

Results from Figs. 3.2c&d indicate that N, S-CQDs have narrower band gap than TiO₂, and thus capable of exciting the electron that participate in Cr (VI) reduction at relatively lower energy level (irradiation by visible light rather than UV light).

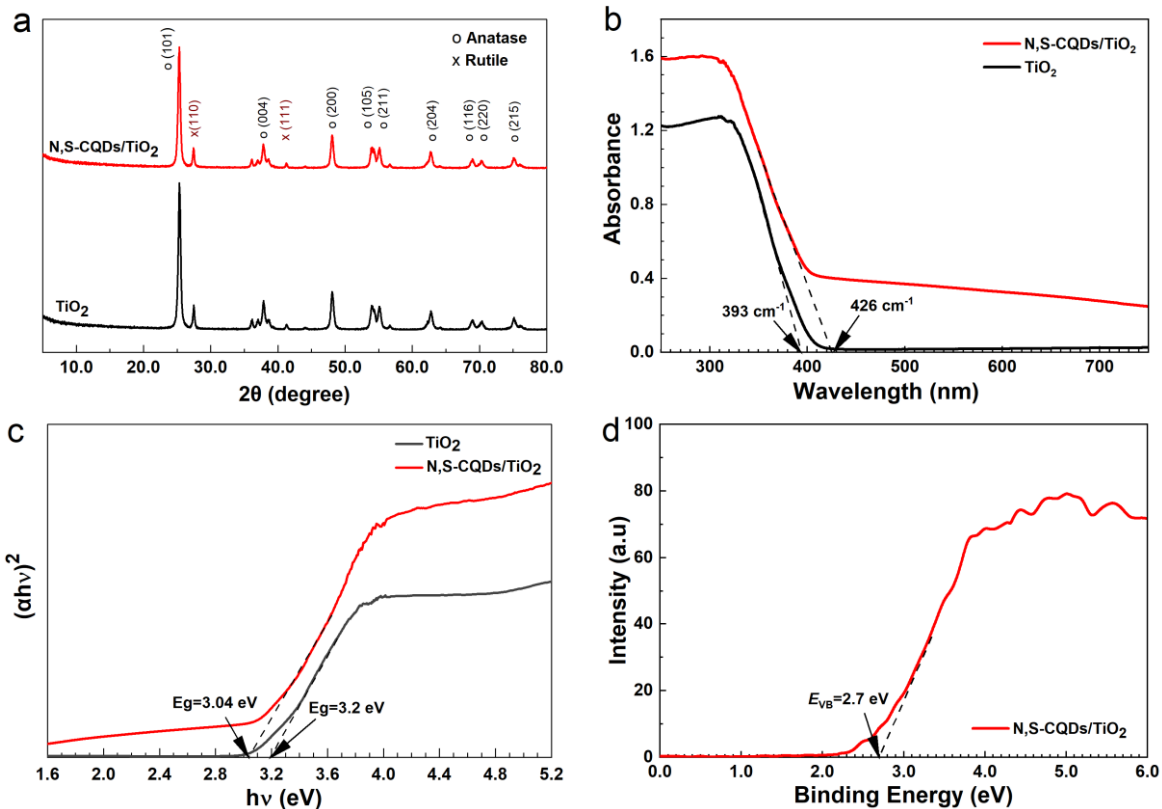


Figure 3. 2. Powder XRD (a), diffuse reflectance UV/Vis spectra (b), Tauc plot (c), and valence band XPS spectra of N, S-CQDs/TiO₂.

3.3.2 Photocatalytic study of N, S-CQDs/TiO₂ composite

The photocatalytic performance of the N, S-CQDs/TiO₂ composite was investigated under visible light irradiation ($\lambda_{\text{ex}} > 420 \text{ nm}$) for the reduction of Cr (VI). Fig. 3.3a compares the concentration changes of Cr (VI) with time in the presence of N, S-CQDs/TiO₂, pure TiO₂ (P25) and in the absence of photocatalysts. Without the use of any photocatalyst, reduction of Cr (VI) was undetectable. In the presence of photocatalysts, roughly 3.0% and 10.0% of Cr (VI) was adsorbed under dark condition by TiO₂ and N, S-CQDs/TiO₂ composite respectively. After 3 h of visible light irradiation, Cr (VI) was completely reduced to Cr (III) by N, S-CQDs/TiO₂, whereas less than 20.0% of Cr (VI) was reduced to Cr (III) by pristine TiO₂ due to its extremely low visible response. The improved photocatalytic reduction rate by N, S-CQDs/TiO₂ was mainly due to the incorporation of N, S-CQDs in the TiO₂ particles, which has improved light harvesting efficiency of visible light (400-600 nm) and hence enhanced photocatalytic capability.

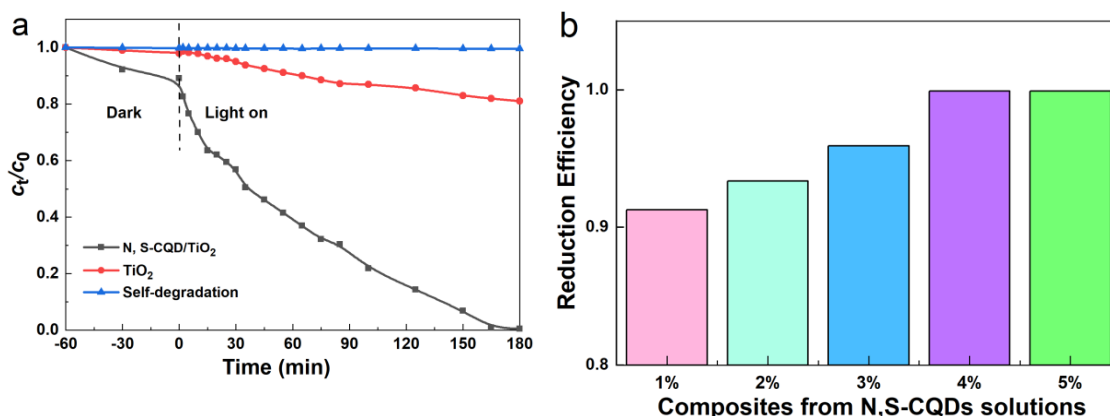


Figure 3. 3. Photocatalytic reduction of Cr (VI) over N, S-CQDs/TiO₂ prepared from 4% N, S-CQDs solution) (a); efficiency of photoreduction of Cr (VI) by N, S-CQDs/TiO₂ composites prepared from different weight percentages of N, S-CQDs solutions

The reduction efficiencies of Cr (VI) by N, S-CQDs/TiO₂ composites prepared by impregnation of TiO₂ into 1.0-5.0 w% of N, S-CQDs solutions are illustrated in Fig. 3.3b. Results indicated that the amounts of N, S-CQDs embedded on TiO₂ increase with the increasing concentration of N, S-CQDs solutions. Nonetheless, there is no significant increase of the embedded N, S-CQDs when solution concentration is equal or higher than 4.0%. As such, the N, S-CQDs/TiO₂ composite prepared by impregnating TiO₂ with 4.0 w% of N, S-CQDs solution were used for all the subsequent experiments.

3.3.3 Effect of pH on photocatalytic performance

In an aqueous solution, the relative fractional abundance of Cr (VI) species (e.g. H₂CrO₄(aq), HCrO₄⁻, Cr₂O₇²⁻, and CrO₄²⁻) varies with pH [7, 50]. To investigate the pH effect on the photocatalytic performance of the prepared N, S-CQDs/TiO₂ composite, reduction of Cr (VI) was carried out under different pH (2.0, 3.0, 4.0, and 5.8*) of initial Cr (VI) solutions.

As seen from Fig. 3.4a, the N, S-CQDs/TiO₂ composite can reduce Cr (VI) more efficiently under acidic conditions. With the increase of solution pH, the final reduction rate decreases from 99.88% at pH2.0 to 75.70% at pH3.0, 62.90% at pH4.0 and 46.18% at pH5.8. This is due to the increase in the amount of negative surface charge on the N, S-CQDs/TiO₂ with increasing solution pH, which leads to the increased electrostatic repulsion between the catalyst and Cr (VI) species. Consequently, the migration of Cr (VI) species to the surface of the catalyst was inhibited, resulting in the reduced Cr (VI) reduction rate.

The influence of solution pH on the reduction kinetics was determined (Fig. 3.4b) using the first and second order kinetic equations (Eq. (3-4) & Eq. (3-5)) and the derived reduction rate constants were summarized in Table 3.1. Results from Fig. 3.4b and Table 3.1 reveal that the reduction rate constants also decrease with the increasing solution pH.

* pH5.8 is the natural pH value of the Cr (VI) aqueous solution

$$\ln(c_t/c_0) = -k_1 t \quad (3-4)$$

$$\frac{1}{c_t} - \frac{1}{c_0} = k_2 t \quad (3-5)$$

where k_1 is the apparent 1st order rate constant, k_2 is the 2nd order rate constant, and t is the time.

Results from Table 3.1 indicated that the 1st order rate equation provided better description of the experimental kinetic data than the 2nd order rate equation.

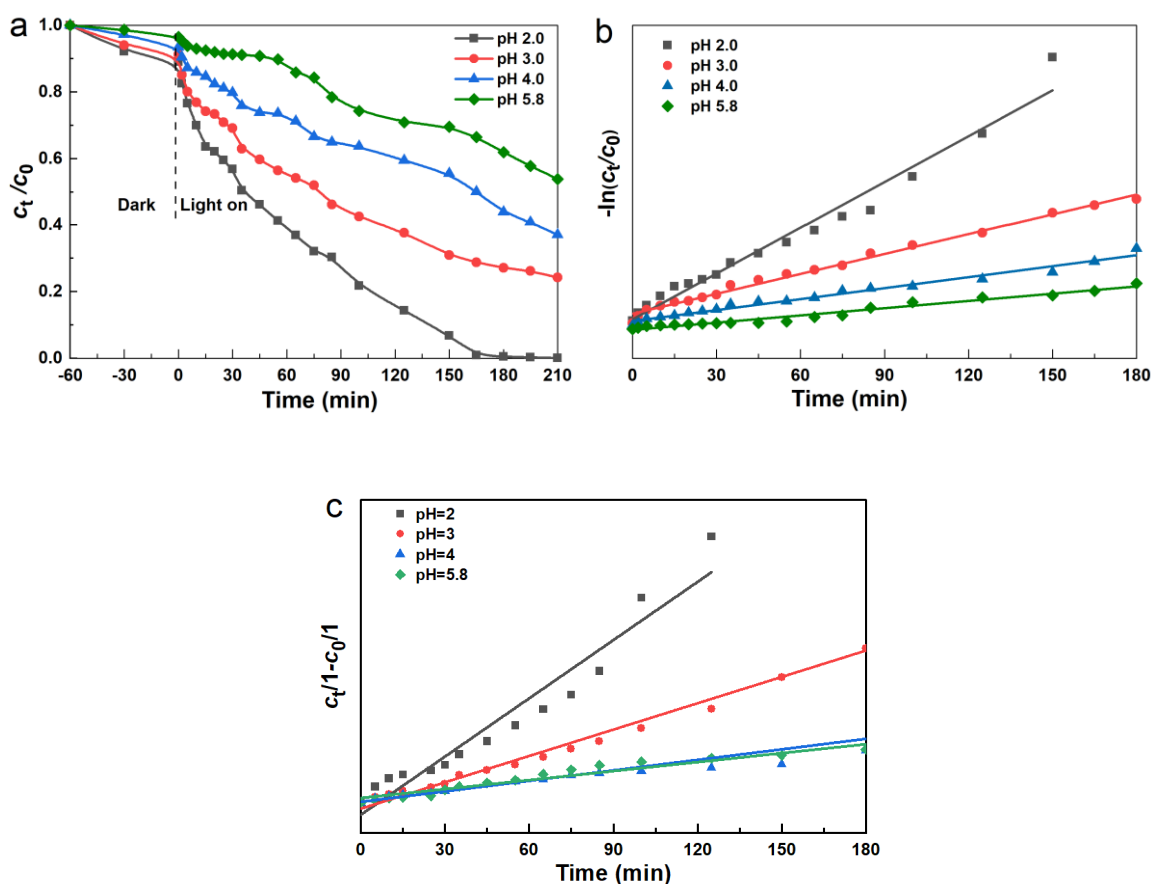


Figure 3. 4. Photocatalytic degradation of Cr (VI) at different pH values by N, S-CQDs/TiO₂ under visible light irradiation (a), first-order (b) and second order (c) reduction kinetics of Cr (VI) at different pH values. Reaction condition: Cr (VI) concentration = 20.0 mg/L, catalyst dosage = 1.0 g/L.

Table 3.1 Reduction rate constants of Cr (VI) at different pH by N, S-CQDs/TiO₂ under visible light irradiation.

Catalyst dosage (g/L)	c_0 (mg/L)	Solution pH	1 st order		2 nd order	
			k_1 (min ⁻¹)	R ²	k_2 (L mg ⁻¹ min ⁻¹)	R ²
1.0	20.0	2.0	2.49×10^{-2}	0.849	3.2×10^{-2}	0.79
1.0	20.0	3.0	6.48×10^{-3}	0.991	1.45×10^{-2}	0.985
1.0	20.0	4.0	3.57×10^{-3}	0.990	5.77×10^{-3}	0.874
1.0	20.0	5.8	2.35×10^{-3}	0.983	4.93×10^{-3}	0.945

3.3.4 Effect of initial concentration of Cr (VI)

The effects of initial concentration of Cr (VI) on the photocatalytic activity of the N, S-CQDs/TiO₂ nanocomposite were also studied with the results being illustrated in Fig. 3.5. With the same catalyst dosage, reaction temperature and solution pH, the reduction efficiency of Cr (VI) decreases when higher initial concentration of Cr (VI) was used. This is obvious because there is a maximum of active sites on the surface of the N, S-CQDs/TiO₂ nanocomposite (50.0 mg), which corresponds to a specific reduction capacity of Cr (VI). Moreover, photocatalyst deactivation is more severe in concentrated Cr (VI) solutions because more Cr(OH)₃ can be deposited on the surface of the photocatalyst. Finally, solution with high concentration of Cr (VI) absorbs more incident visible light, lowering the photon flux received by N, S-CQDs/TiO₂ nanocomposite and the penetration of incident visible light into Cr (VI) aqueous solution [51].

The first-order reduction rate constants of Cr (VI) with different initial Cr (VI) concentrations were determined by linear regression (Fig. 3.5b) and the derived rate constants were listed in Table 3.2.

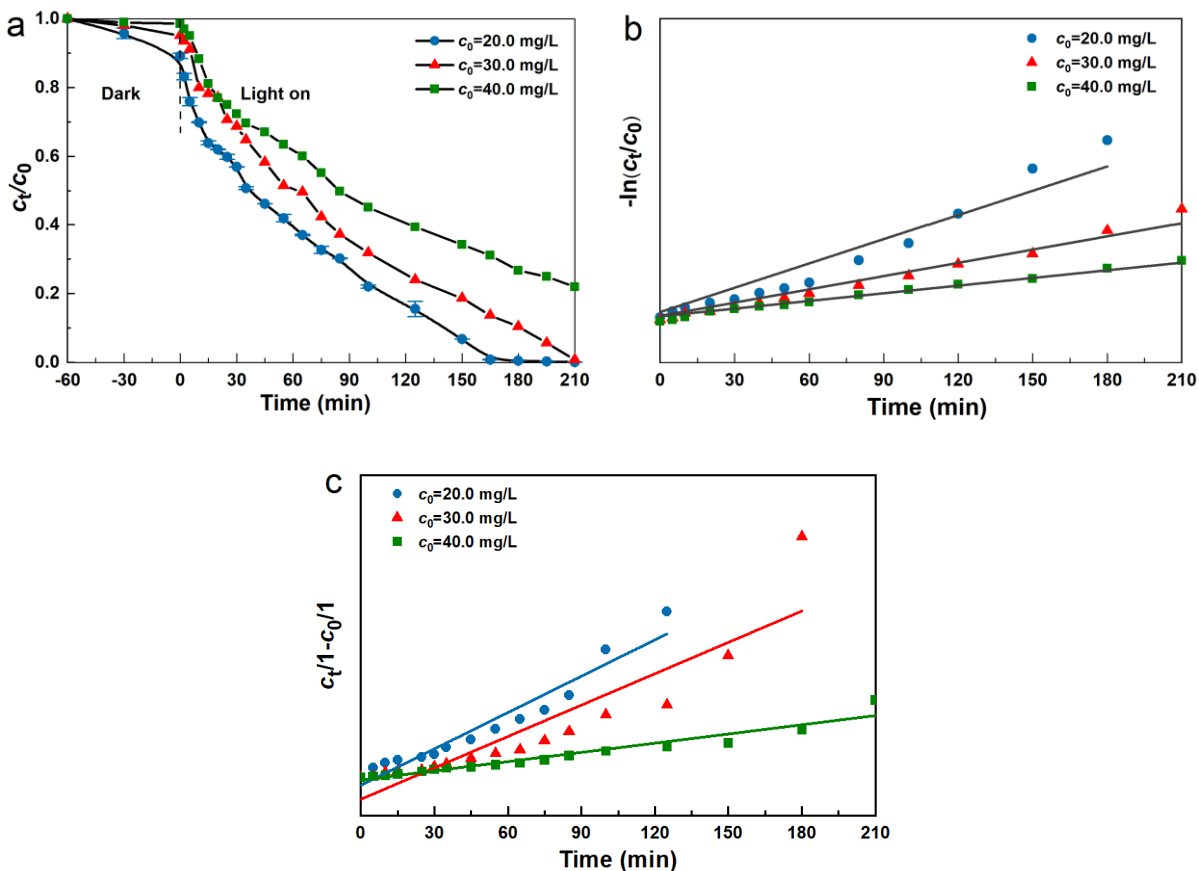


Figure 3.5. Photocatalytic degradation of Cr (VI) at different initial concentration by N, S-CQDs/TiO₂ under visible light irradiation (a), first-order (b) and second order (c) reduction kinetics of Cr (VI) at different initial concentration.

Table 3.2 Reduction rate constants of Cr (VI) at different initial concentration of Cr (VI) by N, S-CQDs/TiO₂ under visible light irradiation

Catalyst dosage (g/L)	c_0 (mg/L)	Solution pH	1 st order		2 nd order	
			k_1 (min ⁻¹)	R^2	k_2 (L mg ⁻¹ min ⁻¹)	R^2
1.0	20.0	3.0	2.00×10^{-2}	0.894	3.2×10^{-2}	0.929
1.0	30.0	3.0	1.09×10^{-2}	0.947	2.76×10^{-2}	0.825
1.0	40.0	3.0	6.31×10^{-3}	0.970	8.11×10^{-3}	0.930

3.3.5 Recyclability

To further verify the chemical stability and reusability of the prepared N, S-CQDs/TiO₂ composite, cyclic tests of photocatalytic reduction of Cr (VI) were carried out. After each photocatalytic reaction, the N, S-CQDs/TiO₂ powders were separated from the solution by centrifugation (4000 rpm for 25 minutes) and washed with DI water. After drying at 70 °C in an oven, the N, S-CQDs/TiO₂ composite was used for the next cycle of photoreduction experiment. The reusability studies for N, S-CQDs/TiO₂ in four reaction cycles are shown in Fig. 3.6. After two cycles, no detectable loss of photoactivity is observed, however, the photoreduction efficiency decreases by 18.0% after the fourth cycle. It may be due to the adsorption of oxide/hydroxide forms of Cr(III) (such as Cr(III)_xO_y and Cr(OH)₃) onto the surfaces of N, S-CQDs/TiO₂ nanocomposite, which could not be efficiently removed by washing [52]. It's also probable that Ti–O–C connection cleaved after four reaction cycles, leading to the reduced photocatalytic activity [53].

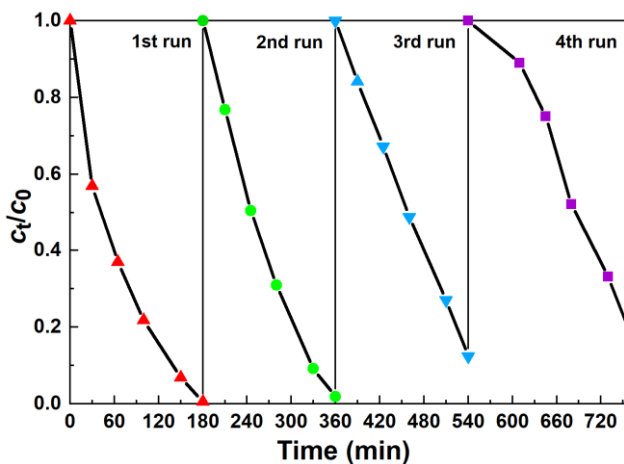


Figure 3. 5. Reusability of N, S-CQDs/TiO₂ nanocomposites toward degradation of Cr (VI) for four reaction cycles.

3.3.6 Photocatalytic reduction mechanisms

Based on the above results and discussions, it is very clearly that the incorporation of N, S-CQDs into TiO₂ leads to enhanced photocatalytic reduction of Cr (VI) in the aqueous medium. Such performance enhancement of N, S-CQDs/TiO₂ is attributed to the extended light absorption range and the reduced band gap energy of the composite. As seen from Figs. 3.1g and 3.2b, incorporating π -conjugated N, S-CQDs into TiO₂ significantly extend the light absorption edge and thus improve the visible light harvesting. Moreover, the electronic coupling of the π states of N, S-CQDs and the conduction band (CB) states of TiO₂ induces a narrower nano-hybrid band gap compared to pure TiO₂ and brings about a reduced band gap energy [16].

Based on the widely reported working mechanism of semiconductor photocatalysts, a possible pathway for the reduction of Cr (VI) by N, S-CQDs/TiO₂ composite under visible light irradiation was speculated. A schematic diagram of the plausible mechanism for Cr (VI) reduction was presented in Fig. 3.7. When the N, S-CQDs/TiO₂ composite is exposed to visible light ($\lambda \geq 420$ nm), the photon energy absorbed by the composite stimulates the generation of electrons (e⁻) from the VB of the composite, and the photo-excited electrons are then quickly transferred from VB to the CB of the composite, leaving holes (h⁺) in the VB of the composite. Holes in the VB are involved in the oxidation of H₂O to O₂, accompanied with the release of reactive protons (H⁺). The excited electrons reduce the toxic Cr (VI) species (mainly HCrO₄⁻ and Cr₂O₇²⁻ over pH2.0–6.0) to less toxic Cr (III) at the CB of the composite. The photocatalytic reduction of Cr (VI) by N, S-CQDs/TiO₂ can be described by the following reactions.





(3-8)

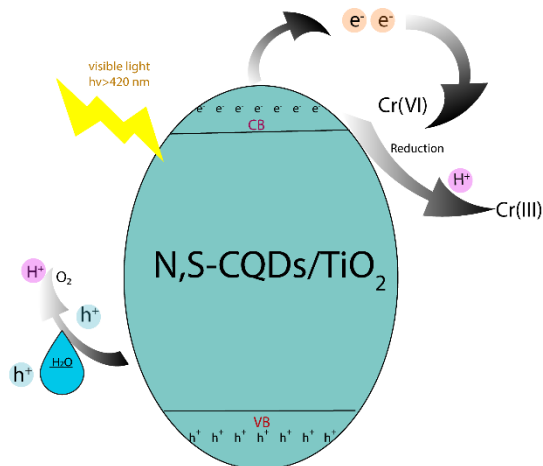


Figure 3. 6. Schematic diagram of photocatalytic reduction of Cr (VI) by N, S-CQDs/TiO₂ composite

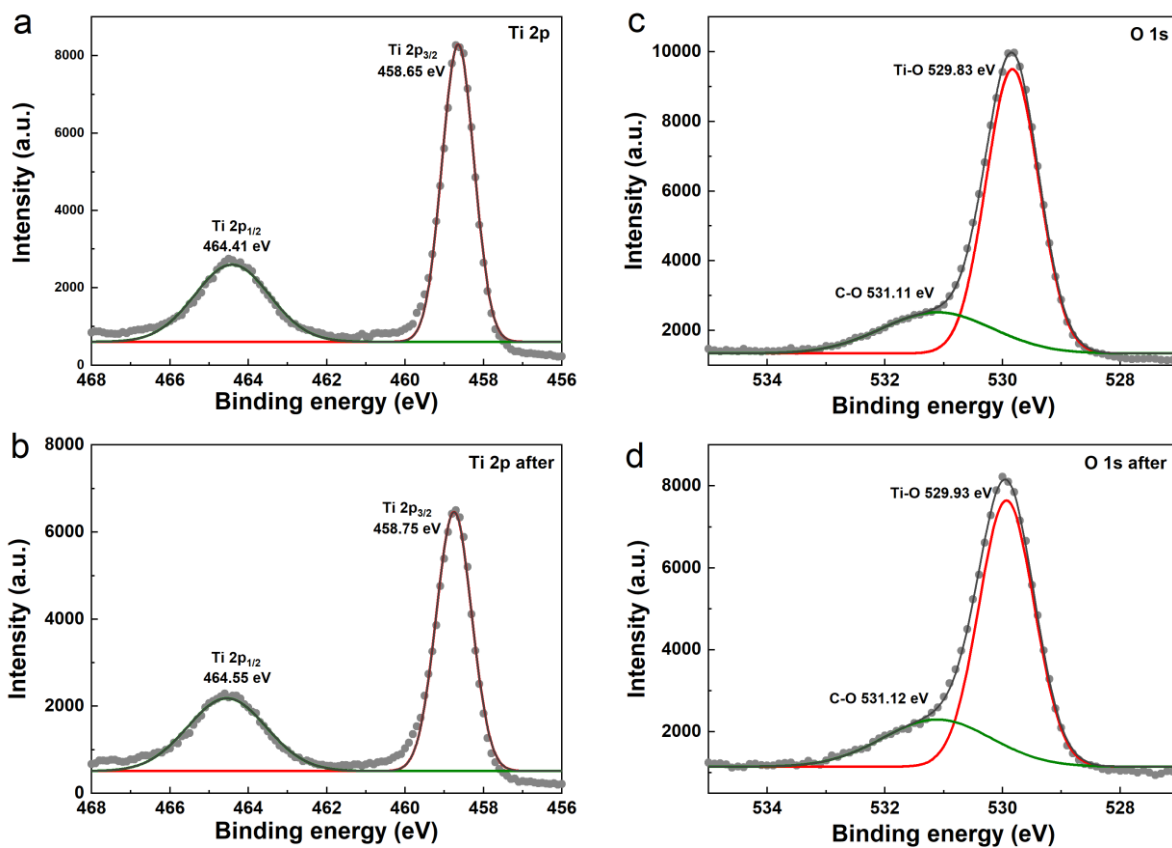


Figure 3. 7. High resolution XPS spectra and deconvoluted BE peaks of Ti 2p, and O 1s before and after photocatalytic reduction of Cr (VI)

To verify the speculated working mechanism of Cr (VI) reduction by N, S-CQDs/TiO₂, high resolution XPS spectra of Ti 2p, O 1s and Cr 2p of the composite before and after Cr (VI) reduction were measured. Fig. 3.8a shows the XPS spectrum of Ti 2p in the fresh composite, which has the doublet at 458.65 and 464.41 eV, responsible for Ti 2p_{3/2} and Ti 2p_{1/2}, correspondingly [54]. After Cr (VI) reduction, the binding energy (BE) peaks of Ti 2p_{3/2} and Ti 2p_{1/2} shift toward higher binding energy (Fig. 3.8b) to 458.75 and 464.55 eV, revealing that Ti donates electrons during the photocatalytic reduction process. In the O 1s XPS spectrum of the fresh catalyst (Fig. 3.8c), two deconvoluted BE peaks at 529.83 and 531.11 eV are attributed to the Ti–O, C–O of the Ti-O-C bond formed in the prepared composite. After Cr (VI) reduction, the corresponding peaks all shift slightly to high BE positions at 529.93 and 531.12 eV (Fig. 3.8d) [55, 56]. No significant BE peaks of Cr 2p were observed from N, S-CQDs/TiO₂ before and after Cr (VI) reduction, indicating that the reduction of Cr (VI) was not accompanied by the formation of Cr(OH)₃ (precipitate) significantly. XPS results prove that that the photo-generated electrons contribute to Cr (VI) reduction under visible light irradiation.

3.4 Reduction of Cr (VI) from Real Water Samples

To further test the stability and photocatalytic activity of the as-prepared N, S-CQDs/TiO₂ composite, reduction of Cr (VI) in real water samples were conducted under the same reactions conditions as those in DI water. The surface water collected from Robin Hood Bay Landfill (NL, Canada) was selected to replace DI water for the photocatalytic reduction of Cr (VI). Fig. 3.9 shows the reduction kinetics of Cr (VI) from surface water with two different initial concentrations. It can be seen from Fig. 3.9 that the 98.0% and 89.0% of Cr (VI) has been removed and reduced by N, S-CQDs/TiO₂ from surface water within 3 hours with initial concentrations of Cr (VI) being 20.0 and 40.0 mg/L, respectively. The reduction rate constants are 0.0283 and 0.0125 min⁻¹ for the

two cases as illustrated in the inset of Fig. 3.9. These results reveal that the prepared N, S-CQDs/TiO₂ nanocomposite can effectively reduce Cr (VI) from real water samples under visible light irradiation.

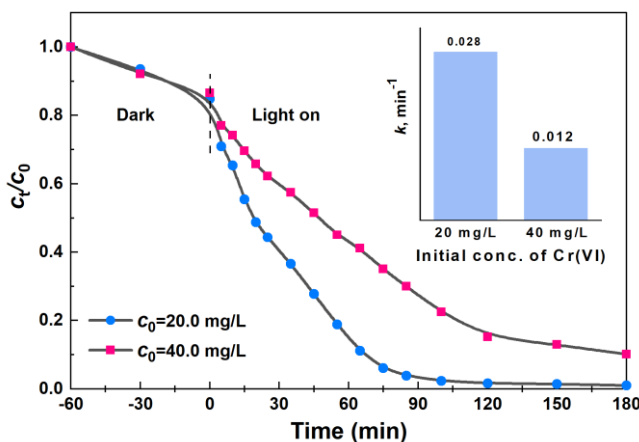


Figure 3. 8. Photocatalytic degradation of Cr (VI) from surface wastewater by N, S-CQDs/TiO₂ with different initial concentration of Cr (VI)

3.5 Conclusion

In this study, a facile method was employed to prepare the N, S-CQDs/TiO₂ nanocomposite as visible-light-responsive photocatalyst to reduce Cr (VI) under acidic conditions. The prepared nanocomposite was characterized using TEM, FTIR, XPS, XRD, UV-Vis DRS and PL spectroscopy. N, S-CQDs/TiO₂ exhibited an extended photo absorption range, enhanced charge separation and photocatalytic ability. The effects of the N, S-CQDs contents in the composite, the pH of Cr (VI) solution, and the initial concentration of Cr (VI) were investigated to optimize the photocatalytic reduction of Cr (VI) under visible light ($\lambda \geq 420$ nm) irradiation. Our experimental results indicate that the N, S-CQDs/TiO₂ nanocomposite prepared by impregnation of TiO₂ with 4 wt% of N, S-CQDs solutions exhibited the highest reduction performance at pH2.0, leading to complete reduction of Cr (VI) with the initial Cr (VI) concentration being 20.0 mg/L. Moreover,

the N, S-CQDs/TiO₂ composite showed rather good reusability, still being able to reduce ~90% of Cr (VI) from aqueous solution during the fourth reaction cycle. The decrease in reduction efficiency of the prepared composite is mainly due to the exfoliation of N, S-CQDs from the surface of TiO₂ particles.

References

- [1] J. Liu, K. Huang, K. Xie, Y. Yang, H. Liu, An ecological new approach for treating Cr(VI)-containing industrial wastewater: photochemical reduction, *Water Res.* 93 (2016), 187–194.
- [2] Z. Chen, Y. Li, M. Guo, F. Xu, P. Wang, Y. Du, P. Na, One-pot synthesis of Mn-doped TiO₂ grown on graphene and the mechanism for removal of Cr(VI) and Cr(III), *J. Hazard. Mater.* 310 (2016), 188–198.
- [3] A. Zhitkovich, Chromium in drinking water: Sources, metabolism, and cancer risks, *Chem. Res. Toxicol.* 24 (2011), 1617–1629.
- [4] H. Chen, Y. Shao, Z. Xu, H. Wan, Y. Wan, S. Zheng, D. Zhu, Effective catalytic reduction of Cr(VI) over TiO₂ nanotube supported Pd catalysts, *Appl. Catal. B Environ.* 105(2011), 255–262.
- [5] Y. Gao, W. Sun, W. Yang, Q. Li, Palladium nanoparticles supported on amine-functionalized glass fiber mat for fixed-bed reactors on the effective removal of hexavalent chromium by catalytic reduction, *J. Mater. Sci. Technol.* 34 (2018), 961–968.
- [6] J. J. Testa, M. A. Grela, M. I. Litter, Heterogeneous photocatalytic reduction of chromium(VI) over TiO₂ particles in the presence of oxalate: Involvement of Cr(V) species, *Environ. Sci. Technol.* 38 (2004), 1589–1594.
- [7] B. A. Marinho, R. O. Cristóvão, R. Djellabi, J. M. Loureiro, R. A. R. Boaventura, V. J. P. Vilar, Photocatalytic reduction of Cr(VI) over TiO₂-coated cellulose acetate monolithic structures using solar light, *Appl. Catal. B Environ.* 203 (2017), 18–30.
- [8] G. Yuan, F. Li, K. Li, J. Liu, J. Li, S. Zhang, Q. Jia, H. Zhang, Research progress on photocatalytic reduction of Cr(VI) in polluted water, *Bull. Chem. Soc. Jpn.* 94 (2021), 1142–1155.
- [9] C.-Y. Chen, T.-C. Wei, J.-Y. Li, Broadband photocatalytic activity of mesoporous Cd(II)-doped TiO₂, *ChemistrySelect* 2 (2017), 3648–3656.
- [10] Z. Jin, Y.-X. Zhang, F.-L. Meng, Y. Jia, T. Luo, X.-Y. Yu, J. Wang, J.-H. Liu, X.-J. Huang, Facile synthesis of porous single crystalline ZnO nanoplates and their application in photocatalytic reduction of Cr(VI) in the presence of phenol, *J. Hazard. Mater.* 276 (2014), 400–407.
- [11] S. Wojtyła, T. Baran, Insight on doped ZnS and its activity towards photocatalytic removing of Cr(VI) from wastewater in the presence of organic pollutants, *Mater. Chem. Phys.* 212 (2018), 103–112.

- [12] C. Hou, Y. Zhang, J. Li, A. Zhu, In-situ hydrothermal synthesis of CeO₂/SnS₂ heterojunction for use as a new efficient visible-light-driven photocatalyst, *Mater. Lett.* 213(2018), 154–157.
- [13] L. Zhang, C.-G. Niu, X.-J. Wen, H. Guo, X.-F. Zhao, D.-W. Huang, G.-M. Zeng, A facile strategy to fabricate hollow cadmium sulfide nanospheres with nanoparticles-textured surface for hexavalent chromium reduction and bacterial inactivation, *J. Colloid Interface Sci.* 514 (2018), 396–406.
- [14] J.-C. Wang, J. Ren, H.-C. Yao, L. Zhang, J.-S. Wang, S.-Q. Zang, L.-F. Han, Z.-J. Li, Synergistic photocatalysis of Cr(VI) reduction and 4-Chlorophenol degradation over hydroxylated α -Fe₂O₃ under visible light irradiation, *J. Hazard. Mater.* 311 (2016), 11–19.
- [15] F. Zhang, Y. Zhang, G. Zhang, Z. Yang, D.D. Dionysiou, A. Zhu, Exceptional synergistic enhancement of the photocatalytic activity of SnS₂ by coupling with polyaniline and N-doped reduced graphene oxide, *Appl. Catal. B Environ.*, 236 (2018), 53–63.
- [16] Y. Zhang, K. Hawboldt, J. Zhang, J. Lu, L. Chang, A. Dwyer, Carbonaceous nanomaterial-TiO₂ heterojunctions for visible-light-driven photocatalytic degradation of aqueous organic pollutants, *Appl. Catal. A-Gen.* 630 (2022), 118460.
- [17] K.R. Reddy, M. Hassan, V.G. Gomes, Hybrid nanostructures based on titanium dioxide for enhanced photocatalysis, *Appl. Catal. A-Gen.* 489 (2015), 1–16.
- [18] K. Lee, H. Yoon, C. Ahn, J. Park, S. Jeo, Strategies to improve the photocatalytic activity of TiO₂: 3D nanostructuring and heterostructuring with graphitic carbon nanomaterials, *Nanoscale* 11 (2019), 7025–7040.
- [19] K.A.S. Fernando, S. Sahu, Y. Liu, W.K. Lewis, E.A. Gulians, A. Jafariyan, P. Wang, C.E. Bunker, Y.-P. Sun, Carbon quantum dots and applications in photocatalytic energy conversion, *ACS Appl. Mater. Interfaces* 7 (2015), 8363–8376.
- [20] H. Li, D. Huang, L. Qin, G. Zeng, C. Lai, M. Cheng, S. Ye, B. Song, X. Ren, X. Guo, Selective prepared carbon nanomaterials for advanced photocatalytic application in environmental pollutant treatment and hydrogen production, *Appl. Catal. B: Environ.* 239(2018), 408–424.
- [21] S. Y. Lim, W. Shen, Z. Gao, Carbon quantum dots and their applications, *Chem. Soc. Rev.* 44 (2015), 362–381.
- [22] R. Liu, H. Li, L. Duan, H. Shen, Y. Zhang, X. Zhao, In situ synthesis and enhanced visible light photocatalytic activity of C-TiO₂ microspheres/carbon quantum dots, *Ceram. Int.*, vol. 43 (2017), 8648–8654.

- [23] J. Zhang, Q. Liu, H. He, F. Shi, G. Huang, B. Xing, J. Jia, C. Zhang, Coal tar pitch as natural carbon quantum dots decorated on TiO₂ for visible light photodegradation of rhodamine B, *Carbon* 152 (2019), 284–294.
- [24] C. Burda, X. Chen, R. Narayanan, M.A. El-Sayed, Chemistry and properties of nanocrystals of different shapes, *Chem. Rev.* 105 (2005), 1025–1102.
- [25] H. Li, X. He, Z. Kang, H. Huang, Y. Liu, J. Liu, S. Lian, C.H.A. Tsang, X. Yang, S.-T. Lee, Water-soluble fluorescent carbon quantum dots and photocatalyst design, *Angew. Chem. Int. Ed.* 49 (2010), 4430–4434.
- [26] S. Kim, B.-K. Yoo, Y. Choi, B.-S. Kim, O.-H. Kwon, Time-resolved spectroscopy of the ensembled photoluminescence of nitrogen- and boron/nitrogen-doped carbon dots. *Phys. Chem. Chem. Phys.* 20 (2018), 11673–11681.
- [27] J. Zhou, X. Shan, J. Ma, Y. Gu, Z. Qian, J. Chen, H. Feng, Facile synthesis of P-doped carbon quantum dots with highly efficient photoluminescence. *RSC Adv.* 4 (2014), 5465–5468.
- [28] Q. Xu, P. Pu, J. Zhao, C. Dong, C. Gao, Y. Chen, J. Chen, Y. Liu, H. Zhou, Preparation of highly photoluminescent sulfur-doped carbon dots for Fe (III) detection. *J. Mater. Chem. A*, 3 (2015), 542–546.
- [29] D. Lu, P. Fang, W. Wu, J. Ding, L. Jiang, X. Zhao, C. Li, M. Yang, Y. Li, D. Wang, Solvothermal-assisted synthesis of self-assembling TiO₂ nanorods on large graphitic carbon nitride sheets with their anti-recombination in the photocatalytic removal of Cr(VI) and rhodamine B under visible light irradiation, *Nanoscale* 9 (2017), 3231–3245.
- [30] Y. Li, Z. Liu, Y. Wu, J. Chen, J. Zhao, F. Jin, P. Na, Carbon dots-TiO₂ nanosheets composites for photoreduction of Cr(VI) under sunlight illumination: Favorable role of carbon dots, *Appl. Catal. B Environ.* 224 (2018), 508–517.
- [31] C. Shi, H. Qi, Z. Sun, K. Qu, Z. Huang, J. Li, M. Dong, Z. Guo, Carbon dot-sensitized urchin-like Ti³⁺ self-doped TiO₂ photocatalysts with enhanced photoredox ability for highly efficient removal of Cr⁶⁺ and RhB, *J. Mater. Chem. C* 8 (2020), 2238–2247.
- [32] L. Xu, L. Yang, X. Bai, X. Du, Y. Wang, P. Jin, Persulfate activation towards organic decomposition and Cr(VI) reduction achieved by a novel CQDs-TiO₂-x/rGO nanocomposite, *Chem. Eng. J.* 373 (2019), 238–250.
- [33] D. Choi, S. Ham, D.-J. Jang, Visible-light photocatalytic reduction of Cr(VI) via carbon quantum dots decorated TiO₂ nanocomposites, *J. Environ. Chem. Eng.* 6 (2018), 1–8.

- [34] L. Xu, X. Bai, L. Guo, S. Yang, P. Jin, L. Yang, Facial fabrication of carbon quantum dots (CDs)-modified N-TiO_{2-x} nanocomposite for the efficient photoreduction of Cr(VI) under visible light, *Chem. Eng. J.* 357 (2019), 473–486.
- [35] S. Zhu, Q. Meng, L. Wang, J. Zhang, Y. Song, H. Jin, K. Zhang, H. Sun, H. Wang, Y. Bai, Highly photoluminescent carbon dots for multicolor patterning, sensors, and bioimaging, *Angew. Chem. Int. Ed.* 52 (2013), 3953–3957.
- [36] R. Behnood, G. Sodeifian, Novel ZnCo₂O₄ embedded with S, N-CQDs as efficient visible-light photocatalyst, *J. Photochem. Photobiol. Chem.*, 405 (2021), 112971.
- [37] Z. Gao, Z. Lin, X. Chen, H. Zhang, Z. Huang, A fluorescent probe based on N-doped carbon dots for highly sensitive detection of Hg²⁺ in aqueous solutions, *Anal. Methods* 8(2016), 2297–2304.
- [38] D. Qu, M. Zheng, L. Zhang, H. Zhao, Z. Xie, X. Jing, R.E. Haddad, H. Fan, Z. Sun, Formation mechanism and optimization of highly luminescent N-doped graphene quantum dots, *Sci. Rep.* 4 (2014), 5294.
- [39] H. Ding, H.-M. Xiong, Exploring the blue luminescence origin of nitrogen-doped carbon dots by controlling the water amount in synthesis, *RSC Advance*, 5 (2015), 66528–66533.
- [40] M. Wu, Y. Wang, W. Wu, C. Hu, X. Wang, J. Zheng, Z. Li, B. Jiang, J. Qiu, Preparation of functionalized water-soluble photoluminescent carbon quantum dots from petroleum coke, *Carbon* 78 (2014), 480–489.
- [41] L. Qie, W. Chen, X. Xiong, C. Hu, F. Zou, P. Hu, Y. Huang, Sulfur-doped carbon with enlarged interlayer distance as a high-performance anode material for sodium-ion batteries, *Adv. Sci.* 2(2015), 1500195.
- [42] D. Saini, J. Kaushik, A.K. Garg, C. Dalai, S.K. Sonkar, N, S-codoped carbon dots for nontoxic cell imaging and as a sunlight-active photocatalytic material for the removal of chromium, *ACS Appl. Bio. Mater.* 3 (2020), 3656–3663.
- [43] K. Jiang, S. Sun, L. Zhang, Y. Lu, A. Wu, C. Cai, H. Lin, Red, green, and blue luminescence by carbon dots: full-color emission tuning and multicolor cellular imaging, *Angew. Chem. Int. Ed.* 54 (2015), 5360–5363.
- [44] H. Tian, K. Shen, X. Hu, L. Qiao, W. Zheng, N, S co-doped graphene quantum dots-graphene-TiO₂ nanotubes composite with enhanced photocatalytic activity, *J. Alloys Compd.* 691 (2017), 369–377.

- [45] M. Ouzzine, A.J. Romero-Anaya, M.A. Lillo-Ródenas, A. Linares-Solano, Spherical activated carbon as an enhanced support for TiO₂/AC photocatalysts, *Carbon*, 67 (2014), 104–118.
- [46] M.T. Genc, G. Yanalak, G. Arslan, I.H. Patir, Green preparation of carbon quantum dots using Ginkgo biloba to sensitize TiO₂ for the photohydrogen production, *Mater. Sci. Semicond. Process.* 109 (2020), 104945.
- [47] Y.-Q. Zhang, D.-K. Ma, Y.-G. Zhang, W. Chen, S.-M. Huang, N-doped carbon quantum dots for TiO₂-based photocatalysts and dye-sensitized solar cells, *Nano Energy*, 2 (2013), 545–552.
- [48] H. Eskandarloo, A. Badiei, M.A. Behnajady, TiO₂/CeO₂ Hybrid photocatalyst with enhanced photocatalytic activity: optimization of synthesis variables, *Ind. Eng. Chem. Res.* 53 (2014), 7847–7855.
- [49] T. Tachikawa, M. Fujitsuka, T. Majima, Mechanistic insight into the TiO₂ photocatalytic reactions: Design of new photocatalysts, *J. Phys. Chem. C* 111(2007), 5259–5275.
- [50] X. Gao, C. Guo, J. Hao, Y. Zhang, M. Li, Z. Zhao, Efficient removal of Cr (VI) by modified sodium alginate via synergistic adsorption and photocatalytic reduction, *Appl. Surf. Sci.* 579 (2022), 15225.
- [51] Y.C. Zhang, M. Yang, G. Zhang, D.D. Dionysiou, HNO₃-involved one-step low temperature solvothermal synthesis of N-doped TiO₂ nanocrystals for efficient photocatalytic reduction of Cr(VI) in water, *Appl. Catal. B Environ.* 142–143 (2013), 249–258.
- [52] W. Ji, In situ surface assembly of core-shell TiO₂-copper(I) cluster nanocomposites for visible-light photocatalytic reduction of Cr(VI), *Appl. Catal. B Environ.* 205 (2017), 368–375.
- [53] M. Rahbar, M. Mehrzad, M. Behpour, S. Mohammadi-Aghdam, M. Ashrafi, S, N co-doped carbon quantum dots/TiO₂ nanocomposite as highly efficient visible light photocatalyst, *Nanotechnology* 30 (2019), 505702.
- [54] W. Baran, E. Masternak, D. Sapińska, A. Sobczak, E. Adamek, Synthesis of new antibiotics derivatives by the photocatalytic method: A screening research, *Catalysts*, 11 (2021), 9-1102.
- [55] R. Zhang, S. Qi, J. Jia, B. Torre, H. Zeng, H. Wu, X. Xu, Size and refinement edge-shape effects of graphene quantum dots on UV–visible absorption, *J. Alloys Compd.*, 623 (2015), 186–191.
- [56] H. Yu, Y. Zhao, C. Zhou, L. Shang, Y. Peng, Y. Cao, Carbon quantum dots/TiO₂ composites for efficient photocatalytic hydrogen evolution, *J. Mater. Chem. A*, 2 (2014), 10-3344.

Chapter 4. Synergistic Photocatalytic Reduction of Cr (VI) and Erythromycin Degradation by Carbon Quantum Dots-Sensitized TiO₂ under visible-light irradiation

4.1 Introduction

Very similar to toxic heavy metal ions, persistent organic pollutants (POPs), such as dyes, pesticides, pharmaceuticals, endocrine disruptors, etc. can be found in all types of environmental compartments. POPs refer to intentionally or unintentionally produced chemicals that possess relatively high chemical resistance and are able to persist in the environment for several years or decades before breaking down [1, 2]. Many POPs are mutagenic and carcinogenic, some damage nerve and endocrine systems of human body and harm the ecological balance [3]. Their presence in the aquatic environment is currently a worldwide problem [4]. Even though various physical processes, such as adsorption, membrane filtration, coagulation and flocculation have been applied to remove POPs from the environment, these methods only concentrate or transfer the recalcitrant organic pollutants from water to solid phase [5]. Degradation of POPs is by far the most effective and economic method to eliminate them from the environment.

Over the last few decades, great efforts have been devoted to developing environmentally sustainable and energy-efficient degradation processes for POPs, among which biocatalysts [6], photocatalysis [7, 8] and electrocatalysis [9] have been widely investigated. Compared with biocatalysts and electrocatalysis, photocatalytic degradation of POPs demonstrates the advantages of high degradation efficiency, environmentally benign nature, use of solar light as a renewable energy source, and low cost [10, 11]. Typically, four steps are involved in the photocatalytic degradation of POPs, which include i) absorption of light (with energy higher than the band gap

energy) by photocatalysts (semiconductors); ii) separation of photogenerated electron-hole pairs within the semiconductors; iii) migration of charge carriers to the surface of photocatalysts; and iv) redox reactions between charge carriers and the target POPs [12]. It is apparent that the properties of photocatalysts play a key role in such degradation processes. Currently, developing non-toxic and visible-light active photocatalysts for degradation of POPs is crucial.

A variety of semiconductors have been fabricated for photocatalytic degradation of POPs under visible light irradiation. Narrow band-gap metal oxides/metal sulfides and their hybrids, such as WO_3 , BiOBr , CdS , Sn_3O_4 , $\text{CdS}/\text{CuInS}_2$, $\text{CeO}_2/\text{ZnIn}_2\text{S}_4$, $\text{MnWO}_4/\text{WO}_3$, etc., have been applied for visible-light driven photodegradation of POPs [12-16]. In general, these photocatalysts can degrade the refractory organic pollutants to low levels. Nonetheless, there is high probability of secondary pollution due to the leaching of heavy metal ions during the degradation process. As such, modification of non-toxic wide-band-gap semiconductors (e.g., TiO_2 , ZnO) for visible-light-driven photocatalytic degradation of POPs is a better option [1].

As discussed in Chapter 2, carbon quantum dots (CQDs) sensitized TiO_2 has been confirmed to be efficient in degrading various POPs under sunlight or visible-light irradiations. Many novel CQDs-sensitized TiO_2 composites have been fabricated for photocatalytic degradation of POPs over the past decade. CQDs loaded TiO_2 composites have been fabricated for the photocatalytic degradation of various dyes, e.g., methylene blue (MB), methyl orange (MO), rhodamine B (RhB), and acid red 88 (AR88) [17-20]. The band gap energies of the prepared CQDs/ TiO_2 composites were much narrower than that of pure TiO_2 , leading to the enhanced visible light absorption and significant improvement in the degradation efficiency of organic dyes. CQDs sensitized TiO_2 nanocomposites also demonstrate good photodegradation performance of phenols. A CQDs/ TiO_2 composite of 20:1 TiO_2 /CQDs mass ratio prepared by one-step sol-gel method was able to

completely degrade nonylphenol ethoxylate (50.0 mg/L) with a catalyst dosage of 1.0 g/L after 60 min exposure of visible light [21]. Recently, a novel photocatalytic membrane was fabricated by incorporating N, S-CQDs/TiO₂ nanocomposite on polysulfide membrane for the photodegradation of a pharmaceutical compound, diclofenac (DCF) in water. The prepared composite was able to degrade 62.3 % of DCF under visible light irradiation, which was 20-fold higher than that by pure TiO₂ under the same operating conditions [22]. So far, the application of CQDs-sensitized TiO₂ composites to the photodegradation of pharmaceutical compounds have not been widely reported, more efforts should be devoted to the development of efficient visible-light-active CQDs/TiO₂ composites for the degradation of antibiotics and the most used medicines to mitigate their environmental impacts.

Erythromycin (ERY, Fig. 4.1), an antibiotic widely used for the treatment of respiratory tract infections, skin infections, pelvic inflammatory disease and syphilis, was selected as an example of POPs in this study to test the photocatalytic activity of the N, S-CQDs/TiO₂ composite under visible-light irradiation. ERY can last up to a year while still acting as an antibiotic [23], and it was added to the US Environmental Protection Agency's Contaminants Candidate List 3 in 2009, and the European Union designated ERY as a high-risk priority substance in its Decision 2015/495/EU [24]. It is therefore important to develop effective degradation methods to eliminate the risky ERY from aquatic system.

In the current work, the N, S-CQDs/TiO₂ composite was used as a visible-light-active photocatalyst to reduce Cr (VI) and degrade ERY synergistically. The effects of initial substrate concentration, catalyst dosage, and effective radicals were thoroughly examined. The degradation kinetics data were obtained by linear regression. Based on the experimental results, a plausible mechanism for

the synergistic photocatalytic reduction of Cr (VI) and ERY degradation by N, S-CQDs/TiO₂ was proposed.

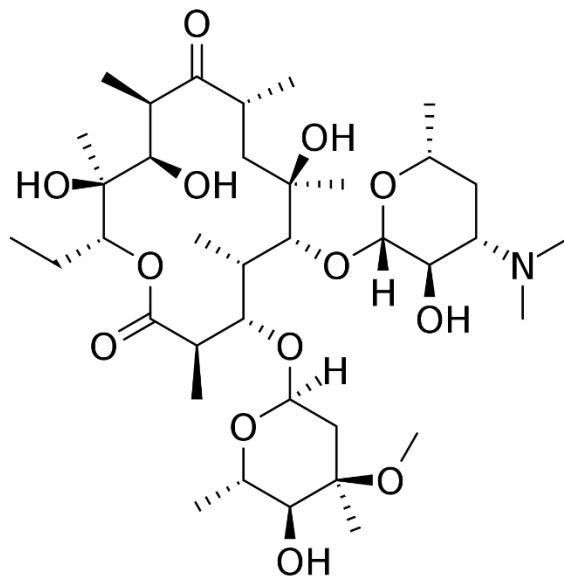


Figure 4. 1. The chemical structure of erythromycin [23]

4.2 Materials and Methods

4.2.1 Materials, synthesis, and characterization of N, S-CQDs/TiO₂

Citric Acid (99.9%), thiourea (99.4%), sodium sulfite, commercially P25 (TiO₂), sodium dichromate dihydrate (Na₂Cr₂O₇·2H₂O), diphenylcarbazine (DPC), erythromycin (C₃₇H₆₇NO₁₃, 99%), and analytical grade of sulfuric acid, hydrochloric acid, phosphoric acid, and sodium hydroxide were purchased from Fisher Scientific and were used as received without further purification. The ultrapure water was used as solvent in all the experiments.

The synthetic and characterization methods of the N, S-CQDs/TiO₂ are the same as those reported in Chapter 3. They are not repeated here for brevity. Based on the obtained photocatalytic reduction

results of Cr (VI), the N, S-CQDSs/TiO₂ composite prepared by immersing TiO₂ in 4.0 w% of N,S-CQDs solutions was used as the photocatalyst for synergistic removal of Cr (VI) and ERY in this work.

4.2.2 Synergistic photocatalytic reduction of Cr (VI) and ERY degradation

Batch experiments were carried out for the synergistic photocatalytic reduction of Cr (VI) and ERY degradation in a 100 ml jacketed reactor using N, S-CQD/TiO₂ composite as the catalyst irradiated by visible light (300-W xenon lamp, $\lambda \geq 420$ nm). The reaction temperature was controlled by a Julabo FP50-HL refrigerated/heating circulator. In a typical experiment, 50.0 mg of the N, S-CQDs/TiO₂ was added to 50.0 mL of Cr (VI)-ERY binary solutions (each with initial concentrations of 10.0, 20.0, 30.0, and 40.0 mg/L) in the reactor and the initial pH of the binary solutions was adjusted to 2.0 with 1.0 M H₂SO₄ and NaOH solutions. The suspension was stirred in dark for 1 h to eliminate the influence of adsorption, and then photocatalytic reactions were initiated by switching on the xenon lamp. At each sampling time (e.g., 2, 5, 10, 15, and 20 min ...to 180 min), 1.0 mL aliquot of suspension was withdrawn from the reactor and filtered using 0.22 μ m membrane filter. The Cr (VI) concentration was determined spectrophotometrically in the supernatant using the method as discussed in Chapter 3. The remaining ERY concentration in the solution was analyzed by an Agilent HPLC-MS system equipped with a C18 column (5 μ m, 250 \times 4.6 mm) with a UV detector at 365 nm. A mixture of ethanol and water at a 40:60 (v/v) ratio was used as the mobile phase with a flow rate of 1.0 mL/min at 25 °C. The sample injection volume was 10 μ L.

Four scavengers were utilised in binary degradation to identify the active radical species. Triethanolamine (TEOA, 10 mmol/L), benzoquinone (BQ, 10 mmol/L), isopropyl alcohol (IPA, 10 mmol/L), and ethanol (10 mmol/L) were employed as scavengers of holes (h⁺), electrons (e⁻),

$\bullet\text{OH}$, and $\text{O}_2^{\bullet-}$ respectively. During the experiments, one kind of radical scavenger was added to the reaction suspension and the other conditions remained the same ($\text{pH}=2$, $T=30\text{ }^\circ\text{C}$, photocatalyst dosage is 1.0 g/L).

4.3. Results and Discussion

4.3.1 Characterization

XPS was employed to characterize the chemical composition of the N, S-CQDs-TiO₂ composite. The XPS survey spectrum of N, S-CQDs-TiO₂ nanocomposite in Fig. 4.2 revealed that the composite was mainly made up of Ti, O, N, and C with O/Ti atom ratio very close to 2.0, indicating no variation in the metal oxide surface composition, and confirmed the presence of N, S-CQDs deposited on TiO₂ albeit the content level of N, S-CQDs in the composite is very low.

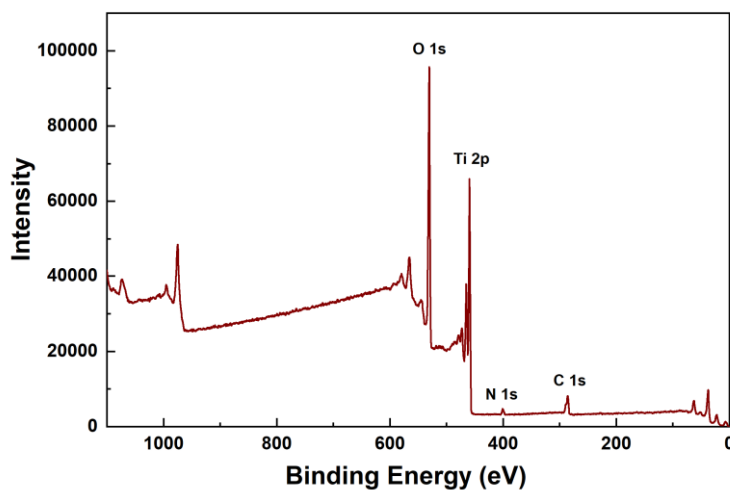


Figure 4. 2. XPS survey spectrum of N, S-CQDs/TiO₂

4.3.2 Photocatalytic study of N, S-CQDs/TiO₂ nanocomposite

The photocatalytic behaviour of the nanocomposite was investigated under visible light irradiation ($\lambda_{\text{ex}} \geq 420$ nm) for simultaneous photocatalytic reduction of Cr (VI) and ERY degradation. Figure 4.3 displays the variations of Cr (VI) and ERY concentrations versus irradiation time in the presence of N, S-CQDs/TiO₂ and pure TiO₂. As seen from Fig. 4.3a, the capacity of the N, S-CQDs/TiO₂ composite to reduce Cr (VI) was much greater than that of pure TiO₂. After 180 min exposure of visible light, Cr (VI) was completely reduced to Cr (III) by N, S-CQDs/TiO₂, whereas only 2.7% of Cr (VI) was reduced to Cr (III) by TiO₂. Two main causes contributed to the performance improvement by N, S-CQDs/TiO₂. Firstly, incorporation of N, S-CQDs into TiO₂ helped to increase the visible-light-harvesting efficiency. Secondly, consumption of h⁺ by the degradation of ERY at the valence band prevented the recombination of photogenerated electron-hole pairs, leading to complete degradation of ERY and reduction of Cr (VI). In the absence of photocatalysts, reduction of Cr (VI) was undetectable, illustrating that Cr (VI) is stable under visible light.

According to the experimental results presented in chapter 3, acidic environment is favorable to Cr (VI) reduction, as such, synergistic Cr (VI) reduction and ERY degradation experiments by N, S-CQDs/TiO₂ were also performed at low pH (pH 2.0). However, the acidic environment has strong influence on the ERY degradation because ERY is not stable and can self-degrade under the acidic conditions. Results from Fig. 4.3b indicated that without the use of any catalysts and the exposure of visible light, about 47.0% of ERY degraded within 1 h. Nonetheless, the use of N, S-CQDs/TiO₂ in photocatalytic degradation process did help the attainment of the complete degradation of ERY after 3 h of visible light irradiation, compared with the other two scenarios in which 69.0% of ERY degraded without the use of any catalysts and about 73.0% of ERY degraded

with pure TiO_2 being used as the photocatalyst. The main reason for the increased ERY degradation by N, S-CQDs/ TiO_2 lies in the fact that more H^+ can be produced from the H_2O oxidation by holes under the visible light irradiation compared with that by pure TiO_2 . Results from Fig. 4.3 reveal that acid conditions are beneficial to both Cr (VI) reduction and ERY degradation.

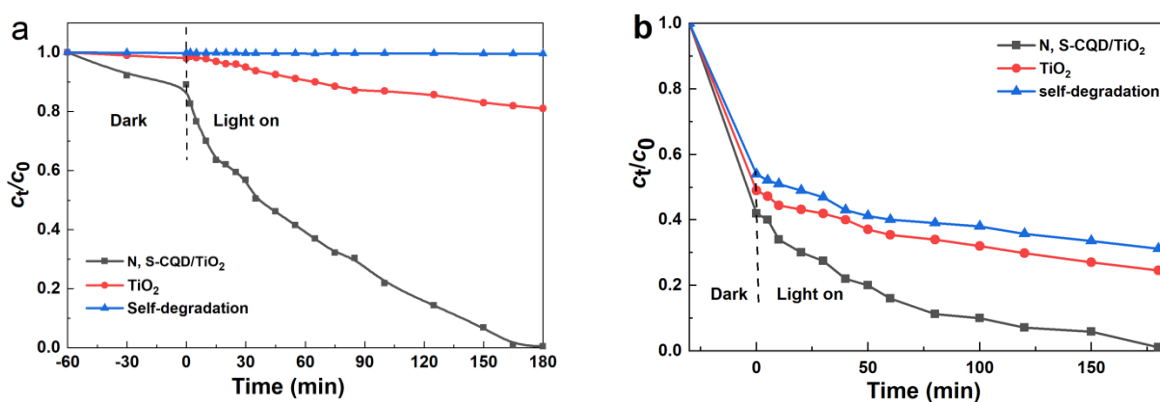


Figure 4. 3. Photocatalytic reduction of Cr (VI) (a) and ERY degradation (b) over TiO_2 and N, S-CQDs/ TiO_2

4.3.3 Effect of initial concentrations of Cr (VI) and ERY

The effect of initial concentrations of Cr (VI) and ERY in the Cr (VI)-ERY system on the synergistic reduction-degradation efficiency was presented in Fig. 4.4. When relatively low initial concentration (20.0 mg/L for each) was used, complete reduction of Cr (VI) and complete degradation of ERY were achieved by N, S-CQDs/ TiO_2 within 3 h of visible light irradiation. When the initial concentration increased to 30.0 and 40.0 mg/L, ERY degradation efficiency was reduced to 96.0% and 90 %, respectively, whereas the reduction rate of Cr (VI) was 100.0% and 93.0% respectively. Compared to single Cr (VI) reduction system, the reduction efficiency of Cr (VI) in binary system is better. This can be explained by the fact that electrons and holes can both

be utilized in a binary system, lowering the rate of electron-hole recombination, which resulted in improved photocatalytic performance.

The influence of initial concentrations on the reduction and degradation kinetics have been determined using the first- and second-order kinetic equations (Eq. 4-1 and Eq. 4-2) and the derived reduction rate constants are summarized in Table 4.1 and Table 4.2 respectively. Results from Fig. 4.4 as well as Tables 4.1 and 4.2 indicate that rate constants of Cr (VI) reduction and ERY degradation decrease with the increasing initial concentrations and the 1st order rate equation better describes the experimental kinetic data in general.

$$\ln(c_t/c_0) = -k_1 t \quad (4-1)$$

$$\frac{1}{c_t} - \frac{1}{c_0} = k_2 t \quad (4-2)$$

where k_1 is the 1st order rate constant, k_2 is the 2nd order rate constant, and t is the time.

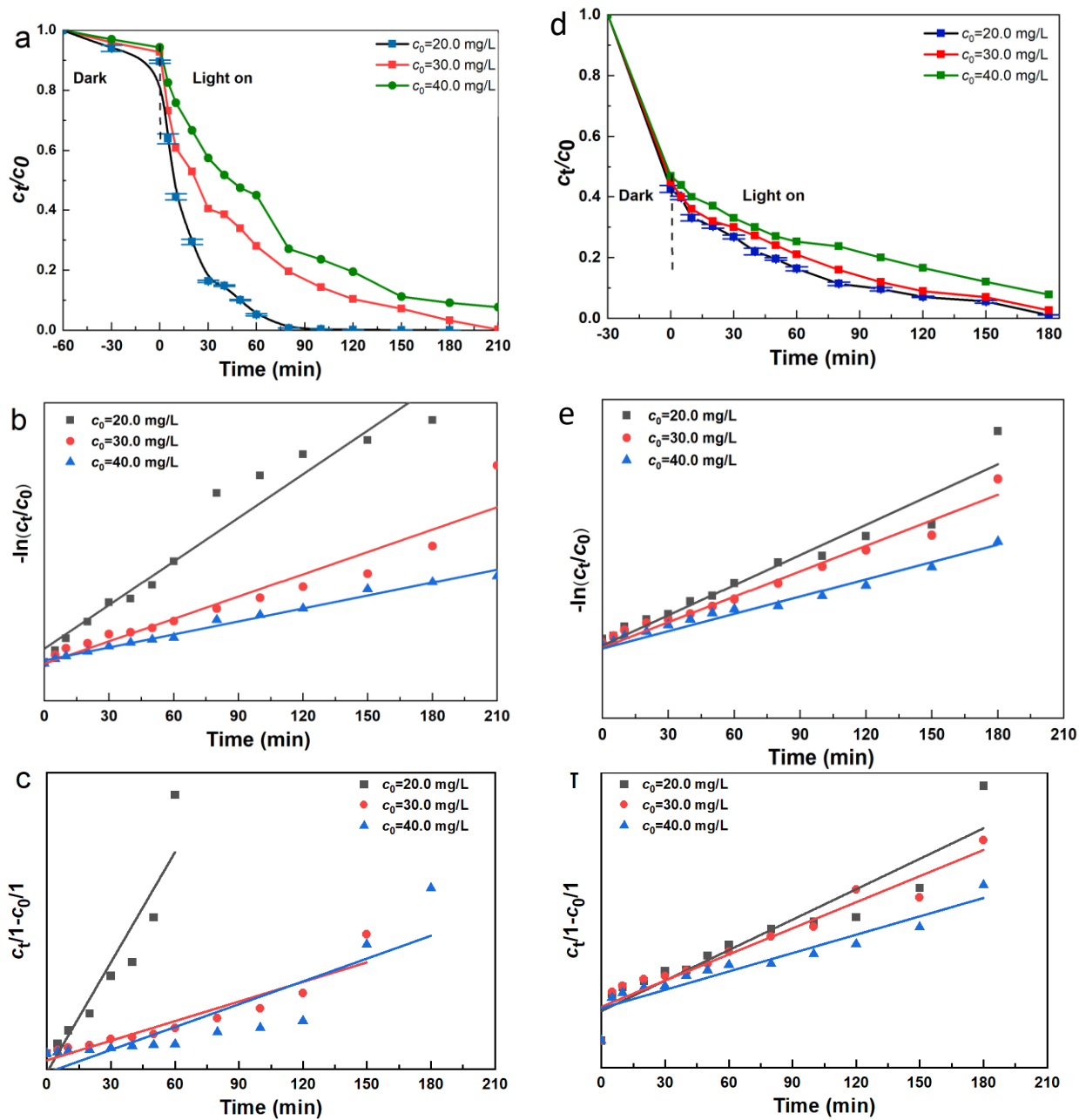


Figure 4. 4. Photocatalytic reduction of Cr (VI) (a, b & c) and ERY degradation (d, e & f) by N, S-CQDs/TiO₂ at different initial concentrations

Table 4.1 The 1st order rate constants of Cr (VI) reduction and ERY degradation at different initial concentrations by N, S-CQDs/TiO₂ under visible light irradiation

c_0 (Cr (VI)) mg/L	c_0 (ERY) mg/L	$k_{Cr(VI)}$ min ⁻¹	R^2	k_{ERY} L mg ⁻¹ min ⁻¹	R^2
20.0	20.0	4.15×10^{-2}	0.843	1.73×10^{-2}	0.945
30.0	30.0	2.13×10^{-2}	0.912	1.47×10^{-2}	0.971
40.0	40.0	1.23×10^{-2}	0.986	9.98×10^{-3}	0.944

*Note: Catalyst dosage: 1.0 g/L, solution pH: 2.5 for all reactions.

Table 4.2 The 2nd order rate constants of Cr (VI) reduction and ERY degradation at different initial concentrations by N, S-CQDs/TiO₂ under visible light irradiation

c_0 (Cr (VI)) mg/L	c_0 (ERY) mg/L	$k_{Cr(VI)}$ min ⁻¹	R^2	k_{ERY} L mg ⁻¹ min ⁻¹	R^2
20.0	20.0	2.35×10^{-1}	0.856	1.89×10^{-2}	0.881
30.0	30.0	4.18×10^{-2}	0.870	1.62×10^{-2}	0.923
40.0	40.0	4.87×10^{-2}	0.755	1.14×10^{-2}	0.878

*Note: Catalyst dosage: 1.0 g/L, solution pH: 2.5 for all reactions

4.3.4 Radicals trapping experiments

It is well-known that free radicals, such as $\bullet OH$, $O_2^{\bullet -}$, and h^+ generated by the redox reactions between photoinduced charges and H₂O/O₂ can decompose large organic pollutants into small molecules [25-28]. To determine the main active free radicals that take part in the photocatalytic degradation of ERY, radical trapping experiments were conducted with four types of radical scavengers and the results were illustrated in Fig. 4.5. As shown in Fig. 4.5, all the added scavengers could inhibit the degradation of ERY in the Cr (VI)-ERY system. The photocatalytic degradation rate of ERY by N, S-CQDs/TiO₂ composite is effectively decreased to 53% in the presence of TEOA, showing that holes (h^+) played the most important role in the photocatalytic oxidation process. Among the four radical scavengers, ethanol had the least influence (90.5%) on

the ERY degradation, indicating that the amount of $O_2^{\bullet-}$ generated from the reactions is quite low. The $\bullet OH$ and e^- scavengers, IPA and BQ, also exhibited significant effect on the ERY degradation, leading to the reduced ERY degradation efficiencies (63% and 81.2% respectively). The results of radical trapping experiments confirmed the existence of photo-excited charges and the formation of $\bullet OH$ and $O_2^{\bullet-}$ radicals and suggested that h^+ and $\bullet OH$ were the major active species for ERY degradation in the Cr (VI)-ERY binary system.

Reactions involved in the photocatalytic degradation of ERY can be described as follows [29, 30]:

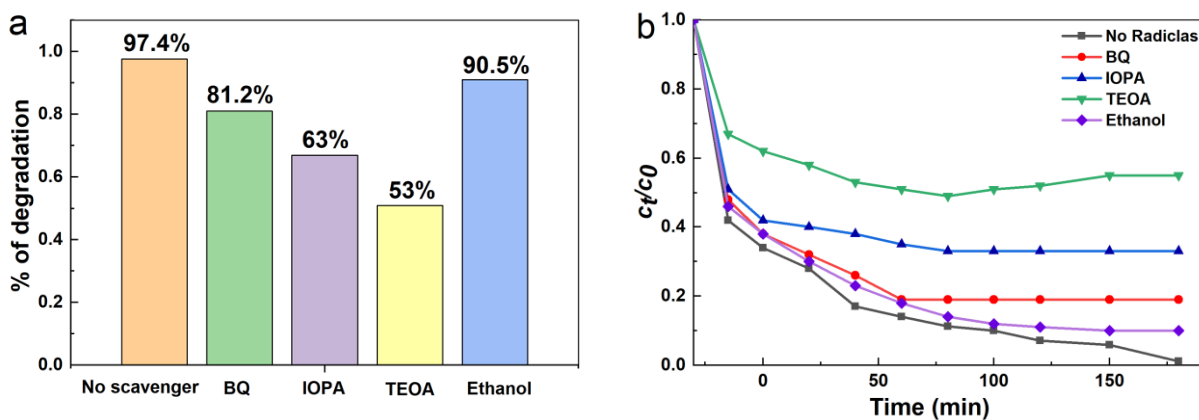
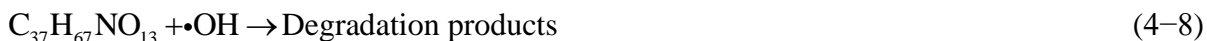
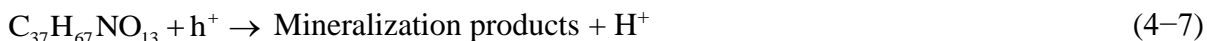


Figure 4. 5. ERY degradation in the presence of different radicals' scavengers.

4.3.5 Photocatalytic mechanisms

Based on the obtained results and previous studies [31, 32], a possible mechanism for the synergistic photocatalytic reduction of Cr (VI) and degradation of ERY by the N, S-CQDs/TiO₂ nanocomposite is depicted in Fig. 4.6. Upon the exposure to the visible light, electrons were generated from the valence band (VB) of N, S-CQDs/TiO₂ and then quickly transferred to the conduction band (CB), resulting in photo-excited e⁻/h⁺ pairs. Such photo-excited e⁻/h⁺ pairs will stimulate redox reactions when they are transferred to the semiconductor surface by the formation of strong radicals (•OH, O₂^{•-}, etc.) [33, 34]. They may also be caught in the semiconductor lattice at faulty locations or may be recombined as heat or light emissions to dissipate energy. For synergistic reduction of Cr (VI) and photodegradation of ERY by N, S-CQDs/TiO₂, the recombination of e⁻/h⁺ pairs was greatly reduced by instantly consuming electrons and holes in the redox reactions at CB and VB. Specifically, photo-generated electrons transferred from VB to the CB of the composite were captured by Cr (VI) ions, leading to the reduction of Cr (VI) to Cr (III). Concurrently, holes in the VB of the composite were involved in a series of oxidization reactions. The photocatalytic activity of the N, S-CQDs/TiO₂ composite was greatly improved. In addition, strong acidic medium provided a high concentration of H⁺, as a result, more •OH radicals were produced for photocatalytic destruction of ERY [35].

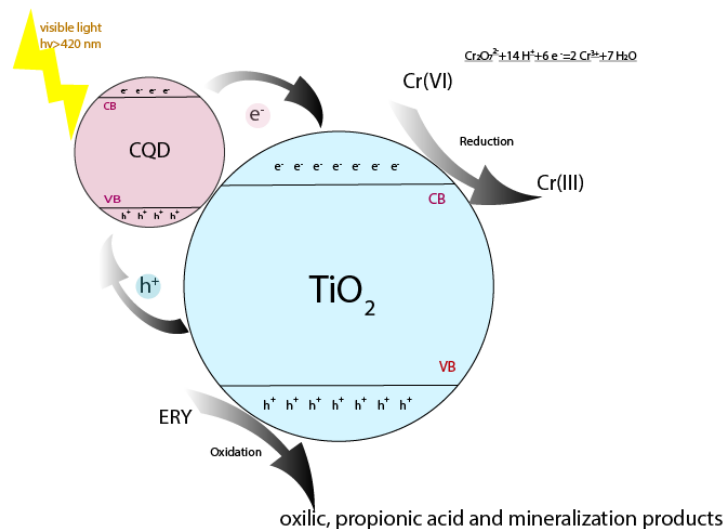


Figure 4. 6. Photocatalytic mechanism of synergic Cr (VI) reduction and ERY degradation by N, S-CQDs/TiO₂

4.3.6 Recyclability

We conducted four cycles of reusability experiments to assess the stability of the N, S-CQDs/TiO₂ nanocomposite. It was observed from Fig 4.7 that the N, S-CQDs/TiO₂ maintained its high catalytic activity after four consecutive runs, the reduction rate of Cr (VI) decreased from 100% to 94.1%, while the degradation efficiency of ERY decreased slightly from 100% to 92.0%. Results from Fig. 4.7 demonstrated that the prepared N.S-CQDs/TiO₂ exhibited very good chemical stability and can be used repeatedly for batch experiments. A continual decrease of the photocatalytic activity could be caused by the occupation of oxides/hydroxides of Cr (III) on the active sites of N, S-CQDs/TiO₂ composite or the cleaving of the Ti–O–C connection.

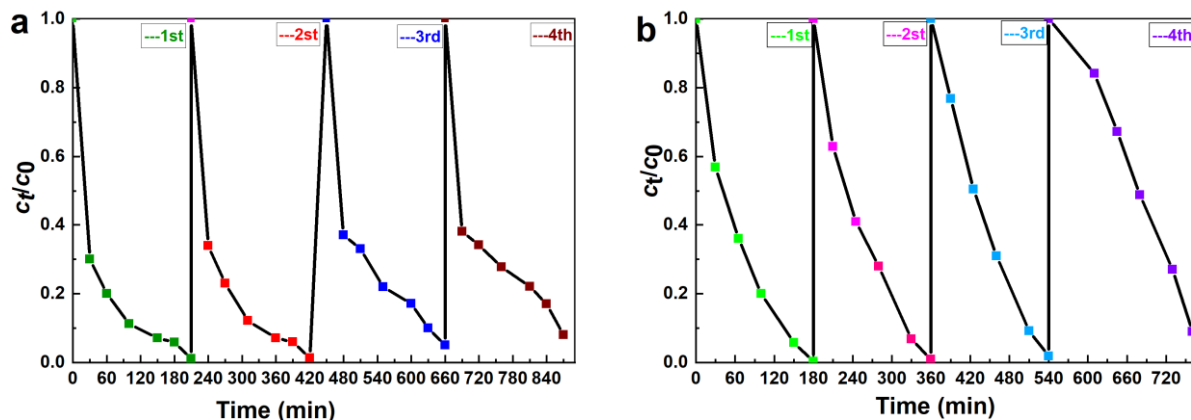


Figure 4. 7. Reusability of N, S-CQDs/TiO₂ nanocomposite for (a) ERY degradation, and (b) reduction of Cr (VI) with four reaction cycles.

4.4 Conclusion

In this study, N, S-CQDs sensitized TiO₂ composite was used for the first time to synergistically reduce Cr (VI) and degrade ERY from water solutions. The N, S-CQDs/TiO₂ demonstrated high photocatalytic performance under visible light irradiation, leading to complete reduction of Cr (VI) and photodegradation of ERY at pH2.0 with the initial concentration of 20.0 mg/L for Cr (VI) and ERY and a catalyst dosage of 1.0 g/L. Moreover, the composite also exhibited very high chemical stability, less than 10% decrease of Cr (VI) reduction rate and ERY degradation efficiency were achieved after four sequential runs. The results from radical trapping experiments confirmed that h⁺ and •OH were the major active species for ERY degradation, whereas photo-generated electrons reduced Cr (VI) to Cr (III) in the Cr (VI)-ERY binary system. Due to the effective consumption of e⁻/h⁺ pairs in CB and VB of the composite, the reduction efficiency of Cr (VI) was significantly improved in binary system compared to the single Cr (VI) reduction system, implying that synergistic photocatalytic removal of heavy metal ions and POPs is a feasible approach to mitigate water pollution.

References

- [1] K.C. Jones, P de Voogt, Persistent organic pollutants (POPs): State of the science, *Environ. Pollut.* 100 (1999), 209–221.
- [2] J. Wang, R.P.J. Hoondert, N.W. Thunnissen, D. van de Meent, A. Jan Hendriks, Chemical fate of persistent organic pollutants in the arctic: Evaluation of simplebox, *Sci. Total Environ.* 720 (2020), 137579.
- [3] Y. Pi, X. Li, Q. Xia, J. Wu, Y. Li, J. Xiao, Z. Li, Adsorptive and photocatalytic removal of persistent organic pollutants (POPs) in water by metal-organic frameworks (MOFs), *Chem. Eng. J.* 337 (2018), 351–371.
- [4] H. Dong, G. Zeng, L. Tang, C. Fan, C. Zhang, X. He, Y. He, An overview on limitations of TiO₂-based particles for photocatalytic degradation of organic pollutants and the corresponding countermeasures, *Water Res.* 79 (2015), 128–146.
- [5] C. Visvanathan, R.B. Aim, K. Parameshwaran, Membrane separation bioreactors for wastewater treatment, *Crit. Rev. Environ. Sci. Technol.* 30 (2000), 1–48.
- [6] N.H. Tran, T. Urase, H.H. Ngo, J. Hu, S.L. Ong, Insight into metabolic and cometabolic activities of autotrophic and heterotrophic microorganisms in the biodegradation of emerging trace organic contaminants, *Bioresour. Technol.* 146 (2013), 721–731.
- [7] F. Creutzig, P. Agoston, J.C. Goldschmidt, G. Luderer, G. Nemet, R.C. Pietzcker, The underestimated potential of solar energy to mitigate climate change, *Nat. Energy* 2 (2017), 17140.
- [8] S. Chu, Y. Cui, N. Liu, The path towards sustainable energy, *Nat. Mater.* 16 (2017), 16–22.
- [9] E. Brillas, C.A. Martínez-Huitle, Decontamination of wastewaters containing synthetic organic dyes by electrochemical methods, An updated review, *Appl. Catal. B Environ.* 166 (2015), 603–643.
- [10] J. Zhang, Y. Wu, M. Xing, S. A. K. Leghari, S. Sajjad, Development of modified N doped TiO₂ photocatalyst with metals, nonmetals and metal oxides, *Energy Environ. Sci.* 3 (2010), 715.
- [11] M. Rahbar, M. Mehrzad, M. Behpour, S. Mohammadi-Aghdam, M. Ashrafi, S. N co-doped carbon quantum dots/TiO₂ nanocomposite as highly efficient visible light photocatalyst, *Nanotech.* 50 (2019), 505702.
- [12] F. Stelo, N. Kublik, S. Ullah, H. Wender, Recent advances in Bi₂MoO₆ based Z-scheme heterojunctions for photocatalytic degradation of pollutants, *J. Alloys Compd.* 829 (2020), 154591.

- [13] L.X. Yang, Y. Xiao, S.H. Liu, Y. Li, Q.Y. Cai, S.L. Luo, G.M. Zeng, Photocatalytic reduction of Cr (VI) on WO₃ doped long TiO₂ nanotube arrays in the presence of citric acid, *Appl. Catal. B: Environ.* 94 (2010), 142–149.
- [14] Q. Fan, Y. Huang, C. Zhang, J. Liu, L. Piao, Y. Yu, S. Zuo, B. Li, Superior nanoporous graphitic carbon nitride photocatalyst coupled with CdS quantum dots for photodegradation of RhB, *Catal. Today* 264 (2016), 250–256.
- [15] Y.C. Chang, J.C. Lin, S.Y. Chen, L.Y. Hung, Y.R. Lin, C.Y. Chen, Complex SnO₂ nanoparticles and nanosheets with enhanced visible-light photocatalytic activity, *Mater. Res. Bull.* 100 (2018), 429–433.
- [16] C. Hao, Y. Tang, W. Shi, F. Chen, F. Guo, Facile solvothermal synthesis of a Z-scheme 0D/3D CeO₂/ZnIn₂S₄ heterojunction with enhanced photocatalytic performance under visible light irradiation, *Chem, Eng. J.* 402 (2020), 126165.
- [17] D. Pan, J. Jiao, Z. Li, Y. Guo, C. Feng, Y. Liu, L. Wang, M. Wu, Electrophoretic fabrication of highly D. Panrobust, efficient, and benign heterojunction photoelectrocatalysts based on graphene-quantum-dot sensitized TiO₂ nanotube arrays, *J. Mater. Chem. A* 1 (2013), 3551–3555.
- [18] D. Pan, J. Jiao, Z. Li, Y. Guo, C. Feng, Y. Liu, L. Wang, M. Wu, Efficient separation of electron–hole pairs in graphene quantum dots by TiO₂ heterojunctions for dye degradation, *ACS Sustainable Chem. Eng.* 3 (2015), 2405–2413.
- [19] J. Zhang, Q. Liu, H. He, F. Shi, G. Huang, B. Xing, J. Jia, C. Zhang, Coal tar pitch as natural carbon quantum dots decorated on TiO₂ for visible light photodegradation of rhodamine B. *Carbon* 152 (2019), 284–294.
- [20] M. Rahbar, M. Mehrzad, M. Behpour, S. Mohammadi-Aghdam, M. Ashrafi, S, N co-doped carbon quantum dots/TiO₂ nanocomposite as highly efficient visible light photocatalyst, *Nanotechnology* 30 (2019), 505702.
- [21] H. Liang, X. Tai, Z. Du, Photocatalytic degradation of nonylphenol ethoxylate and its degradation mechanism, *J. Mol. Liq.* 302 (2020), 112567.
- [22] W.S. Koe, W.C. Chong, Y.L. Pang, C.H. Koo, M. Ebrahim, A.W. Mohammad, Novel nitrogen and sulphur co-doped carbon quantum dots/titanium oxide photocatalytic membrane for in-situ degradation and removal of pharmaceutical compound, *J. Water Process Eng.* 33 (2020), 101068.
- [23] M. Patel, R. Kumar, K. Kishor, T. Mlsna, C. U. Pittman, D. Mohan, Pharmaceuticals of emerging concern in aquatic systems: chemistry, occurrence, effects, and removal methods, *Chem. Rev.*, 119 (2019), 3510–3673.

- [24] E. U. Commission, Study on the review of the list of critical raw materials, *Eur. Comm. Bruss. Belg.*, 2017
- [25] L. Xie, T. Du, J. Wang, Y. Ma, Y. Ni, Z. Liu, L. Zhang, C. Yang, J. Wang, Recent advances on heterojunction-based photocatalysts for the degradation of persistent organic pollutants, *Chem. Eng. J.* 426 (2021), 130617.
- [26] F. Zhao, Y. Rong, J. Wan, Z. Hu, Z. Peng, B. Wang, High photocatalytic performance of carbon quantum dots/TNTs composites for enhanced photogenerated charges separation under visible light, *Catal. Today* 315 (2018), 162–170.
- [27] R. Ma, S. Zhang, T. Wen, P. Gu, L. Li, G. Zhao, F. Niu, Q. Huang, Z. Tang, X. Wang, A critical review on visible-light-response CeO₂-based photocatalysts with enhanced photooxidation of organic pollutants, *Catal. Today* 335 (2019), 20–30.
- [28] H. Yi, D. Huang, L. Qin, G. Zeng, C. Lai, M. Cheng, S. Ye, B. Song, X. Ren, X. Guo, Selective prepared carbon nanomaterials for advanced photocatalytic application in environmental pollutant treatment and hydrogen production, *Appl. Catal. B Environ.*, 239 (2018), 408–424.
- [29] Y. Zhang, K. Hawboldt, J. Zhang, J. Lu, L. Chang, A. Dwyer, Carbonaceous nanomaterial-TiO₂ heterojunctions for visible-light-driven photocatalytic degradation of aqueous organic pollutants, *Appl. Catal. A-Gen.* 630 (2022), 118460.
- [30] Y. Baran, E. Masternak, D. Sapińska, A. Sobczak, E. Adamek, Synthesis of new antibiotics derivatives by the photocatalytic method: A screening research, *Cataly.*, 9 (2021), 1102.
- [31] J. Chen, J. Shu, Z. Anqi, H. Juyuan, Z. Yan, J. Chen, Synthesis of carbon quantum dots/TiO₂ nanocomposite for photo-degradation of rhodamine B and cefradine, *Diam. Relat. Mater.*, 70 (2016), 137–144.
- [32] W. Ji, J. Qu, C. Li, J. Wu, S. Jing, F. Gao, Y. Lv, C. Liu, In situ surface assembly of core-shell TiO₂-copper(I) cluster nanocomposites for visible-light photocatalytic reduction of Cr (VI), *Appl. Catal. B Environ.*, 205 (2017), 368–375.
- [33] B. Gao, G. Z. Chen, G. Li Puma, Carbon nanotubes/titanium dioxide (CNTs/TiO₂) nanocomposites prepared by conventional and novel surfactant wrapping sol-gel methods exhibiting enhanced photocatalytic activity, *Appl. Catal. B Environ.*, 3 (2009), 503–509.
- [34] T. Tachikawa, M. Fujitsuka, T. Majima, Mechanistic insight into the TiO₂ photocatalytic reactions: Design of new photocatalysts, *J. Phys. Chem. C*, 14 (2007), 5259–5275.

[35] Mohammad. Abdullah, G. K. C. Low, R. W. Matthews, Effects of common inorganic anions on rates of photocatalytic oxidation of organic carbon over illuminated titanium dioxide, *J. Phys. Chem.*, 17 (1990), 6820–6825.

Chapter 5. Conclusions and Recommendations

5.1 Conclusions

In this study, the N, S-CQDs were synthesized from citric acid and thiourea through the hydrothermal method. The prepared N, S-CQDs exhibit strong visible light adsorption over the wavelength range of 420-620 nm. Accordingly, N, S-CQDs were employed as a photosensitizer to modify TiO₂ and the resulting nanocomposite was used as a photocatalyst for the degradation of toxic contaminants in the water. The prepared nanocomposite was characterized using TEM, UV-Vis, FTIR, XRD and XPS analyses. This composite simultaneously exhibited an extended photo response range, enhanced charge separation, transportation properties and photocatalytic ability.

N, S-CQDs/TiO₂ nanocomposite prepared by immersing TiO₂ into 4 wt% of N, S-CQDs solutions followed by calcination at 150 °C was first used to reduce Cr (VI) from water solutions. The prepared composite exhibited the highest reduction efficiency at pH2.0, leading to complete reduction of Cr (VI) after 3 h's exposure to visible light with the initial Cr (VI) concentration being 20.0 mg/L and catalyst dosage being 1.0 g/L. Experimental results also demonstrated that high solution pH and high initial Cr (VI) concentration led to decreased reduction rate of Cr (VI). Moreover, more than 98.0% of Cr (VI) ($c_0 = 20.0$ mg/L) was reduced by the prepared composite under visible light irradiation from real water sample (surface water), indicating their great promise in practical wastewater treatment.

The N, S-CQDs/TiO₂ nanocomposite was then employed as the photocatalyst for synergistic photocatalytic reduction of Cr (VI) and degradation of erythromycin (ERY) from water under visible light irradiation. Due to the instant consumptions of photo-generated electrons and holes at

conduction and valence bands, the composite showed improved Cr (VI) reduction efficiency in the binary Cr (VI)-ERY system compared to single Cr (VI) system, leading to complete reduction of Cr (VI) and 96.0% degradation of ERY with the increased initial concentration ($c_0 = 30.0$ mg/L for each) and catalyst dosage being 1.0 g/L. The composite also exhibited very high chemical stability, and less than 10% decrease of Cr (VI) reduction rate and ERY degradation efficiency were achieved after four sequential runs. The results from radical trapping experiments confirmed that h^+ and $\bullet OH$ were the major active species for ERY degradation, whereas photo-generated electrons reduced Cr (VI) to Cr (III) in the Cr (VI)-ERY binary system.

5.2 Recommendations for future work

In recent years, tremendous efforts have been made regarding the synthesis of efficient, low-cost, and environmentally friendly CQDs-semiconductor materials. Because carbon quantum dots have complex structure and difference in properties, there is still significant scope to enhance their utilization.

Some recommendations for future work include:

- (1) The optical characteristics of CQDs are influenced by their size and surface imperfections. However, there are yet no methodologies or procedures that can exactly control the magnitude and population of flaws in CQDs. More attention should be directed to the synthesis of CQDs with well-defined and atom-precise structures.
- (2) Doping procedures and surface passivation methods can be used more effectively to boost the quantum yield of CQDs produced.
- (3) The photostability of CQD-based photocatalysts is overlooked. The oxygenic groups on the surface of CQDs are significantly depleted after prolonged irradiation and photocatalytic activity.

The depletion of surface functional groups may have a major impact on their photocatalytic activity, so this issue should be taken seriously. Furthermore, to ensure long-term stability of these photocatalytic systems, additional focus should be directed to the creation of strong CQDs.

(4) The efficiency and photostability of the modified TiO₂ must be increased. The performance of modified TiO₂ is currently limited by the materials' physicochemical properties. Although a modified TiO₂ can degrade pollutants well in the lab, the catalysts' durability and recyclability must be considered in real-world applications.

(5) In this study, the synthesis of composites occurred using the hydrothermal method, which took a long time under high temperature. The process of composition synthetization should also be improved to reduce itself overall cost and energy consumption. In addition, the accurate amount of CQDs on TiO₂ is still under researched. Thus, more CQDs attached on TiO₂ should be achieved to narrower the bandgap of composites.

(6) Moreover, because the collection and reuse of catalysts in water is still inconvenient due to their small size and poor mechanical properties, novel photocatalysts with an easy collection property or new hybrid devices based on photocatalysts with selected substrates (e.g., polymers, metals) are proposed.

(7) Significantly, to make future large-scale adoption cost-effective, extensive experimental research is required. On this subject, there are several chemicals that are expensive. Cost should be considered as a crucial parameter when comparing and enhancing the findings of this field of research.

(8) Finally, erythromycin is not the best choice of POPs for photodegradation because it can self-degrade under acidic conditions, which does not fully reflect the degradation ability of N, S-CQDs/TiO₂. Even while some researchers claim that erythromycin cannot totally dissolve in an acidic environment, there is no evidence available regarding the degradation of the ery-x binary system. Considering this, future research could explore other organic contaminants or other binary system studies.

Appendix A. The Calibration Curve for Cr (VI) UV-Vis Determination

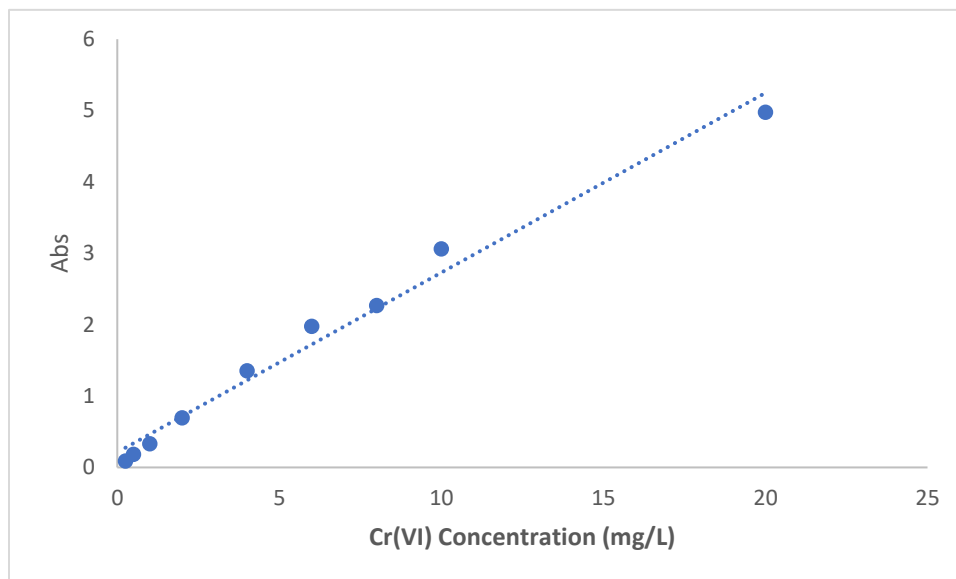


Figure A1. Calibration curve for Cr (VI) concentration determination using UV-Vis absorbance at wavelength of 540 nm.